

**TWO-LAYER EXCHANGE FLOW THROUGH
THE BURLINGTON SHIP CANAL**

by

SUSAN LAVINIA GRECO

B.A.Sc., University of Windsor, 1996

**A THESIS SUBMITTED IN PARTIAL FULFILLMENT OF THE REQUIREMENTS FOR
THE DEGREE OF
MASTER OF APPLIED SCIENCE**

in

**THE FACULTY OF GRADUATE STUDIES
(CIVIL ENGINEERING)**

**We accept this thesis as conforming
to the required standard**

THE UNIVERSITY OF BRITISH COLUMBIA

September 1998

© Susan L. Greco, 1998

In presenting this thesis in partial fulfilment of the requirements for an advanced degree at the University of British Columbia, I agree that the Library shall make it freely available for reference and study. I further agree that permission for extensive copying of this thesis for scholarly purposes may be granted by the head of my department or by his or her representatives. It is understood that copying or publication of this thesis for financial gain shall not be allowed without my written permission.

Department of CIVIL ENGINEERING

The University of British Columbia
Vancouver, Canada

Date 12/09/98

ABSTRACT

In summer, the temperature difference between Hamilton Harbour and Lake Ontario drives a two-layer exchange flow through the Burlington Ship Canal. Warmer Hamilton Harbour water forms the upper layer in the canal before floating out onto the surface of Lake Ontario, while cooler lake water forms the bottom layer in the canal prior to sinking into the harbour's hypolimnion. During periods of exchange flow, large amounts of water are exchanged between the harbour and the lake, thus an understanding of this phenomenon is necessary to determine the water quality of either body. In the summer of 1996, an extensive field study was conducted to obtain a better understanding of exchange flow dynamics in the Burlington Ship Canal.

Acoustic Doppler Current velocity Profiler (ADCP) and Conductivity-Temperature-Depth (CTD) profiles measured during 5 drifts along the canal from a boat on July 25, 1996 were analyzed in the present study. Differential Global Positioning System (DGPS) was employed to determine surface location within the canal. Density in the canal was calculated from temperature and conductivity using a lakewater equation of state. A hyperbolic tangent function was fit to each of the velocity and density profiles in the ship canal. This fit provided a convenient way of characterizing the density and velocity of each layer, the interface location, and thickness of the interface. Flows into and out of Hamilton Harbour were

estimated by integrating the velocity profiles with respect to depth. By forcing control locations at the ends of the Burlington Ship Canal, a line was calculated as an initial estimate of the interface profile using the measured flow for each layer and the density difference. As a first approximation, the line provides a reasonable fit to the data. However, unsteadiness in the flow limits the validity of the concept of hydraulic control and other aspects of steady 2-layer hydraulics. Predictions of the interface fit should be extended to account for unsteady effects. In addition, barotropic and frictional effects should be considered.

All of the drifts, except for one where mixing was caused by the passage of a large ship through the canal rather than exchange flow, exhibit similar mixing patterns. The bulk Richardson number associated with velocity, $J_s = 0.30$, and the bulk Richardson number associated with density, $J_\eta = 0.25$. These values compare very favourably with published values of J from theoretical, numerical, and experimental work. In the Burlington Ship Canal, mixing may be predicted once the background flow is known. Unfortunately, steady, 2-layer hydraulics cannot provide an accurate estimate of the background flow.

TABLE OF CONTENTS

ABSTRACT.....	II
TABLE OF CONTENTS.....	IV
LIST OF TABLES	VII
LIST OF FIGURES	VIII
LIST OF SYMBOLS.....	XI
ACKNOWLEDGEMENTS.....	XIV
1 INTRODUCTION	1
1.1 Objectives.....	3
1.2 Scope	4
2 LITERATURE REVIEW.....	8
2.1 Remedial Action Plan.....	8
2.2 Water Quality Modeling.....	9
2.3 Two-Layer Exchange Flow.....	11
2.4 Interfacial Mixing.....	12
3 REVIEW OF HYDRAULIC THEORY	14
3.1 Assumptions	14
3.2 Equations of Motion	14
3.3 Review of Froude Numbers.....	15

3.3.1	Composite Froude Number	16
3.3.2	Internal and External Froude Number	17
3.3.3	Stability Froude Number	18
3.3.4	Relationship between Froude Numbers	19
3.4	Energy and Shear Stress	19
3.5	Exchange Flow	21
3.6	Linear Theory	23
4	FIELD WORK.....	27
4.1	Field Site	27
4.2	Moored Instrumentation	28
4.3	Boat Instrumentation	29
4.3.1	Survey Method.....	30
4.3.1.1	Time Zones.....	31
4.3.1.2	Drift Labeling.....	31
4.3.1.3	Drift D	32
4.3.2	DGPS	33
4.3.2.1	Position in the Canal	33
4.3.3	ADCP	34
4.3.3.1	Location of ADCP pings.....	35
4.3.3.2	Bottom Topography.....	35
4.3.4	CTD.....	36
4.3.4.1	Location of CTD Casts.....	36
4.3.4.2	Comparison of ADCP and CTD.....	37
5	ANALYSIS OF BOAT DATA FOR JULY 25, 1996.....	48
5.1	Velocity.....	48
5.1.1	Velocity Profiles.....	51
5.1.1.1	Velocity of each layer	51
5.1.1.2	Interface Position Along the Canal	52
5.1.1.3	Thickness of Velocity Interface	53
5.1.1.4	Flow rates.....	54
5.1.1.5	Exchange flow strength parameter.....	56
5.1.2	Velocity variation along the canal.....	57
5.2	Equation of State.....	57
5.3	Temperature and Conductivity Data.....	60
5.3.1	Density Profiles.....	60
5.3.1.1	Density of each layer.....	61

5.3.1.2	Interface Position Along the Canal	61
5.3.1.3	Thickness of Density Interface	62
5.3.2	Temperature Profiles	63
5.4	Parameter Summary	63
6	DISCUSSION	77
6.1	Interfacial Mixing	77
6.2	Applicability of Two-Layer Hydraulics	79
7	CONCLUSIONS AND RECOMMENDATIONS	92
7.1	Suggestions for further research	93
	BIBLIOGRAPHY	94
	APPENDIX A – LIST OF COMPUTER PROGRAMS FOR DATA ANALYSIS	97
	APPENDIX B – DRIFT D RESULTS	99

LIST OF TABLES

Table 2 - 1	Some water quality parameters in western Lake Ontario and Hamilton Harbour (Adapted from Barica, et al., 1988).....	11
Table 4 - 1	Survey drift labeling.....	32
Table 4 - 2	Points along centreline of Burlington Ship Canal.....	34
Table 4 - 3	Some differences in ADCP and CTD data collection.....	37
Table 5 - 1	Smoothing of one velocity profile.....	50
Table 5 - 2	Interface location by the position of maximum shear and by.....	53
Table 5 - 3	Exchange flow strength classification.....	56
Table 5 - 4	Density, velocity, and flow for each layer averaged over the drift.....	64
Table 6 - 1	Richardson Numbers.....	79
Table 6 - 2	Linear theory solutions for each of the five drifts.....	80

LIST OF FIGURES

Figure 1 - 1 Schematic of exchange flow through the Burlington Ship Canal (Adapted from Hamblin, 1989).....	5
Figure 1 - 2 Mass Balance around Hamilton Harbour (Adapted from Hamblin & Lawrence, 1990).....	6
Figure 1 - 3 (a)-(c) Flow regimes in the Burlington Ship Canal.	7
Figure 3 - 1 (a) Top view for flows; (b) side view for one-layer flow; and (c) side view for two-layer exchange flow (Adapted from Lawrence, 1990b).	25
Figure 3 - 2 Shear stress acting on an element in two-layer exchange flow (Adapted from Zhu, 1996).....	26
Figure 4 - 1 Plan view of field site showing Hamilton Harbour, Burlington Ship Canal and Lake Ontario (Adapted from Ling, et al., 1993).	38
Figure 4 - 2 (a) Simplified plan and (b) and cross-section views of exchange flow in the Burlington Ship Canal (Adapted from Greco, et al., 1998).....	39
Figure 4 - 3 (a) Plan and (b) Section view of canal showing location of moored instrumentation (Figure prepared by R. Pieters, 1996).	40
Figure 4 - 4 Velocity of moored ADCP data on July 25, 1996 plotted on depth versus time.	41
Figure 4 - 5 Plan view of a typical boat transect in the Burlington Ship Canal.	42
Figure 4 - 6 Section view of CTD yo-yo's for Drift E.	43
Figure 4 - 7 Sample density and velocity profiles along the canal.	44
Figure 4 - 8 Plan view of non-dimensional boat and ADCP data collection position.	45
Figure 4 - 9 Bottom depth along the centreline of the canal for all Drifts.	46
Figure 4 - 10 Plan view of non-dimensional boat and CTD data collection position.....	47
Figure 5 - 1 (a) Sample velocity and (b) density profiles with fitted hyperbolic tangent functions.	66
Figure 5 - 2 Layer velocities and barotropic component along the length of the canal for Drifts A, B, C, and E.....	67
Figure 5 - 3 Interface height along the length of the canal from velocity for Drifts A, B, C, and E.....	68
Figure 5 - 4 The difference in using the position of maximum shear, $h_{1m.s.}$, and position of zero velocity, $h_{1u=0}$, to locate the interface.	69

Figure 5 - 5 Layer and net flow rate per unit width along the length of the canal for Drifts A, B, C, and E.....	70
Figure 5 - 6 Velocity variation for Drifts A, B, C, and E.....	71
Figure 5 - 7 (a) Temperature-Salinity diagram and (b) Temperature-Conductivity plot for all Drifts.....	72
Figure 5 - 8 Sample (a) conductivity, (b) temperature, and (c) density profile.....	73
Figure 5 - 9 Density of top and bottom layers along the length of the canal for Drifts A, B, C, and E.....	74
Figure 5 - 10 Interface height along the length of the canal from density for Drifts A, B, C, and E.....	75
Figure 5 - 11 Temperature profiles from CTD along canal for Drifts A, B, C, and E.....	76
Figure 6 - 1 Thickness of the velocity interface, δ , mixing length scale, $\Delta U^2/g'$, and bulk Richardson number from velocity profiles, J_δ , for Drifts A, B, C, and E.....	83
Figure 6 - 2 Thickness of the density interface, η , mixing length scale, $\Delta U^2/g'$, and bulk Richardson number from density profiles, J_η , for Drifts A, B, C, and E.....	84
Figure 6 - 3 Bulk Richardson number from velocity for Drifts A, B, C, and E.....	85
Figure 6 - 4 Richardson number from density for Drifts A, B, C, and E.....	86
Figure 6 - 5 Interface from density and velocity profiles compared to linear interface for Drifts A, B, C, and E.....	87
Figure 6 - 6 Variation of internal energy head, EI, and net flow, q, along the length of the canal for Drifts A, B, C, and E.....	88
Figure 6 - 7 Variation of composite Froude number along the length of the canal for Drifts A, B, C, and E.....	89
Figure 6 - 8 Variation of stability Froude number along the length of the canal for Drifts A, B, C, and E.....	90
Figure 6 - 9 Exchange flow strength parameter for Drifts A, B, C, and E.....	91
Figure B - 1 Layer velocities and barotropic component along the length of the canal for Drift D.....	100
Figure B - 2 Interface height along the length of the canal for Drift D.....	101
Figure B - 3 Flow rate per unit width in top and bottom layers along the length of the canal determined from velocity profiles for Drift D.....	102
Figure B - 4 Velocities plotted depth against distance for Drift D.....	103
Figure B - 5 Density of top and bottom layers along the length of the canal for Drift D.....	104
Figure B - 6 Interface height along the length of the canal from density profiles for Drift D.....	105
Figure B - 7 Temperature profiles along the length of the canal for Drift D.....	106
Figure B - 8 Thickness of the velocity interface, δ , mixing length scale, $\Delta U^2/g'$, and bulk Richardson number from velocity profiles, J_δ , for Drift D.....	107
Figure B - 9 Thickness of the density interface, η , mixing length scale, $\Delta U^2/g'$, and bulk Richardson number from density profiles, J_η , for Drifts A, B, C, and E.....	108
Figure B - 10 Bulk Richardson number plot for velocity for Drift D.....	109
Figure B - 11 Bulk Richardson number plot for density for Drift D.....	110

Figure B - 12	Comparison of interface location with linear interface for Drift D.....	111
Figure B - 13	Variation of internal energy head, E_i , and net flow, q , along the length of the canal for Drift D.....	112
Figure B - 14	Variation of composite Froude number along the length of the canal for Drift D.	113
Figure B - 15	Variation of stability Froude number along the length of the canal for Drift D.	114
Figure B - 16	Exchange flow strength parameter for Drift D.	115

LIST OF SYMBOLS

ρ	density
η	thickness of the density interface
$\eta' = \delta/h$	dimensionless thickness of the density interface
δ	thickness of the velocity interface
$\delta' = \delta/h$	dimensionless thickness of the velocity interface
τ	shear stress
ρ_i	density for layer i
ΔS_f	friction slope
$\Delta U = u_1 - u_2 $	velocity difference between the two layers
+	top layer direction (left-to-right)
-	bottom layer direction (right-to-left by convention)
$\varepsilon = (\rho_2 - \rho_1)/\rho_2 = 1 - r$	relative density difference between the layers
a	horizontal offset from the centre in hyperbolic tangent fit to velocity profiles
A	horizontal offset from the centre in hyperbolic tangent fit to density profiles
A_j	cross-sectional area of layer j
b	horizontal scale in hyperbolic tangent fit to velocity profiles
B	horizontal scale in hyperbolic tangent fit to density profiles
$b(x)$	width of flow varying in the x-direction
c	vertical distance to the centre of the profile in hyperbolic tangent fit to velocity profiles
C	vertical distance to the centre of the profile in hyperbolic tangent fit to density profiles
C	conductivity
d	vertical scale in hyperbolic tangent fit to velocity profiles
D	vertical scale in hyperbolic tangent fit to density profiles

E	mechanical energy per unit volume
E_I	internal energy for two-layer flow
E_j	mechanical energy per unit volume for layer j
F	Froude number
F_Δ	stability Froude number
f_b	bottom friction coefficient
F_E	external Froude number
f_I	interfacial friction coefficient
F_I	internal Froude number
f_s	surface friction coefficient
f_w	side wall friction coefficient
g	gravitational acceleration
$g' = \epsilon g$	modified gravitational acceleration
G	composite Froude number
h	total depth of flow
H	average height of canal (≈ 10 m)
$h_{I_{m.s.}}$	depth to interface at point of maximum shear
$h_{I_{u=0}}$	depth to interface at point of zero velocity
h_b	bottom depth
h_i	depth of each layer
$hs(x)$	height of bottom topography varying in the x-direction
$i = 1, 2$	top layer index, bottom layer index
$J = g'\delta/\Delta u^2$	bulk Richardson number
L	total length of canal (≈ 836 m)
$q = q_1 + q_2$	net volumetric flow rate per unit width
q_i	volumetric flow rate per unit width for layer i
$r = \rho_1/\rho_2$	density ratio
x'	Non-dimensional channel length
Re	Reynold's number
S	surface area
t	time from Global Positioning System (GPS)
T	temperature

$u(z)$	horizontal velocity varying in the z-direction
u_i	horizontal velocity for layer I
W	average width of canal (≈ 89 m)
x	horizontal direction
z	vertical depth

ACKNOWLEDGEMENTS

I would like to sincerely thank Dr. Greg Lawrence and Dr. Roger Pieters who provided guidance and encouragement necessary to complete this study. I am indebted to Dr. Rich Pawlowicz for never failing to provide an answer to my endless Matlab questions. Many others in the Department of Oceanography patiently guided me through computer problems including: Carine Vindeirinho, David Eurin, Paal Isaacson, David Jones, and Joe Tam. Ted Tedford must be recognized for his help in the analysis of the moored instrumentation. In addition, I appreciate the support from my family and friends throughout my academic career.

Financial support from the Natural Science and Engineering Research Council (NSERC) is gratefully acknowledged.

1 INTRODUCTION

An important exchange flow of environmental interest in Ontario, Canada is the transfer of polluted Hamilton Harbour water with Lake Ontario water. The harbour lies on the western edge of Lake Ontario. It is a eutrophic water body with high nutrient levels and low dissolved oxygen concentration. In summer, the temperature difference between warmer Hamilton Harbour and cooler Lake Ontario drives an exchange flow through the Burlington Ship Canal. Since the inflow of lake water is the most significant input into the harbour, accurate exchange flow estimates are necessary to determine the harbour's water quality.

The exchange flow is driven by the density difference between Lake Ontario and Hamilton Harbour. Distinct densities layers are a result of both temperature and salinity differences between the waters, but the temperature difference is most important. During periods of exchange flow, warm harbour water forms the top layer in the canal before floating out onto the lake, while cooler lake water forms the bottom layer in the canal before sinking down into the harbour's hypolimnion. In Figure 1 - 1, a side view schematic of exchange flow in the canal is shown.

Exchange flows occur when two water bodies of different density are connected by a constriction. The density difference may be due to salinity, temperature, or sediment

concentration. In these flows, the buoyant top layer flows counter current to the denser bottom layer. Exchange through the Strait of Gibraltar, connecting the Atlantic Ocean with the Mediterranean Sea, has generated considerable interest due to its strategic location and huge flow volume, approximately 10^6 m³/s in either direction (Kinder & Bryden, 1987). The density difference between the layers in this case is attributed to salinity rather than temperature differences. The Mediterranean Sea is approximately 2 psu more saline than the Atlantic Ocean.

On the order of 100 m³/s of water can be exchanged between Hamilton Harbour and Lake Ontario in summertime (Hamblin & Lawrence, 1990). This is a significant contribution to the mass balance around the harbour since it is ten times greater than all other inputs combined. Tributaries supply a flow of 4 m³/s into the harbour; wastewater treatment plants discharge 4.3 m³/s of treated sewage effluent into the harbour; and industries on the south shore use and return 27 m³/s of harbour water. This mass balance is displayed in Figure 1 - 2.

Both exchange flow and unidirectional flow occur in the Burlington Ship Canal. Exchange flow occurs primarily in the summer months from about May-to-October when the temperature difference between the two water bodies is large. This is the period during which the greatest volume of water is transferred. The top layer moves countercurrent to the bottom layer. In unidirectional flow, the entire water column moves in the same direction. However, in the Burlington Ship Canal, it is common for unidirectional flow to alternate direction periodically, due to Helmholtz resonance, see Hamblin (1995). This may result in little actual exchange between the two water bodies since the water column typically changes

direction before any given parcel of fluid can traverse the length of the canal. Note that neither pure exchange flow nor pure unidirectional flow (plug flow) are common. Typically, flow is a combination of the two. Velocities, obtained from moored instrumentation in the canal, depicting strong and weak exchange flow and unidirectional flow are shown in Figure 1 - 3 (a)-(c).

1.1 Objectives

To further our understanding of the dynamics of exchange flow in the Burlington Ship Canal and exchange flow in general, a comprehensive field investigation was conducted in the summer of 1996. Data were collected from the canal by both moored instrumentation and from a boat transecting the length of the canal. The boat completed five drifts along the centreline of the canal recording density parameters, velocity, and position. Vertical temperature, conductivity, and velocity profiles in the canal, obtained from the five drifts, were analyzed for a summertime exchange flow.

The objectives of this study are to:

1. Analyze conductivity, temperature, and velocity profiles obtained from a boat in the Burlington Ship during an exchange flow event;
2. Assess the applicability of two-layer hydraulic theory to exchange flow in the canal;
and
3. Obtain an estimate of interfacial mixing between the two layers.

1.2 Scope

An introduction to the literature on water quality in Hamilton Harbour, exchange flow theory, and exchange flow in the Burlington Ship canal is presented in Chapter 2. Chapter 3 reviews two-layer hydraulic theory including assumptions, equations of motion, Froude numbers, energy, shear stress and frictional considerations. Interfacial mixing between the layers and a method for making an initial estimate of the interface location, using internal hydraulics, are also reviewed. The field study of the Burlington Ship Canal is discussed in Chapter 4. Data collection from moored instrumentation and from the boat is described. The boat data, including velocity, temperature, conductivity, and position from an exchange flow event on July 25, 1996 are analyzed in Chapter 5. Density, velocity, and volumetric flow rates are calculated along the canal and averaged for each drift. The interface position and interfacial thickness determined from both velocity and density profiles are calculated. The results from the analysis of interfacial mixing and the applicability of two-layer hydraulics to the flow in the Burlington Ship Canal are discussed in Chapter 6. In Chapter 7, conclusions and recommendations for additional research are made.

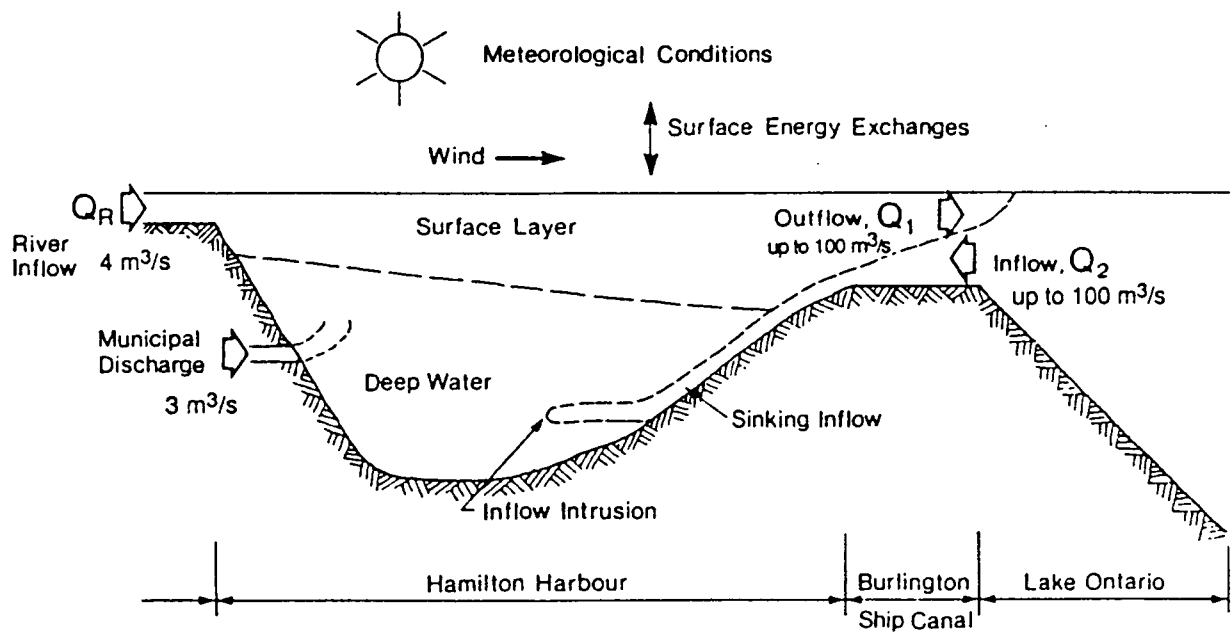


Figure 1 - 1 Schematic of exchange flow through the Burlington Ship Canal (Adapted from Hamblin, 1989).

Exchange flow through the canal occurs between Hamilton Harbour and Lake Ontario when there is a significant temperature difference in summer months. Warm, buoyant outflow from the harbour is denoted by Q_1 and cooler, denser inflow from the lake is denoted by Q_2 .

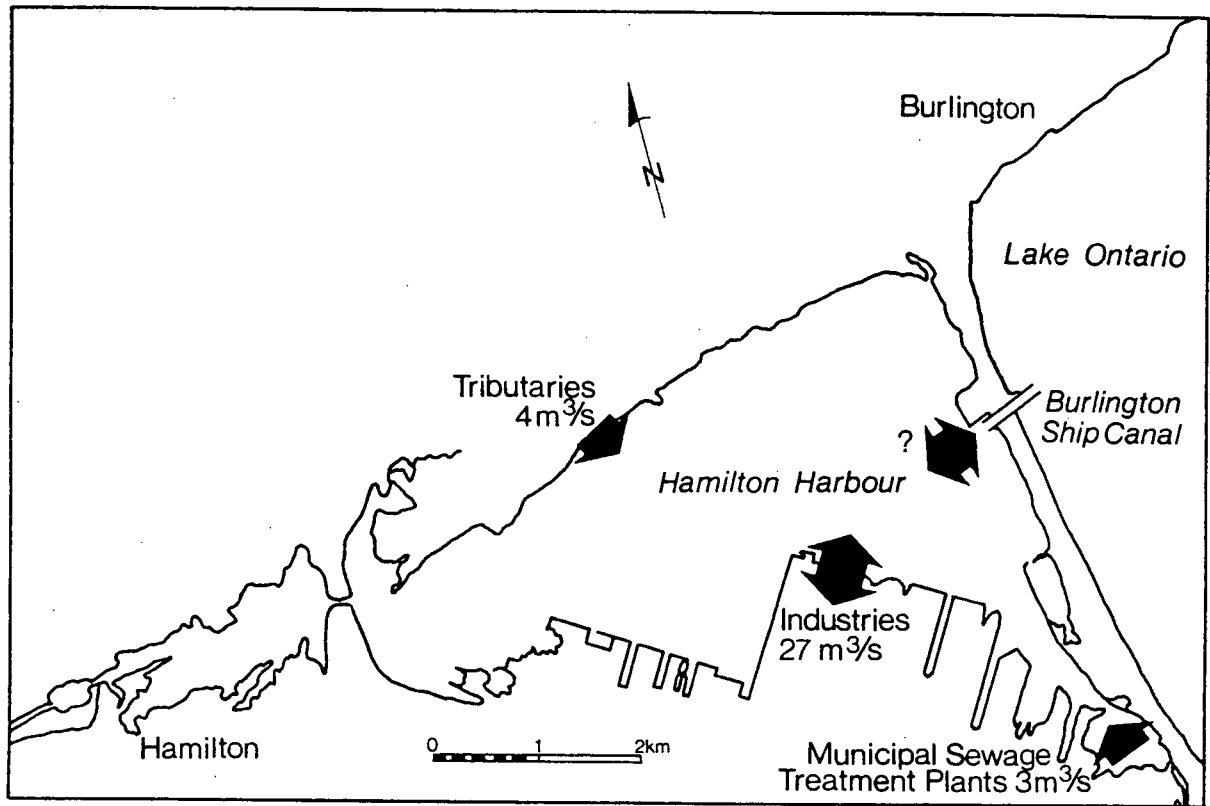


Figure 1 - 2 Mass Balance around Hamilton Harbour (Adapted from Hamblin & Lawrence, 1990). Major inflows and exchanges are shown.

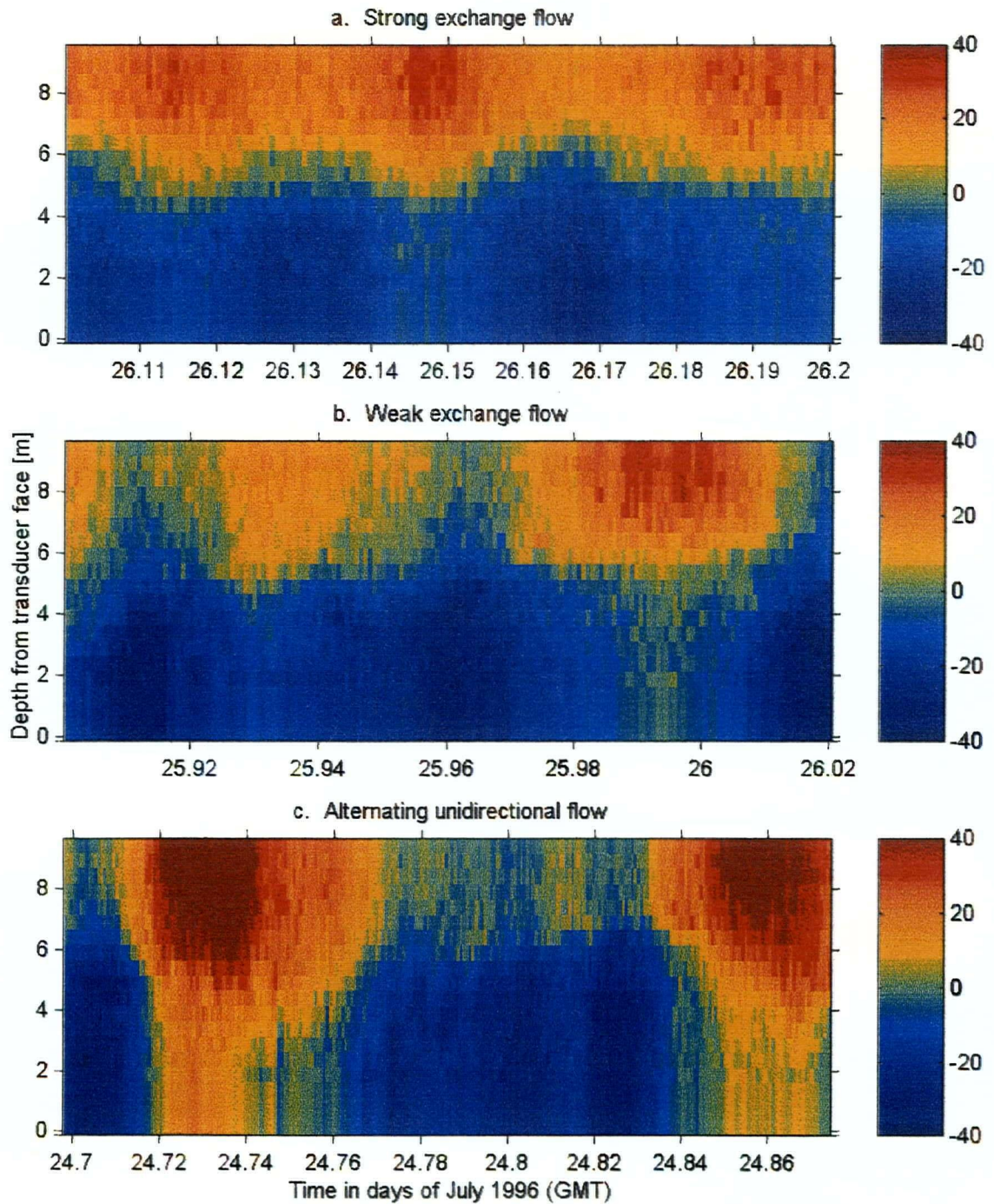


Figure 1 - 3 (a)-(c) Flow regimes in the Burlington Ship Canal. Velocities (in cm/s) from bottom mounted, upward looking moored ADCP in the Burlington Ship Canal are plotted on depth from transducer face and time. The transducer face was located 0.5 m above the bottom of the canal. Hot colours indicate a positive velocity (from Hamilton Harbour to Lake Ontario) while cool colors indicate a negative velocity (from Lake Ontario to Hamilton Harbour).

2 LITERATURE REVIEW

Hamilton Harbour is a eutrophic system whose water quality is improved by exchange flow with Lake Ontario. Water quality in the harbour has become a concern in recent years after the initiation of a Remedial Action Plan for Hamilton Harbour. An understanding of exchange flow is vital to assessing water quality in the harbour.

2.1 Remedial Action Plan

Hamilton Harbour was identified as an Area of Concern (AOC) by the International Joint Commission (IJC) in the 1970's (M.O.E., 1989) because it failed to meet the Ontario Provincial Water Quality Objectives and sediment disposal guidelines. A Remedial Action Plan (RAP) was completed for Hamilton Harbour in 1992 under the auspices of the Canada-U.S. Great Lakes Water Quality Agreement (GLWQA). The RAP stakeholders consisting of members of the public, industry, and government identified six major concerns listed below (M.O.E., 1992).

- Toxic Contamination
- Water Quality
- Bacterial Contamination
- Stresses in Fish and Wildlife
- Urbanization and Land Management
- Access and Aesthetics

The first three concerns are directly related to the harbour's water and described in more detail. The final three are indirectly a result of poor water quality. The water and sediments in Hamilton Harbour are contaminated by metals (including zinc, iron, nickel, and lead) and organic compounds (including PCB's, PAH's, mirex, and DDT). The majority of this type of contamination comes from large industrial operations. The southern shores of Hamilton Harbour house the largest concentration of steel industry in Canada.

Poor water clarity, low dissolved oxygen levels, and odour are a few water quality concerns in the harbour. Erosion of topsoil from farms, streambanks, and construction sites as well as stirring of bottom sediments contribute to the poor water clarity. Excessive nutrients, particularly phosphorus and nitrogen, result in harbour eutrophication. This leads to excessive algal growth and low dissolved oxygen levels.

Four wastewater treatment plants discharge treated effluent into Hamilton Harbour. Severe bacterial contamination of the harbour occurs from combined sewer overflow (CSO) loading after storm events. Installation of retention basins for sewage treatment plants is a recommended and ongoing option to reduce the impact of these events (Stirrup, 1996).

2.2 Water Quality Modeling

The exchange of water through the Burlington Ship Canal is the largest component of the water balance around the harbour. It reduces the harbour's hydraulic residence time thereby improving water quality through dilution and oxygenation. Models for estimating water

quality in Hamilton Harbour have been developed where exchange flow with Lake Ontario is an important input parameter.

Ling, Diamond & MacKay (1993), for example, use a Quantitative Water Air Sediment Interaction (QWASI) fugacity/aquivalence mass balance model to assess the fate of contaminants in Hamilton Harbour. Fugacity (f , Pa) is used rather than concentration (C , mol/m³) as the inter-phase equilibrium criterion. A linear relationship exists between the two, however chemicals always move from a phase with high fugacity to a phase with low fugacity which is simpler than for concentration. Fugacity is unsuitable as an equilibrium criterion for chemicals that have negligible vapour pressure. In these cases, (such as for metals, organometals, ionic compounds), equivalence is used. Chemicals may enter and exit Hamilton Harbour by exchange flow with Lake Ontario. This means accurate exchange flow estimates are required since exchange flow is the most significant flow input/output for Hamilton Harbour.

Hamilton Harbour an important embayment for Lake Ontario since it acts as a stabilization basin for municipal wastewater and industrial effluent and urban runoff. Exchange flow with Lake Ontario reduces the hydraulic residence time of the harbour. Barica, *et al.* (1988) claim that the beneficial effect of dilution by the oligo-to mesotrophic lake far exceeds contamination of western Lake Ontario by the hypereutrophic harbour. Water quality in the harbour would be drastically poorer without the exchange flow. General values for water quality parameters for both bodies of water are shown in Table 2 - 1.

Table 2 - 1 Some water quality parameters in western Lake Ontario and Hamilton Harbour (Adapted from Barica, *et al.*, 1988).

Parameter	Units	Western Lake Ontario (background location)	Hamilton Harbour (Station 256)
Ammonia-Nitrogen	mg/L	0.031	1.661
Nitrate+Nitrite Nitrogen	mg/L	0.306	2.049
Total Phosphorus	mg/L	0.013	0.07
Chlorophyll-a	µg/L	4.2	25.3
Suspended Solids	mg/L	1.11	3.41
Conductivity	µS/cm	333	551

2.3 Two-Layer Exchange Flow

Dick & Marsalek (1973) first noted that two flow regimes existed in the Burlington Ship Canal. They are open channel flow (to-and-fro) with a unidirectional velocity profile created by a water level difference between the two ends of the canal, and exchange flow with buoyant, warm water flowing out of the harbour forming the top layer and dense, cool lake water sinking into the harbour forming the bottom layer. The second regime can be observed in summer months while the first regime occurs during the remainder of the year. Generally, the flow in the canal is a combination of the two regimes with a higher exchange flow component in the summer and a higher unidirectional flow component the remainder of the year. Specific Burlington Ship Canal exchange flow theory and flow calculations are presented in Hamblin & Lawrence (1990).

Armi & Farmer have studied the internal hydraulic theory of exchange flow through the Strait of Gibraltar extensively. Armi & Farmer (1986) examined maximal two-layer exchange flow through a contraction with barotropic flow (net flow in one direction). Farmer & Armi (1986) examined exchange flow over a sill along with the combination of a sill and a contraction.

Kohli (1979) stated that the lake-harbour exchange is important for maintaining and even improving the harbour water quality. During his September study, oscillatory flow (unidirectional flow) persisted in the canal. Total and net daily exchanges from Hamilton Harbour to Lake Ontario were found to be 0.98% and 0.48% of the harbour volume respectively. The net exchange was also found to be toward the lake as calculated from a monthly average.

An alternate method of calculating exchange flow, based on the mass balance of conservative tracers, is presented by Klapwijk & Snodgrass (1985). The model of lake-harbour exchange flow is based on a mass balance of total dissolved substances (TDS) and hypolimnetic temperature. Previously published estimates of exchange flow based on current measurements resulted in unlikely values such as Dick & Marsalek (1973); Palmer & Poulton (1976); and Kohli (1979). This was probably due to inadequate metering of the canal.

2.4 Interfacial Mixing

For two-layer exchange flow, the top layer and bottom layer have distinct characteristics such as temperature and conductivity. The interface between the two layers is a mixed region that exhibits properties of each layer. Effective mixing between the layers is caused by shear instabilities, notably the Kelvin-Helmholtz instability. Lawrence (1990b) hypothesized that under many circumstances hydraulic analysis may be applied to predict maximum mixing layer thickness by $\delta = J(\Delta U)^2/g'$ where J is the bulk Richardson number, ΔU is the velocity difference between the two layers and g' is the reduced gravitational acceleration. This

hypothesis will be tested in the present study. The thickness of the mixed layer is described and calculated in Chapters 5 and 6, respectively.

3 REVIEW OF HYDRAULIC THEORY

To a first approximation, exchange flow through the Burlington Ship Canal can be described by two-layer internal hydraulic theory. Sections 3.1 - 3.5 review two-layer hydraulic theory. Included is a review of the bulk Richardson number, a parameter used to predict mixing between the two layers in exchange flow which is examined in Chapter 6. Section 3.6 describes the "linear theory" which will be compared to the field results in Chapter 6.

3.1 Assumptions

The flows analyzed are based on the assumptions of steady two-layer, two-dimensional, non-rotating, inviscid flow. Free surface deflection and external forcing are assumed to be negligible. The exchange flow is assumed to be driven primarily by the density difference between the two layers rather than by tides or winds.

3.2 Equations of Motion

For steady flow, the motion of layered flows is governed by the conservation of energy,

$$\frac{1}{\rho_j} \frac{\partial E_j}{\partial x} = 0 \quad (3.1)$$

and the continuity equation,

$$\frac{1}{b} \frac{\partial Q_j}{\partial x} = 0 \quad (3.2)$$

where j is the number of layers ($j = 1$ for single layer flow and $j = 2$ for exchange flow); x is the flow direction; ρ_j is the density of layer j ; E_j is the mechanical energy per unit volume; b is the width of flow; and Q_j is the volumetric flow rate. The mechanical energy per unit volume is defined as:

$$E_j = (p + \rho_j g h_j) + \frac{1}{2} \rho_j u_j^2 \quad (3.3)$$

where p is the pressure, assumed hydrostatic, g is the acceleration due to gravity, and h_j and u_j are the depth and velocity of layer j respectively.

3.3 Review of Froude Numbers

Single-layer or open channel hydraulic flow is traditionally classified by the non-dimensional Froude number, F , the ratio of convective velocity to phase speed,

$$F = \frac{u}{\sqrt{gh}} \quad (3.4)$$

where u is the convective velocity and h is the total depth of flow. Flow is classified as follows:

$F < 1$	Subcritical
$F = 1$	Critical (control point)
$F > 1$	Supercritical

Open channel flow is controlled by channel features, such as contractions or changes in surface elevation, that determine a depth-discharge relationship (Henderson, 1966). These features are called hydraulic controls, or simply controls. At a control, the flow is critical and it changes from subcritical to supercritical passing through the control.

3.3.1 Composite Froude Number

In two-layer flow, a composite Froude number, G , is used,

$$G^2 = F_1^2 + F_2^2 - \epsilon F_1^2 F_2^2 \quad (3.5)$$

where the relative density difference, $\epsilon = (\rho_2 - \rho_1) / \rho_2$, the densimetric Froude number for each layer, F_j^2 , is:

$$F_j^2 = \frac{u_j^2}{g' h_j} \quad (3.6)$$

where $j = 1, 2$ and the modified acceleration due to gravity, $g' = \epsilon g$.

In this case, the singularity condition, or internal hydraulic control, occurs where the composite Froude number is unity, $G^2 = 1$, analogous to $F^2 = 1$ in single layer flow. In the Burlington Ship Canal, it has been presumed that controls occurs at each end of the canal (Hamblin & Lawrence, 1990).

When the relative density difference between the layers is small, $\epsilon \ll 1$, the Boussinesq approximation is valid. In the Burlington Ship Canal ϵ is of the order 10^{-3} , thus G^2 can be approximated by:

$$G^2 = F_1^2 + F_2^2 \quad (3.7)$$

Also important in the study of two-layer flow are the internal Froude number, F_I^2 , the external Froude number, F_E^2 , and the stability Froude number, F_Δ^2 defined below.

3.3.2 Internal and External Froude Number

As with the single-layer Froude number, the internal and external Froude numbers are defined as the ratio of convective velocity to phase speed. The celerity or characteristic velocity of external (on surface) and internal (on interface) long waves is the sum of a convective velocity and a phase speed. The external Froude number is the same as the single layer Froude number for Boussinesq two-layer flows,

$$F_E = \frac{\tilde{u}}{\sqrt{gh}} \quad (3.8)$$

where $h = h_1 + h_2$ and the flow weighted mean velocity, $\tilde{u} = (u_1 h_1 + u_2 h_2)/h$. The internal Froude number (Lawrence, 1985, 1990a) is defined as:

$$F_I = \frac{u_1 h_2 + u_2 h_1}{\sqrt{g' h h_1 h_2 (1 - F_\Delta^2)}} \quad (3.9)$$

3.3.3 Stability Froude Number

The interfacial long wave stability Froude number is a representation of the strength of the velocity shear across the interface of the two fluid layers relative to the buoyancy forces. The stability Froude number is defined as:

$$F_\Delta^2 = \frac{\Delta U^2}{g' h} \quad (3.10)$$

where $\Delta U = |u_1 - u_2|$ and h is the total depth of flow. Note that for exchange flows, u_1 and u_2 are of opposite sign so that $\Delta U = |u_1| + |u_2|$. The stability Froude number may be regarded as an inverse bulk Richardson number. It is useful in quantifying the mixing layer thickness, the stability of the flow and its susceptibility to instabilities at the interface. The interface thickness due to shear instabilities, δ , may be predicted using the stability Froude number (Lawrence, 1990a):

$$\delta = J F_\Delta^2 h \quad (3.11)$$

where $J = g'\delta/\Delta U^2$ is the bulk Richardson number due to shear thickness. This work is supported by theoretical work of Miles (1961), Howard (1961), and Corcos & Sherman (1976); the numerical work of Hazel (1972) and Patnaik *et al.* (1976); and the experimental work of Thorpe (1973), Koop & Browand (1979), Lawrence (1985), and Lawrence *et al.* (1991). The estimates of J obtained in these studies vary between 0.25 and 0.32.

3.3.4 Relationship between Froude Numbers

A fundamental relationship between the four aforementioned Froude numbers is defined by Lawrence (1985, 1990a):

$$(1-G^2) = (1-F_A^2)(1-F_E^2)(1-F_I^2) \quad (3.12)$$

For exchange flow through a contraction, the negligible free surface deflection assumption results in $F_E^2 \cong 0$. Accordingly, the relationship between the Froude numbers is simplified to:

$$(1-G^2) = (1-F_A^2)(1-F_I^2) \quad (3.13)$$

Note that G^2 is not simply the ratio of convective velocity to phase speed as is the single-layer Froude number.

3.4 Energy and Shear Stress

The mechanical energy per unit volume is shown below for each layer (Armi, 1986).

$$E_1 = \rho_1 gh + \frac{1}{2} \rho_1 u_1^2 \quad (3.14)$$

$$E_2 = \rho_1 gh + (\rho_2 - \rho_1)gh_2 + \frac{1}{2} \rho_2 u_2^2 \quad (3.15)$$

An equation for the internal energy head, E_i , is obtained by subtracting Equation (3.14) from (3.15) and dividing by the unit weight of the lower layer, $\rho_2 g'$. The internal head for two-layer flow is:

$$E_i = \frac{E_2 - E_1}{\rho_2 g'} = h_2 + \frac{1}{2g'}(u_2^2 - u_1^2) \quad (3.16)$$

Frictional effects are caused by the surface, side walls, bottom, and interface. Energy losses due to friction are represented by shear stresses, τ , at the four surfaces, namely

Surface	$\tau_s = -f_s \rho_1 u_1 u_1 $	(3.17)
---------	----------------------------------	--------

Side wall	$\tau_w = -f_w \rho_j u_j u_j $	(3.18)
-----------	----------------------------------	--------

Bottom	$\tau_b = -f_b \rho_2 u_2 u_2 $	(3.19)
--------	----------------------------------	--------

Interface (upper layer)	$\tau_{i1} = -f_i \rho_1 (\Delta u)^2$	(3.20)
-------------------------	--	--------

Interface (lower layer)	$\tau_{i2} = -f_i \rho_2 (\Delta u)^2$	(3.21)
-------------------------	--	--------

where f_s is the surface friction coefficient, f_w is the wall friction coefficient, f_b is the bottom friction coefficient, and f_i is the interfacial friction coefficient. Conventionally, the upper layer flows in the positive direction (left-to-right) so that $|u_1| = +u_1$ and $|u_2| = -u_2$. The shear stresses are shown on an element of fluid from each layer in Figure 3 - 2. Assuming that the

energy losses are due to the shear stresses on the wall, surfaces and at the interface (Cheung, 1990),

$$\frac{dE_j}{dx} = \frac{\sum \tau_j dS}{A_j dx} \quad (3.22)$$

where S is the surface area and A_j is the cross-sectional area. The left hand side of Equation (3.22) is evaluated by differentiating then summing Equations (3.14) and (3.15). The right side of Equation (3.22) is evaluated by:

$$\frac{\sum \tau_1 dS}{A_1 dx} = -f_w \rho_1 u_1^2 \frac{2}{b} - f_1 \rho_1 \Delta u^2 \frac{1}{h_1} - f_s \rho_1 u_1^2 \frac{1}{h_1} \quad (3.23)$$

$$\frac{\sum \tau_2 dS}{A_2 dx} = f_w \rho_2 u_2^2 \frac{2}{b} + f_1 \rho_2 \Delta u^2 \frac{1}{h_2} + f_b \rho_2 u_2^2 \frac{1}{h_2} \quad (3.24)$$

3.5 Exchange Flow

Equations (3.1) and (3.2) can be reduced to Equation (3.25) (Cheung, 1990).

$$C \frac{\partial v}{\partial x} = D \frac{\partial f}{\partial x} + S \quad (3.25)$$

For single layer flow ($j = 1$):

$$C = \begin{bmatrix} u & g \\ h & u \end{bmatrix} \quad v = \begin{bmatrix} u \\ h \end{bmatrix} \quad D = \begin{bmatrix} -g & 0 \\ 0 & Q \end{bmatrix} \quad f = \begin{bmatrix} hs \\ b^{-1} \end{bmatrix} \quad S = \begin{bmatrix} -f_w u^2 \frac{2}{b} - f_b u^2 \frac{1}{y} - f_s u^2 \frac{1}{h} \\ 0 \end{bmatrix}$$

and for two-layer flow ($j = 2$):

$$C = \begin{bmatrix} u_1 & 0 & g & g \\ 0 & u_2 & rg & g \\ h_1 & 0 & u_1 & 0 \\ 0 & h_2 & 0 & u_2 \end{bmatrix} \quad v = \begin{bmatrix} u_1 \\ u_2 \\ h_1 \\ h_2 \end{bmatrix} \quad D = \begin{bmatrix} -g & 0 \\ -g & 0 \\ 0 & Q_1 \\ 0 & Q_2 \end{bmatrix} \quad f = \begin{bmatrix} hs \\ b^{-1} \end{bmatrix} \quad S = \begin{bmatrix} -f_w u_1^2 \frac{2}{b} - f_I \Delta u^2 \frac{1}{h_1} - f_s u_1^2 \frac{1}{h_1} \\ f_w u_2^2 \frac{2}{b} + f_b u_2^2 \frac{1}{h_2} + f_I \Delta u^2 \frac{1}{h_2} \\ 0 \\ 0 \end{bmatrix}$$

where the density ratio, $r = \rho_1/\rho_2 = (1-\epsilon)$, h_s is the variation in bottom topography, and b is the width of the channel.

The friction slope, ΔS_f , is the sum of the surface, wall, interfacial, and bottom friction slopes.

$$\begin{aligned} \Delta S_f &= \Delta S_{f_s} + \Delta S_{f_w} + \Delta S_{f_I} + \Delta S_{f_b} \\ \Delta S_f &= f_s F_1^2 + \frac{2f_w}{b} [F_1^2 h_1 + F_2^2 h_2] + f_I F_A^2 \frac{h^2}{h_1 h_2} + f_b F_2^2 \end{aligned} \quad (3.26)$$

The internal resistance equation for the case of a wide rectangular channel with zero bed slope is:

$$\frac{dE_1}{dx} = \Delta S_f \quad (3.27)$$

and if we substitute the equation for internal head (3.16) into the resistance equation (3.27), we obtain an equation for the slope of the interface (3.28)

$$\frac{dh_2}{dx} = \frac{\Delta S_f}{1-G^2} \quad (3.28)$$

Equation (3.27) may be integrated with respect to x over the length of the canal to obtain the interface profile that accounts for friction. Finding y_2 at a point of control will provide a boundary condition or starting point.

Equation (3.25) can be solved given the following:

- bathymetry, namely specifying width, $b(x)$, and bottom elevation, $h_b(x)$;
- relative density difference between layers, ϵ ; and
- surface, sidewall, bottom and interfacial friction factors.

However, there is considerable variation in reported values of interfacial friction factors. See Zhu (1996) and Cheung (1990) for reviews. Alternatively, the interfacial friction factor could be determined by fitting solutions of Equation (3.25) to field or laboratory data as done by Cheung (1990).

3.6 Linear Theory

Solution of (3.25) for the Burlington Ship Canal and determination of interfacial friction factors is beyond the scope of this work. Nonetheless, since hydraulic theory would indicate $G^2 = 1$ at both ends of the ship canal, the interface height at each end can be determined as shown below. A first approximation to the interface position within the ship canal is a line between the interface positions at the two ends. In the steady pure exchange flow investigated by Cheung (1990), this turns out to be a good approximation of the full solution

of (3.25). The linear interface connecting the interface height determined from $G^2 = 1$ at each end of the canal will be referred to as the “linear theory” in this work. Linear theory will be compared to field results in Chapter 6.

In a rectangular channel, the ends act as control points where $G^2 = 1$. Using Equation (3.7) for G^2 , and substituting flow per unit width, $q_i = u_i h_i$,

$$G^2 = \frac{q_1^2}{g' h_1^3} + \frac{q_2^2}{g' h_2^3} \quad (3.29)$$

Eliminating h_2 using $h = h_1 + h_2$, results in,

$$G^2 = \frac{q_1^2}{g' h_1^3} + \frac{q_2^2}{g' (h - h_1)^3} = 1 \quad (3.30)$$

at the ends of the ship canal. If the flows, q_1 and q_2 ; the total depth, h ; and the relative density difference between the layers, g' , are known, then (3.29) can be solved. The two real, positive values for h_1 specify the interface position at the two ends of the ship canal. The upper layer, h_1 , is thin at the Lake Ontario end and thick at the Hamilton Harbour end.

Note that some friction effects are incorporated since values of q_1 and q_2 come from the field observations where friction is active. The barotropic flow component (net flow in one direction) is also indirectly accounted for since q_1 and q_2 calculated from the field values are not necessarily equal.

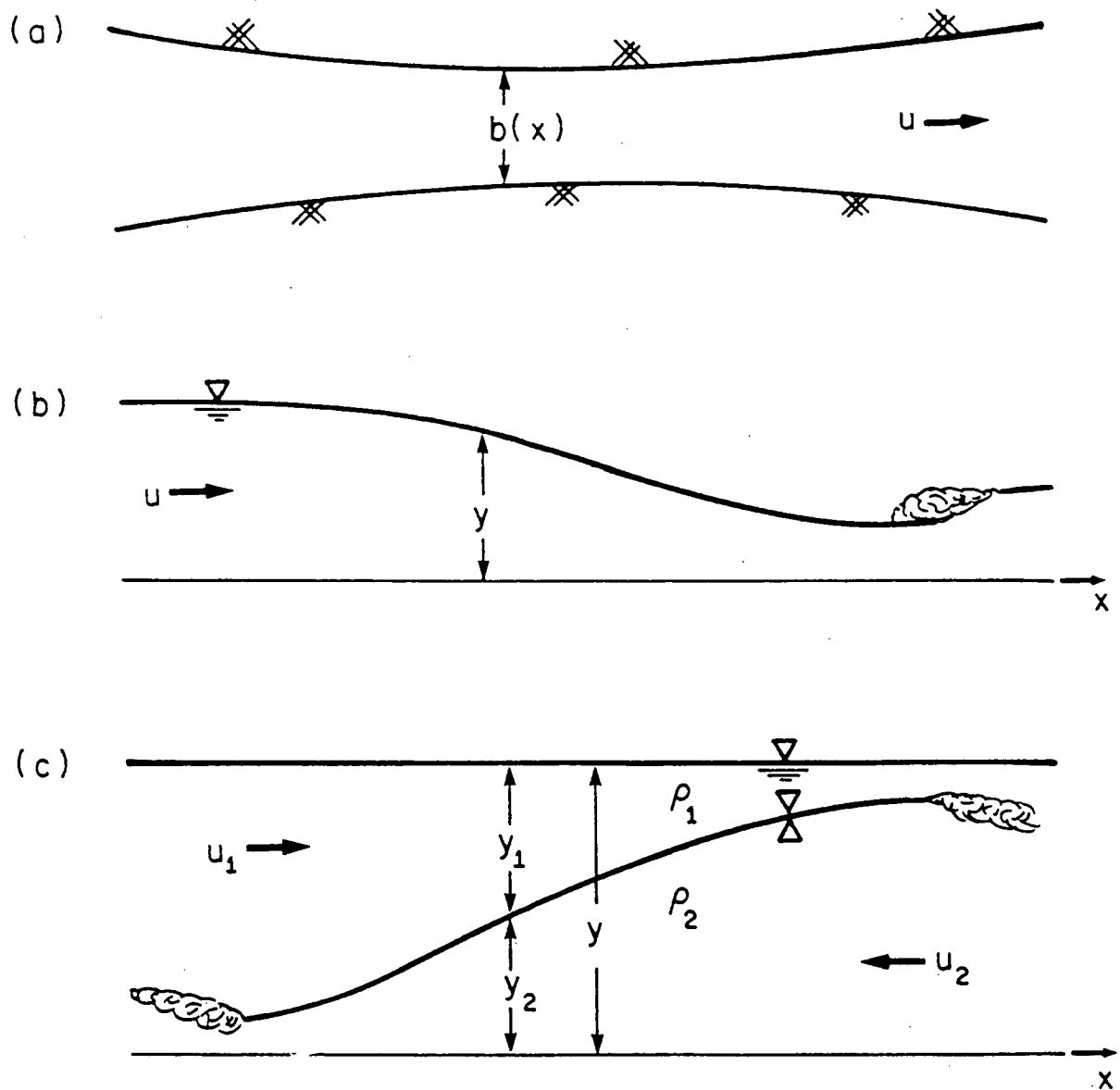


Figure 3 - 1 (a) Top view for flows; (b) side view for one-layer flow; and (c) side view for two-layer exchange flow (Adapted from Lawrence, 1990b).

(a) Top view for 1-layer and 2-layer flow through a contraction of varying width, $b(x)$.

(b) The velocity, u , depth of flow, y , and position, x , for 1-layer flow.

(c) The velocity, u_i , depth of flow, y_i , and density, ρ_i , for each layer are where $i = 1$ for the top layer and $i = 2$ for the bottom layer for 2-layer exchange flow. The flow direction, x , is positive from left-to-right by convention.

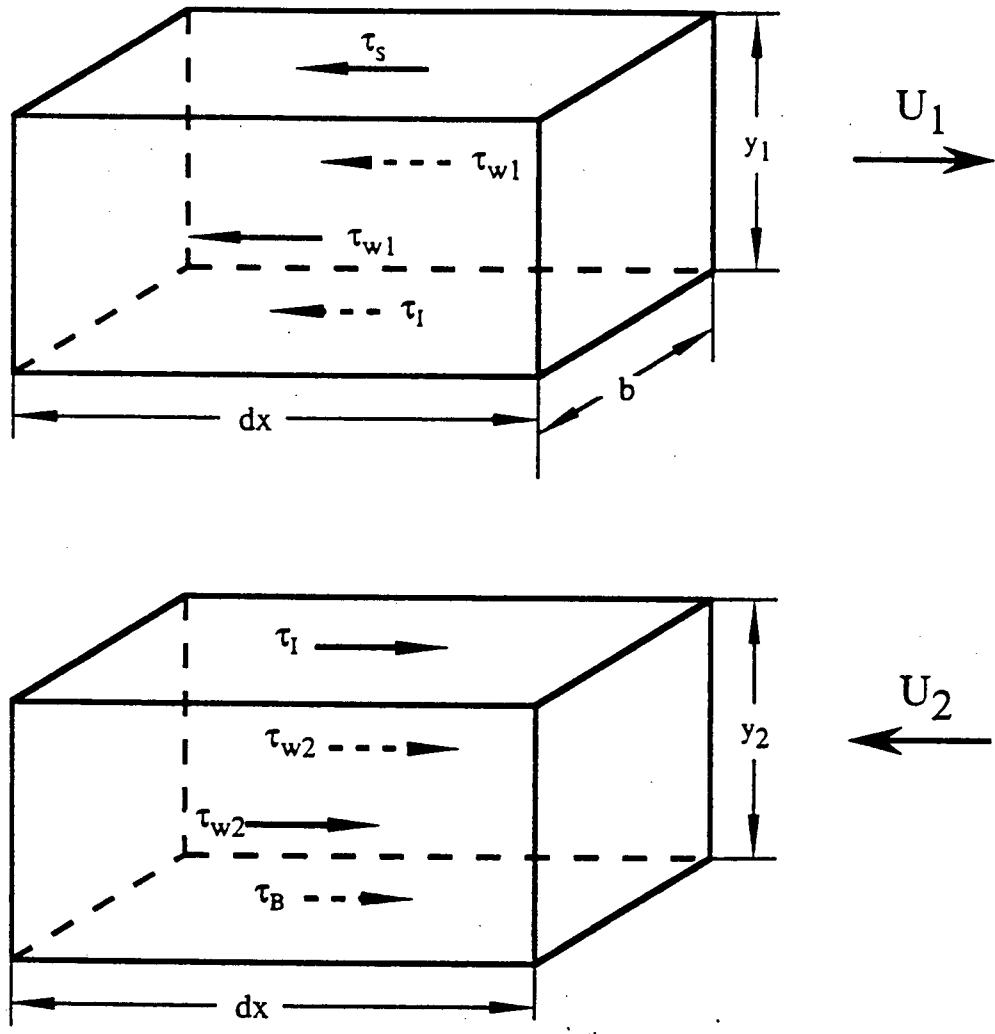


Figure 3 - 2 Shear stress acting on an element in two-layer exchange flow (Adapted from Zhu, 1996).

- | | |
|-----------------------|------------------------------------|
| τ | shear stress |
| subscripts s, w, I, b | surface, wall, interfacial, bottom |
| U_j | average velocity of each layer |
| y_j | depth of each layer |
| dx, b | length, width |
| $j = 1, 2$ | top layer, bottom layer |

4 FIELD WORK

In July and August of 1996, a sampling program, described in Section 4.1, was conducted to improve understanding of exchange flow in the Burlington Ship Canal. A variety of instruments were moored in and around the ship canal as summarized in Section 4.2. Data was also collected from instrumentation mounted on an 8 metre boat as described in Section 4.3. The focus of this work is data collected from the boat on July 25th, 1996.

4.1 Field Site

Hamilton Harbour is an enclosed body of water separated from the western end of Lake Ontario by the Burlington Ship Canal. This triangular shaped harbour is mainly used for shipping by industries located on the southern shores of the harbour. The harbour acts as a drainage basin for a 500 km², half-million inhabitant watershed composed of mixed urban, industrial and agricultural lands. It also acts as a receiving pond for effluent from four sewage treatment plants. The harbour has an east-west dimension of 8 km, a north-south dimension of 5 km and holds approximately $280 \cdot 10^6$ m³ of water. The maximum and mean depths are 23 m and 13 m, respectively (Barica et al, 1988). The Burlington Ship Canal connecting the harbour to the lake is a uniform rectangular canal 836 m long, 89 m wide and, on average, 10 m deep. See Figure 4 - 1 for a plan view of the field site.

Exchange flow in the canal is primarily driven by the temperature difference between Lake Ontario and Hamilton Harbour. In summer months, (May-to-October), the harbour is significantly warmer than the lake. In the canal, the harbour water forms a warm upper layer which spreads out onto the lake, while the cooler lake water forms a lower layer before sinking down into the harbour's hypolimnion. By convention, the velocity is positive as water flows from the harbour to the lake (flowing to the north-east) and negative as water flows from the lake to the harbour (flowing to the south-west). See Figure 4 - 2 for a simplified cross section of the exchange flow through the Burlington Ship Canal.

4.2 Moored Instrumentation

Moored instrumentation in the harbour, lake and canal during the study included 77 temperature and 9 conductivity recorders arranged in 8 chains, 2 gas purging water level meters mounted near each end of the ship canal, 3 pressure recorders with Paroscientific sensors, 2 Brancker pressure sensors, and 3 current meters. Several meteorological stations were also deployed. (See Figure 4-3 (a)).

Two bottom mounted Acoustic Doppler Current Profiles (ADCP's) were moored in the canal, one near each end, as shown in Figure 4 - 3 (b). Unfortunately, the ADCP at the Lake Ontario end failed after the first week of the experiment and will not be discussed further. The ADCP on the Hamilton Harbour end was connected by cable to a computer located in a trailer on shore. For convenience, this ADCP on the west end of the canal will be referred to

as the “moored ADCP”. This provided real time velocity profiles useful in determining steady periods of exchange.

The head of the upward-facing moored ADCP transducer was located about 0.5 m from the bottom of the Burlington Ship Canal and 2 m from the wall. The velocity profiles were smoothed at the top (air-water interface) and bottom to account for sidelobe contamination and signal interference, respectively. The smoothing method used is similar to that described in detail for the boat ADCP in Section 5.1.

Velocity for the moored ADCP on July 25, 1996 are shown in Figure 4 - 4 as a function of depth from the transducer and time. The flow in the canal appears to be weak-to-moderate exchange flow with short periods of unidirectional flow. The fact that the interface changes position with time (i.e. that the layers change thickness at the same position) indicates that flow is unsteady over the day.

4.3 Boat Instrumentation

During the field study, the boat, an 8 m Hourston glasscraft (the “Wagtail”), transected the length of the Burlington Ship Canal obtaining:

- position from Differential Global Positioning System (DGPS),
- velocity profiles from Acoustic Doppler Current Profilers (ADCP), and
- conductivity-temperature-depth (CTD) profiles.

Data for July 25, 1996 are analyzed in Chapter 5. The boat survey method and instrumentation are described below.

4.3.1 Survey Method

On July 25, 1996, data were collected by allowing the boat to repeatedly drift through the ship canal. The boat started at the Hamilton Harbour end of the Burlington Ship Canal, drifted through the canal and out onto Lake Ontario pushed by a small wind from the south-west. Then the boat was driven back to the harbour end to start another drift. Each drift lasted approximately 30 minutes. A typical boat transect is shown in Figure 4 - 5.

Position (DGPS) and velocity (ADCP) were collected continuously during all drifts back and forth. However, because of instrument memory limitations, a continuous record of CTD casts was not obtained. Boat CTD data were collected only during the drifts from the harbour to the lake and gaps exist when the instrument was uploaded to a computer on the boat. Figure 4 - 6 shows the CTD data collection casts for Drift E.

Vertical density (calculated from temperature and conductivity) and velocity profiles were collected for drifts along the length of the Burlington Ship Canal. During periods of exchange flow, the profiles in the canal generally show:

- a top layer with almost constant velocity, u_1 , and density, ρ_1 ;
- a bottom layer with almost constant velocity, u_2 , and density, ρ_2 ; and

- a mixed interfacial layer where the velocity changes from u_1 to u_2 and the density changes from ρ_1 to ρ_2 .

The vertical location and extent of the interfacial layer typifies flow dynamics in the canal. Selected velocity and density profiles from Drift E are plotted along the canal in Figure 4 - 7. The location of the interface between the two layers moves up in the direction of flow of the upper layer (left-to-right) from about $h_1 = 6$ m at the Hamilton Harbour end to $h_1 = 4$ m at the Lake Ontario end.

4.3.1.1 Time Zones

All instrumentation recorded time in Greenwich Mean Time (GMT). The local time in Burlington, Ontario during the study was Eastern Daylight Savings Time (EDST). Records and log book notes are made in EDST. During daylight savings time, GMT is 4 hours ahead of EDST. For example, data collection on July 25, 1996 started at 12:00 GMT or 08:00/8:00 A.M. EDST and ended at 21:00 GMT or 17:00/5:00 P.M. EDST. To convert between the two times during the study (in hours),

$$\text{GMT} = \text{EDST} + 4:00 \quad \text{and} \quad \text{EDST} = \text{GMT} - 4:00.$$

4.3.1.2 Drift Labeling

For five drifts, there is a complete record of both boat ADCP and boat CTD data collection. Two drifts occurred in the morning (Drift A and Drift B) and three drifts occurred in the

afternoon (Drift C, Drift D and Drift E). Drifts in a north-easterly direction (from Hamilton Harbour to Lake Ontario) are denoted as positive drifts while drifts in a south-westerly direction (from Lake Ontario to Hamilton Harbour) are denoted as negative drifts. The drifts and drift labels are summarized in Table 4 - 1.

Table 4 - 1 Survey drift labeling.

Drift Label	Start time (hr GMT)	End time (hr GMT)	ADCP number (direction)	Drift	CTD number	Cast
-				1 (-)		-
A	13.8187	14.5042		2 (+)	18, 19, 20	
-				3 (-)		-
B	15.3801	15.8669		4 (+)	23, 24	
-				5 (-)		-
C	17.2470	17.6471		1 (+)	25, 26, 27	
-				2 (-)		-
D	17.9835	18.5716		3 (+)	28, 29, 30	
-				4 (-)		-
E	19.0377	19.5010		5 (+)	32, 34, 35	
-				6 (-)		-

4.3.1.3 Drift D

The records from the lift bridge above the Burlington Ship Canal indicate the bridge was up from 17.867 – 18.084 hr GMT on July 25, 1996 for the “Canadian Venture”, a dry bulk carrier, travelling from Hamilton Harbour to Lake Ontario. Table 4 –1 reports that Drift D began at 17.984 hr GMT – while the Venture was still in the ship canal. By the time Drift D was completed, the Venture had been out of the ship canal for 0.5 hr. Thus, disturbance in the canal is expected to be greatest at the start of Drift D. This is the case as can be seen from

the velocity for each layer and the interface position shown in Appendix B, Figures B-1 and B-2. The velocity plot is also disturbed (see Figure B-4).

In the St. Lawrence seaway, dry bulk carriers, or ore lakers, range from 200 - 300 m long, 20 - 30 m wide and typically have a draft of 10 m. As a result, they displace on the order of 60,000 m³, or about 7 % of the volume of the Burlington Ship Canal. The draft of these ships is comparable to the depth of the ship canal. Thus substantial disturbance of the water column is expected and observed in Drift D whose behavior is quite erratic compared to the other drifts. Therefore, in Chapters 5 and 6, the results for Drifts A, B, C, and E will be presented in the body text while results for Drift D will be presented in Appendix B.

4.3.2 DGPS

The boat was equipped with Differential Global Positioning System (DGPS) to determine exact surface location within the canal. The DGPS recorded geographical position in latitude and longitude and time in GMT. A DGPS base station was placed on the south edge roof of the Canadian Centre for Inland Waters (CCIW) building which is located north of the canal.

4.3.2.1 Position in the Canal

Geographical position obtained by the GPS was first converted to a surface location, in metres, on an x-y plane. The following conversion was used,

1 minute Latitude N	= 1836 m
1 minute Longitude W	= 1344 m

Then the position was transformed to a dimensionless position along the centreline of the Burlington Ship Canal. The centreline of the canal is oriented 55° east of North. This line passed through a point at the Hamilton Harbour end of the canal (Station 901), a point at the Lake Ontario end of the canal (Station 924), and a point in the middle of the canal (Station 925).

The position along the centreline of the canal was scaled to be from 0 to 1. The scaled centreline co-ordinate, x' = 0 at the Hamilton Harbour end, and x' = 1 at the Lake Ontario end. A record was generated relating GMT time, t , and scaled centreline position along ship canal, x' . The geographical and normalized positions for 3 points in the ship canal are shown in Table 4 - 2.

Table 4 - 2 Points along centreline of Burlington Ship Canal.

Station	Latitude (°N)	Longitude (°W)	Normalized position (x')
Hamilton Harbour end (Station 901)	43° 17' 50"	79° 48' 58"	0.00
Mid-canal (Station 925)	43° 17' 57"	79° 47' 44"	0.46
Lake Ontario end (Station 924)	43° 18' 05"	79° 47' 27"	1.00

4.3.3 ADCP

An RDI 1200 kHz Broadband Acoustic Doppler Current Profiler (ADCP) was attached to a boom over the side of the boat. measuring velocity profiles during all drifts. This ADCP took a vertical velocity profile (a "ping") every 12 seconds resulting in approximately 150 vertical profiles per drift. The bin depth was 0.25 m. The reader is referred to RD Instruments (1998)

for information on the theory and operation of an ADCP. The hope was that during the time to complete one drift (about 30 minutes), the exchange flow would be steady. This is not always the case shown in Chapter 5 due to flow variation during the drifts.

4.3.3.1 Location of ADCP pings

The position of the ADCP pings was interpolated from the time of the pings using the relationship between the scaled centreline position in the canal, x' , and the time from the DGPS record, t . In Figure 4 - 8, the boat position along the centreline of the canal is shown as a function of time and the locations where ADCP readings were obtained are marked. Drifts from the Hamilton Harbour end ($x' = 0$) to the Lake Ontario end ($x' = 1$) were slower and contained more ADCP profiles than the return trips. The ADCP record is continuous for all drifts.

4.3.3.2 Bottom Topography

The ADCP also provided a record of the bottom depth in the ship canal. For each ping, bottom depth was determined from each of the 4 beams. The ADCP automatically corrects for the depth of the instrument below the water surface. Valid values were averaged to obtain an estimate of the bottom depth for each ping. Bottom depth along the centreline varied between 9.9 – 13 m and the average for all drifts was found to be 11 m. Along the centreline, the ends of the canal are deeper than the middle as shown in Figure 4 - 9, a plot of bottom depth along the canal for all Drifts. However, along the width of the canal, the centre is

deeper than the edges. An overall estimate of average canal depth is $h = 9.55$ m (Spiegel, 1989).

4.3.4 CTD

During the drifts from Hamilton Harbour to Lake Ontario an OS 200 Conductivity-Temperature-Depth (CTD) probe was repeatedly lowered and raised through the water column. The OS 200 collected 15.5 records/second where each record is an average of 10 readings. Because of the limited memory in the OS 200, a continuous record was not obtained, as gaps result during times when the instrument was uploaded to a laptop PC on the boat (see Figure 4 - 6). Conductivity and temperature are combined using an equation of state to calculate density in Section 5.1.

4.3.4.1 Location of CTD Casts

The position of a CTD profile in the Burlington Ship Canal was determined from the DGPS record of position and time. Since one profile occurred over a distance rather than at one location, each profile was assumed to have occurred at the midpoint of the CTD downcast. The normalized position of the boat is shown along with the locations of each CTD vertical profile in Figure 4 - 10.

In processing the CTD data, a time for each reading had to be manually assigned in order to obtain position in the canal, since the OS 200 recorded time only at the start of casting and when the memory was full. Casts were assumed to have been raised and lowered at a

constant velocity. Upcasts from the CTD were discarded since it is designed for measurement on the downcast.

4.3.4.2 Comparison of ADCP and CTD

Several differences exist between the operation of the CTD and the ADCP. The CTD measurements do not provide as complete a record as the ADCP. ADCP vertical profiles were taken continuously along the length of the canal (approximately 150 vertical profiles per transect), while the CTD profiles were taken less frequently (approximately 15 vertical profiles per transect). The CTD data contain gaps in the transect due to time spent uploading the CTD instrumentation. Although there were fewer CTD profiles, the vertical distance between measurements was more precise for the CTD (approximately 3 cm) than for the ADCP (approximately 25 cm). Some differences between the ADCP and CTD are summarized in Table 4 - 3.

Table 4 - 3 Some differences in ADCP and CTD data collection.

	Vertical Resolution	Profiles per Drift (1 drift \approx 30 min.)	Operation	Continuous Data?
ADCP	25 cm	150	automatic	Yes
CTD	3 cm	15	manual	No – only on positive drifts and gaps when instrument is uploaded

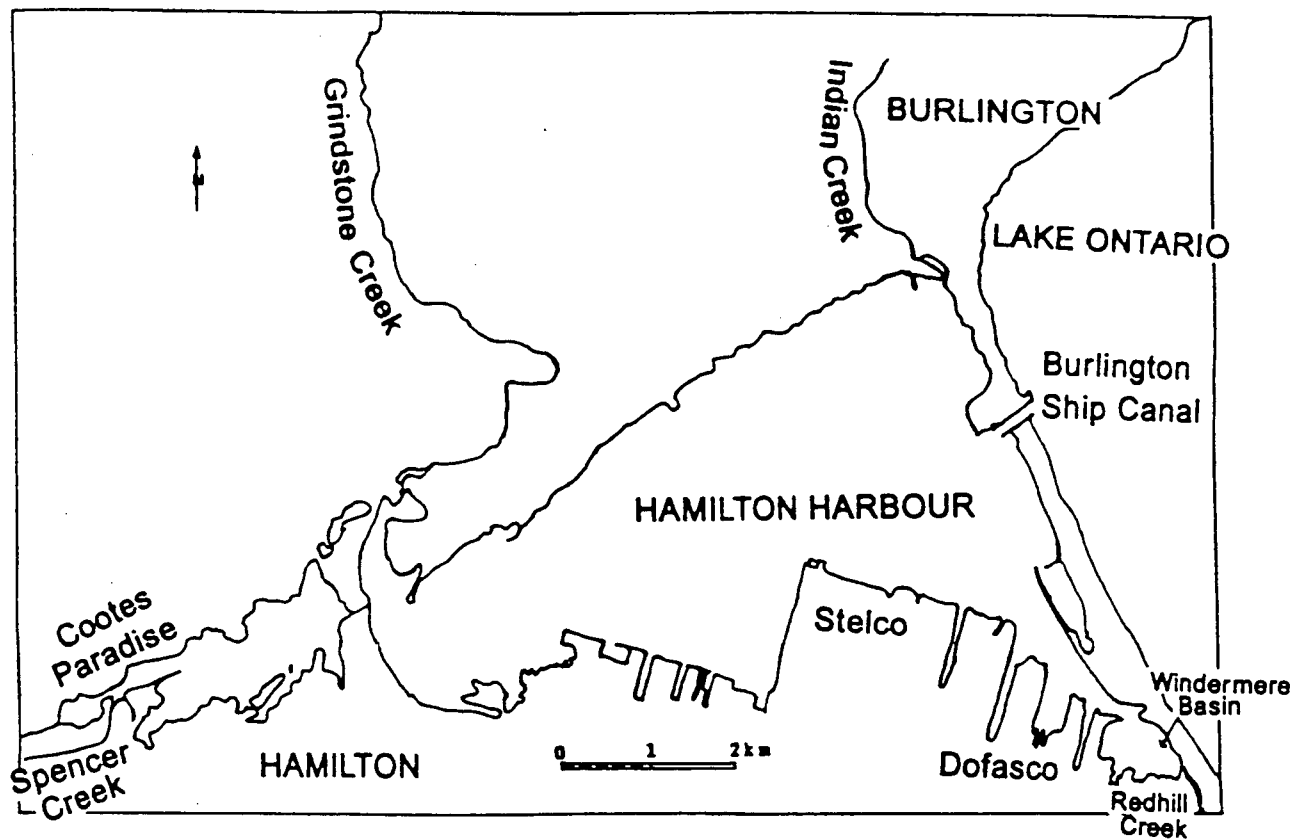


Figure 4 - 1 Plan view of field site showing Hamilton Harbour, Burlington Ship Canal and Lake Ontario (Adapted from Ling, *et al.*, 1993).

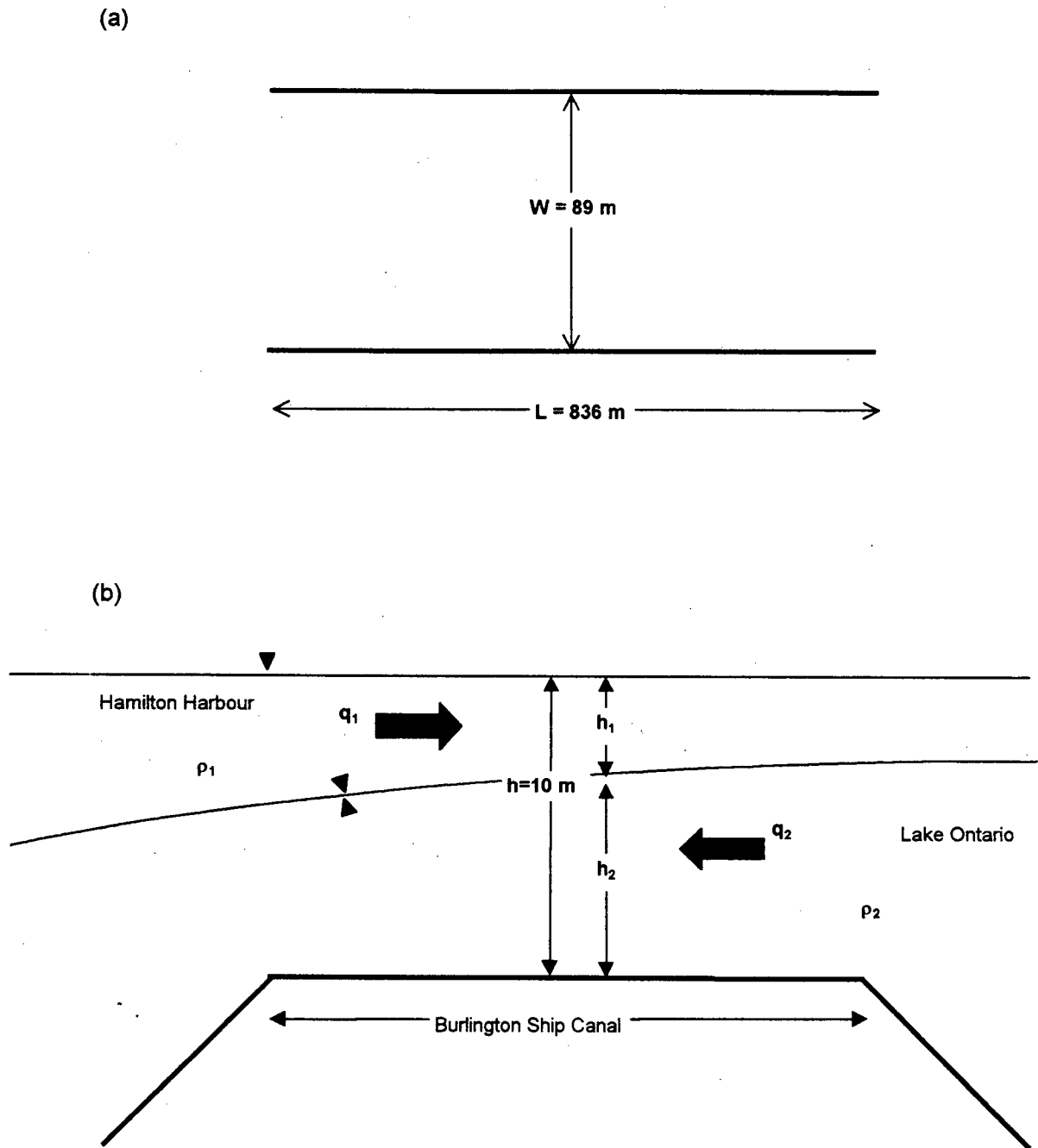


Figure 4 - 2 (a) Simplified plan and (b) and cross-section views of exchange flow in the Burlington Ship Canal (Adapted from Greco, *et al.*, 1998).

(a) In the plan view, the average width, W , and length, L are shown for the rectangular canal.

(b) In the section view, the flow per unit width, q_i , depth of flow, h_i , and density, ρ_i , for each layer are shown for 2-layer exchange flow in the canal where $i = 1$ for the top layer and $i = 2$ for the bottom layer. The flow direction, x , is positive from left-to-right by convention.

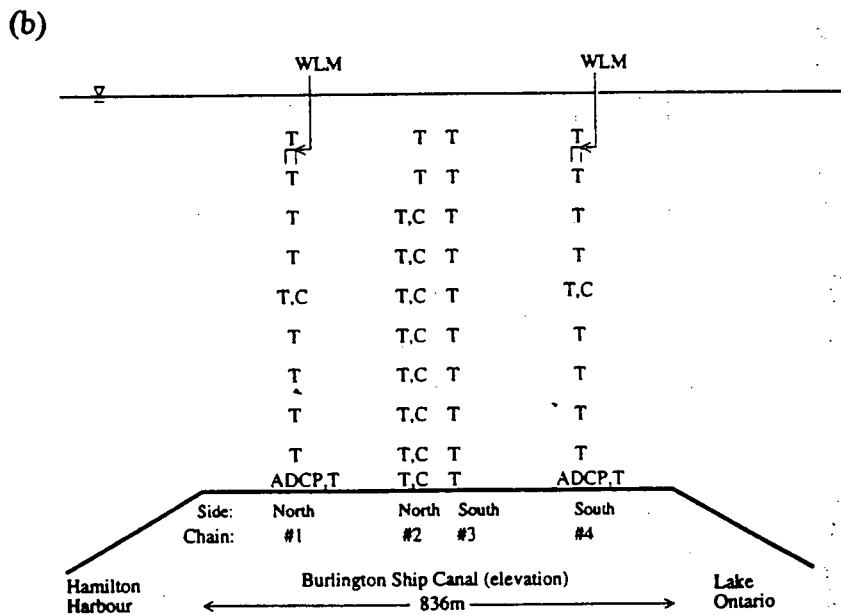
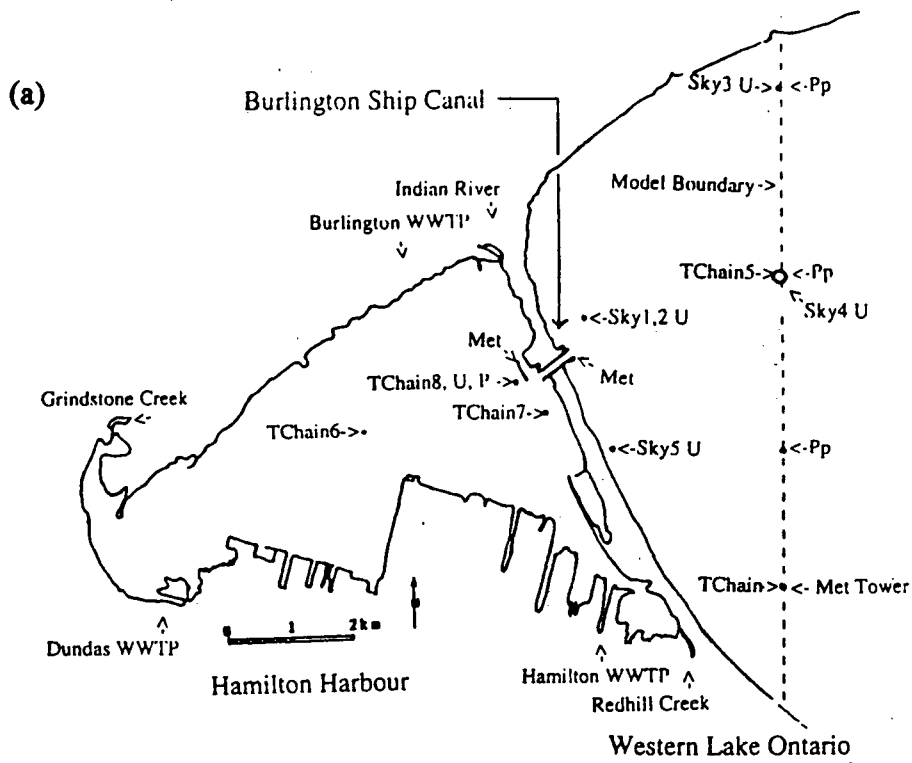


Figure 4 - 3 (a) Plan and (b) Section view of canal showing location of moored instrumentation (Figure prepared by R. Pieters, 1996).

KEY:

T	Temperature sensor	WLM	Water Level Meter
C	Conductivity sensor	Met	Meteorological station
ADCP	Acoustic Doppler Current Profiler	WWTP	Wastewater Treatment Plant discharge

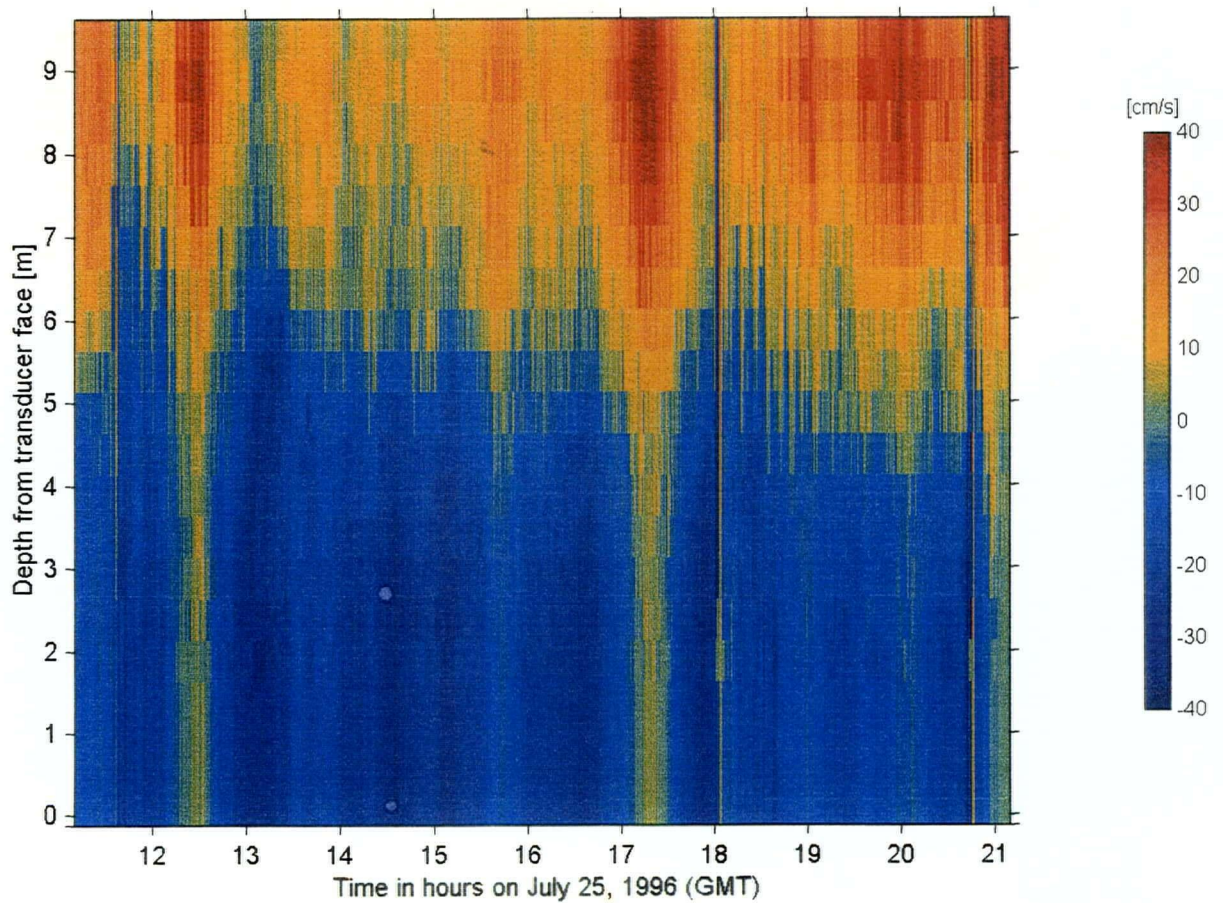


Figure 4 - 4 Velocity of moored ADCP data on July 25, 1996 plotted on depth versus time.

Velocities (in cm/s) from moored, upward looking, bottom mounted ADCP in the Burlington Ship Canal are plotted on depth from ADCP transducer face and time. Hot colours indicate a positive velocity (from Hamilton Harbour to Lake Ontario). The transducer was located 0.5 m above the bottom of the canal. Lift bridge records show the passage of large vessels through the canal at 11.5, 18.0 and 20.8 hours GMT corresponding to the periods where the velocity profile is disturbed.

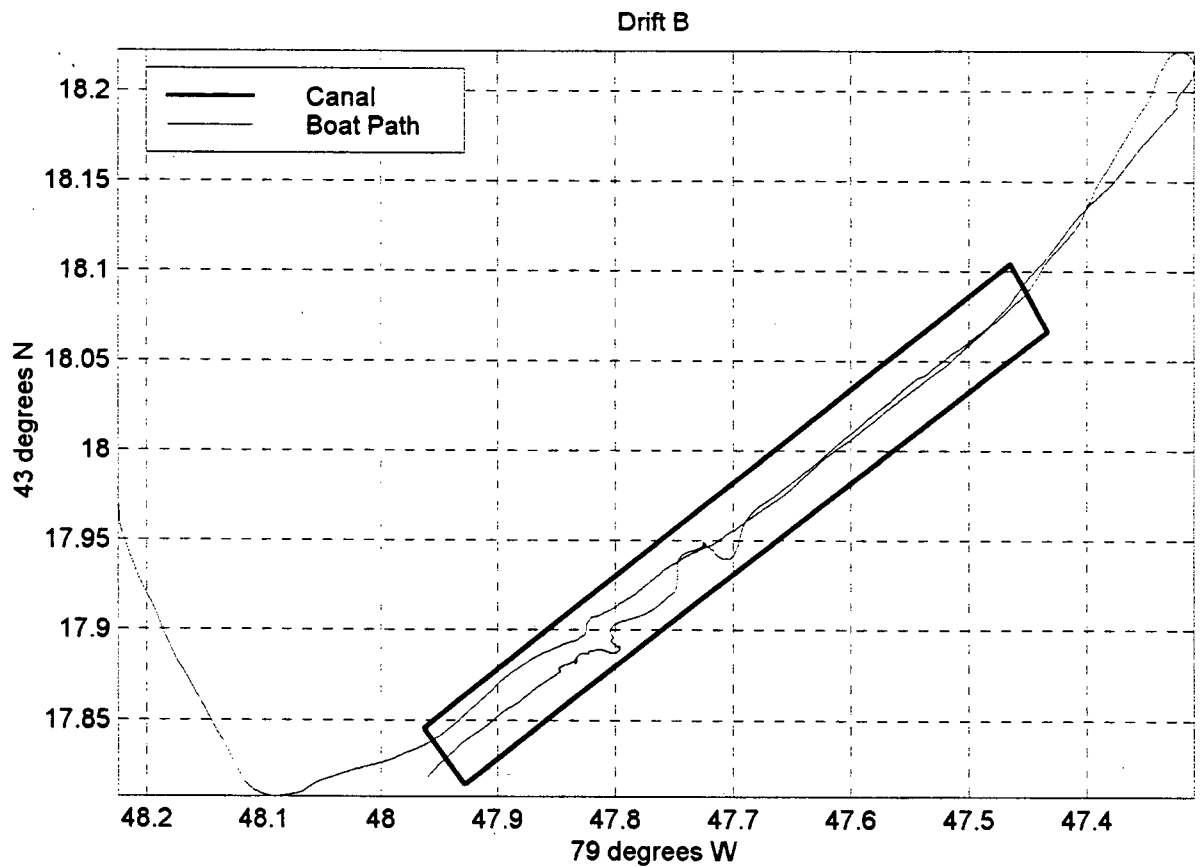


Figure 4 - 5 Plan view of a typical boat transect in the Burlington Ship Canal. This drift, the second of five, began at the southwest end of the canal in Hamilton Harbour, drifted through the canal into Lake Ontario, returned, and finally ended at the Canadian Centre for Inland Waters (CCIW) building in Burlington, northwest of the canal.

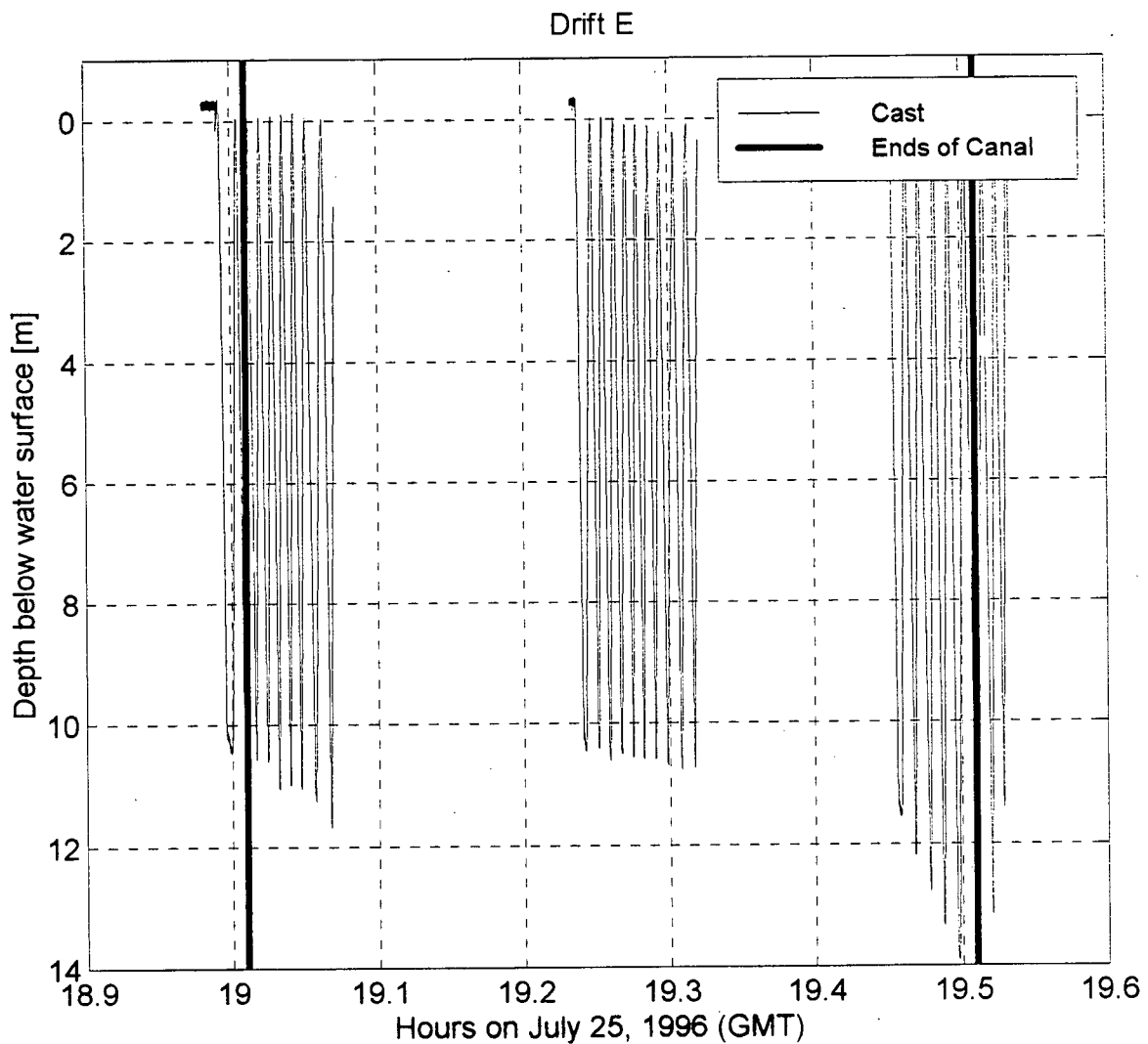


Figure 4 - 6 Section view of CTD yo-yo's for Drift E. Thin lines show the CTD casts (yo-yo's) for Drift E. Thick lines mark the ends of the Burlington Ship Canal. Gaps in the casts indicate times when the OS 200 was uploaded to a computer.

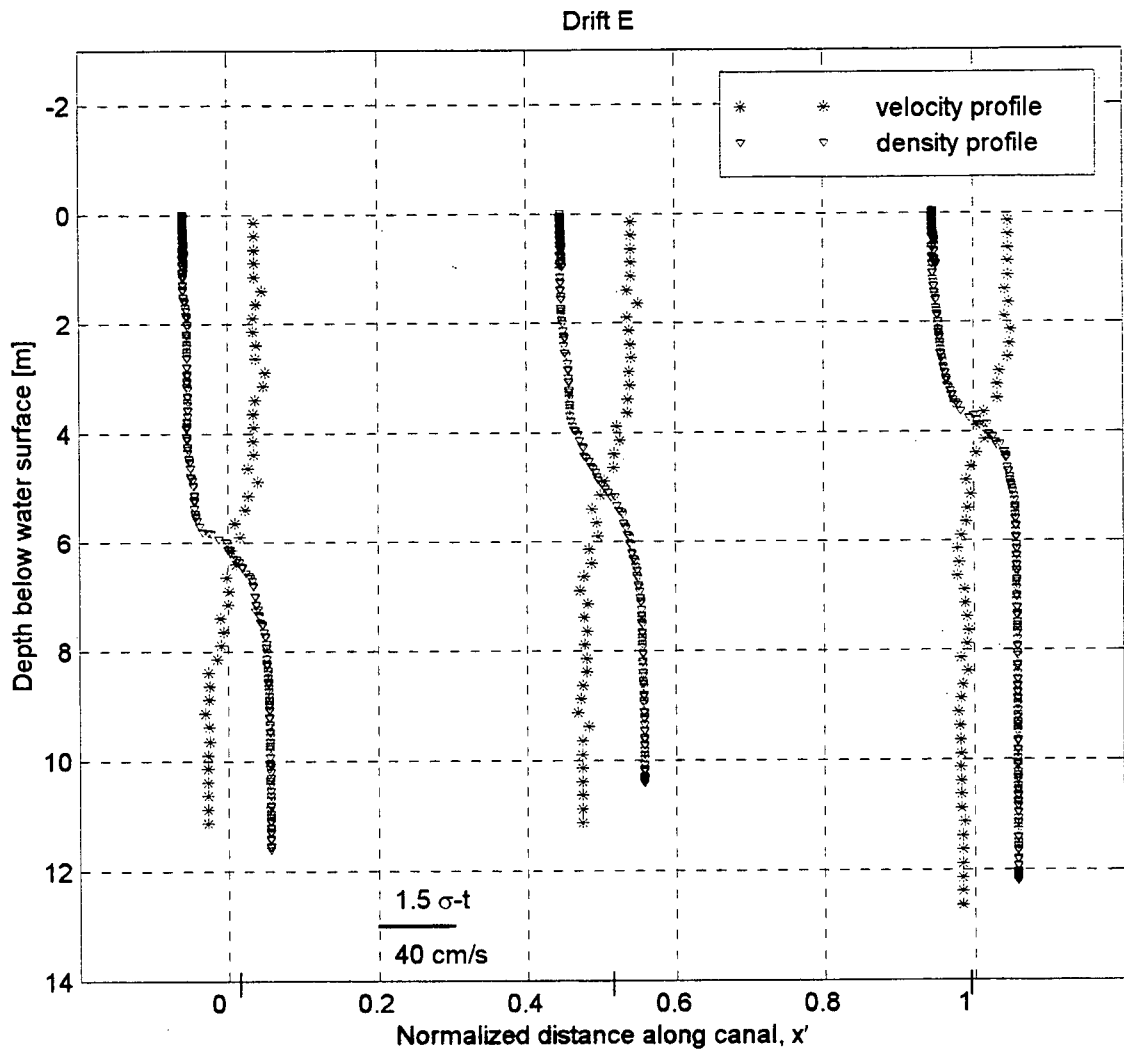


Figure 4 - 7 Sample density and velocity profiles along the canal. Density and velocity profiles are shown at 3 locations along the Burlington Ship Canal during Drift E ($x' = 0.02$; $x' = 0.53$; and $x' = 0.99$). The profiles show a top layer, mixed interfacial layer and bottom layer. A distance of $x' = 0.1$ is equivalent to a density difference of $1.5 \sigma_t$ and a velocity difference of 40 cm/s.

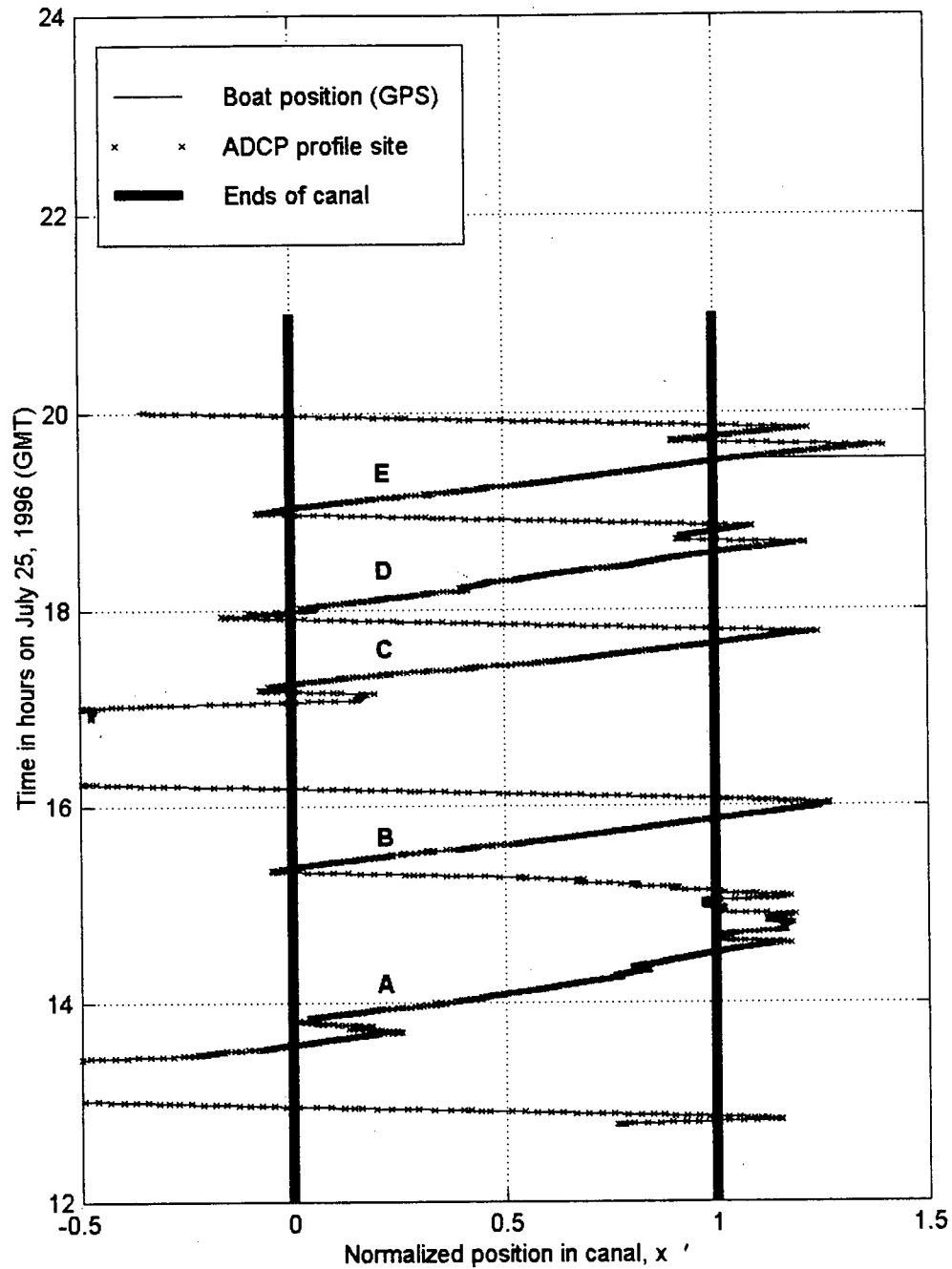


Figure 4 - 8 Plan view of non-dimensional boat and ADCP data collection position. The boat path for all drifts is shown. Drift labels appear slightly above the thin path line (—) marking the locations of velocity profiles (x). Two thick lines (—) indicate the ends of the Burlington Ship Canal. The Hamilton Harbour end of the canal is $x' = 0$ while the Lake Ontario end of the canal is $x' = 1$.

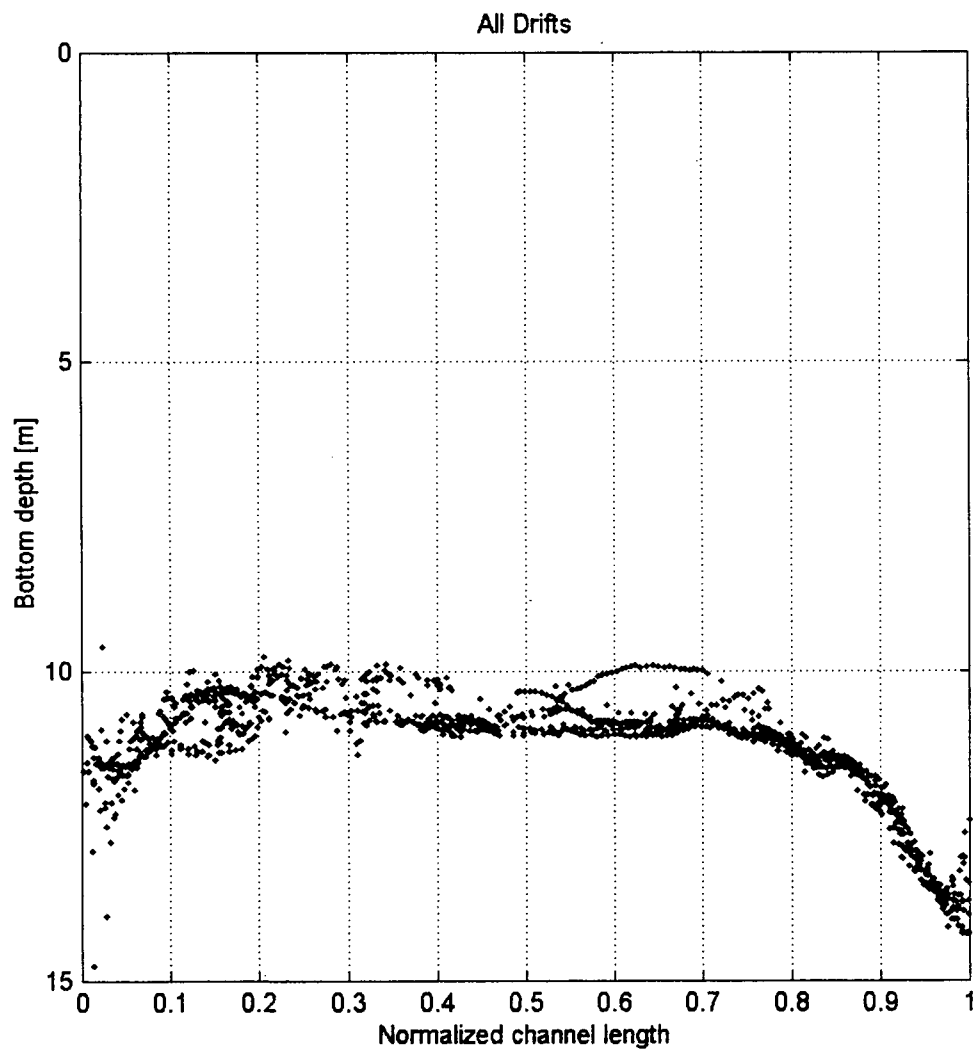


Figure 4 - 9 Bottom depth along the centreline of the canal for all Drifts. Note that the depths along the centreline are deeper than the depths near the sides of the canal. An overall estimate of the bottom depth of the canal is approximately 10 m. The ADCP instrument corrected for the depth of the transducer below the water surface (0.52 m).

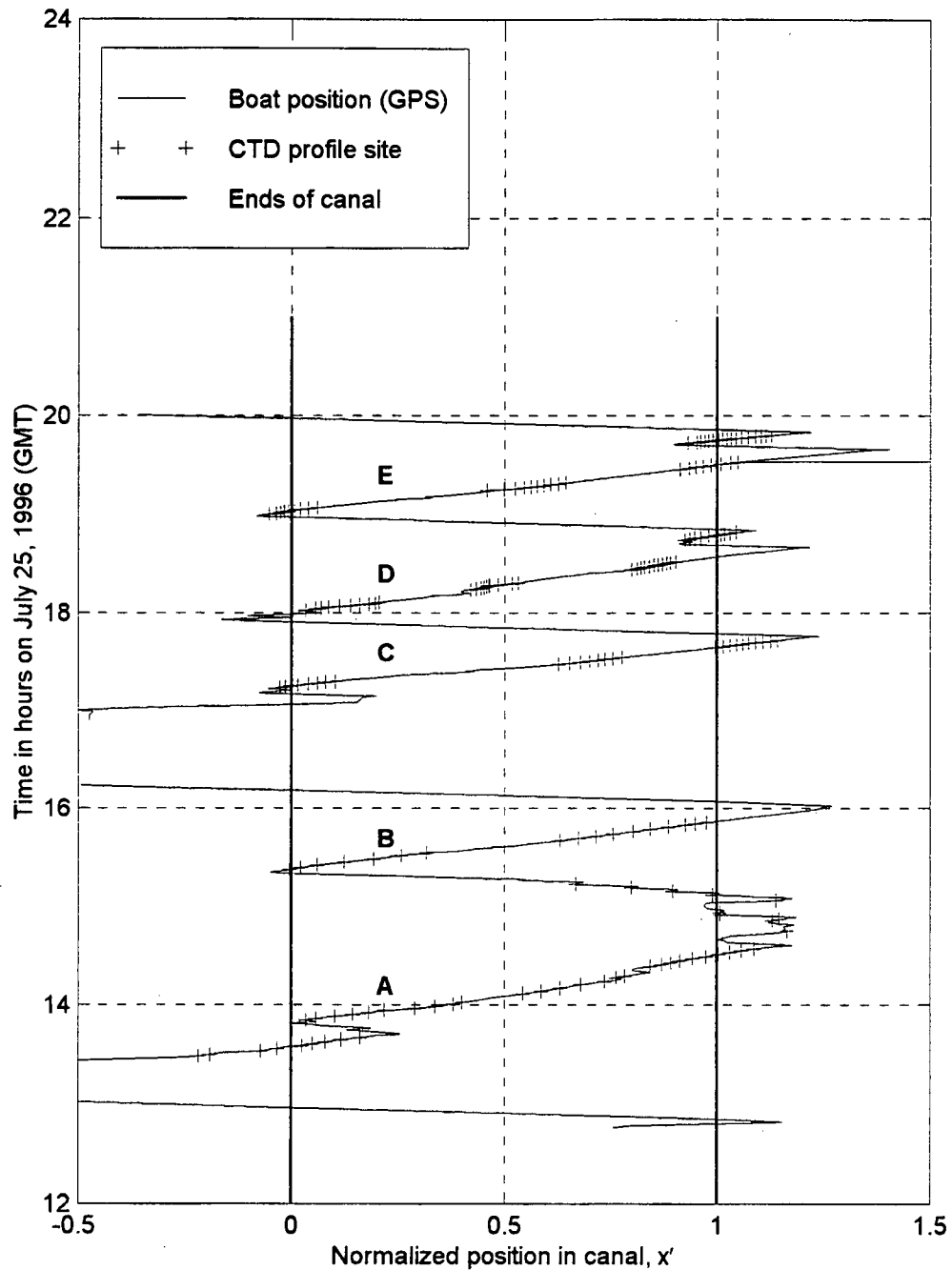


Figure 4 - 10 Plan view of non-dimensional boat and CTD data collection position. The boat path for all drifts is shown. Drift labels appear slightly above the thin path line (—). The locations of density profiles (+) are marked. The thick lines (—) indicate the ends of the Burlington Ship Canal. The Hamilton Harbour end of the canal is $x' = 0$ while the Lake Ontario end of the canal is $x' = 1$.

5 ANALYSIS OF BOAT DATA FOR JULY 25, 1996

The focus of this work is analyzing exchange flow data collected by boat instrumentation during five drifts through the Burlington Ship Canal on July 25, 1996. Since the exchange flow is seldom pure, a classification scheme to evaluate the strength of the exchange flow is developed in Section 5.2. In Sections 5.1 and 5.4, respectively, the velocity profiles and density profiles from the drifts are studied in detail. As the flow is two-layer, a hyperbolic tangent function will be fit to these profiles and utilized to characterize the flow. Section 5.3 outlines the procedure for converting temperature and conductivity into density. Computer programs used in this analysis, written in Matlab and Fortran, are listed in Appendix A.

5.1 Velocity

Velocity obtained by the boat ADCP was analyzed and used to characterize the two-layer exchange flow. Before beginning the analysis, the raw ADCP velocity data were read into the computer and filtered using Matlab. Specifically, the velocity data set was:

- projected onto the centreline of the canal, 55° east of North,
- filtered,
- smoothed at the bottom 15%, and
- extended to and smoothed at the top.

The sign convention for velocity direction is positive for flow out of Hamilton Harbour and negative for flow into Hamilton Harbour. The top layer in the canal, flowing northeast, is warm Hamilton Harbour water, while the bottom layer in the canal, flowing southwest, is cooler Lake Ontario water.

A set of 5 depth bins x 5 time bins was employed in filtering the data. (The total set is 51 depth bins x 2000 time bins.) Outliers were removed from the set by replacing raw velocity values with the median velocity of the set if the raw values exceeded one median-absolute-deviation from the set.

The velocity was smoothed near the free surface to account for the fact that the instrument is still sending out a signal when the first signals return. At the bottom of the canal, the velocity is smoothed to account for sidelobe contamination occurring in the bottom 15 % of the water column. The first ADCP bin reading was 1.39 m below the free surface, so five bins were added to the top of the profile to extend the velocities to the water surface. The surface velocity of these 5 bins was generated by averaging the velocity of bins 7 – 10. The velocity of bin 6, the 1.39 m bin, is not used to calculate the average because the values sometimes seemed to be erroneous. The velocities in the bins occurring 15 % from the bottom are replaced with the average of the 3 bins above the 15 % mark. Table 5 - 1 illustrates the procedure for smoothing one velocity profile. Note, this procedure is nearly identical to the moored ADCP velocity smoothing except the moored instrument is located at the bottom of the canal facing upward instead of at the top of the canal facing downward.

Depth to mid-bin	Bin Velocity [cm/s]	Bin no.	Comments
0.14	5.56	1	Bins added to fill depth up to free surface
*0.39	5.56	2	
*0.64	5.56	3	
0.89	5.56	4	
1.14	5.56	5	
**1.39	0.36	6	Signal interference
1.64	7.20	7	Velocity of these 4 bins is averaged to obtain velocity of 5 added surface bins
1.89	-2.09	8	
2.14	5.74	9	
2.39	11.39	10	
2.64	9.20	11	
2.89	10.39	12	
3.14	9.31	13	
3.39	1.81	14	
///////	///////	///////	
7.89	-27.15	32	
8.14	-17.72	33	
8.39	-26.46	34	
8.64	-28.49	35	
8.89	-29.99	36	Velocity of these 3 bins is averaged to obtain velocity of sidelobe contaminated bins
9.14	-24.41	37	
9.39	-27.45	38	
9.64	-27.28	39	Sidelobe contamination occurring in bottom 15% of water column
9.89	-27.28	40	
10.14	-27.28	41	
10.39	-27.28	42	
10.64	-27.28	43	
10.89	-27.28	44	
11.14	NaN	45	Bottom (NaN = not a number)
11.39	NaN	46	
11.64	NaN	47	
11.89	NaN	48	
12.14	NaN	49	
12.39	NaN	50	
12.64	NaN	51	

Table 5 - 1 Smoothing of one velocity profile.

* The ADCP transducer was located at 0.52 m depth below water surface.

** The first ADCP velocity reading was from bin no. 6 at 1.39 m depth below water surface.

5.1.1 Velocity Profiles

Velocity profiles were fitted with hyperbolic tangent functions by minimizing the sum of the squared error between the boat ADCP profile and the hyperbolic tangent velocity profile. From these profiles the top-layer velocity, bottom-layer velocity, shear thickness and depth to interface were determined. The hyperbolic tangent equation for velocity is shown below,

$$u(z) = a + b * \tanh\left[\frac{(z - c)}{d}\right] \quad (5.1)$$

where $u(z)$ is the velocity in the canal as a function of depth and a , b , c , and d are fit parameters where:

- a = the horizontal velocity offset, [cm/s]
- b = the horizontal scale, (physical meaning discussed below) [cm/s]
- c = vertical distance from the free surface to the point of maximum velocity shear, and [m]
- d = vertical scale (physical meaning discussed below). [m]

A sample velocity profile along with the fitted hyperbolic tangent function and error estimate is shown in Figure 5 – 1(a). The fit parameters from the hyperbolic tangent velocity function characterize the velocity of each layer, the vertical depth to the interface, and the shear thickness. Additionally, the velocity profiles may be integrated with respect to depth to obtain flow.

5.1.1.1 Velocity of each layer

The velocity of each layer is determined from the fitted hyperbolic tangent function. The top layer velocity, $u_1 = a - b$, and the bottom layer velocity, $u_2 = a + b$. The parameter, a , occurs

at the point of maximum shear, or the centre of the velocity profile, and measures the barotropic component of velocity. The velocity difference between the layers, or shear strength, $\Delta U = u_2 - u_1 = 2*b$. The velocities for each layer along with the barotropic component are shown for Drifts A, B, C, and E in Figure 5 - 2. All results for Drift D, described in Section 4.3.1, will be shown in Appendix B. For steady flow, u_1 increases and u_2 decreases along the length of the channel.

5.1.1.2 Interface Position Along the Canal

The interface divides the warm, buoyant upper layer and cool, dense lower layer. The depth of the interface from the velocity profiles can be specified in two ways:

- from the position of maximum shear, $h_{1m.s.} = c$, or
- from the position of zero velocity, $h_{1u=0} = c + d*\text{atanh}(-a/b)$ where $u(h_{1u=0}) = 0$.

The parameters a , b , c , and d are obtained from the fitted velocity profiles. By combining the depth to the interface for each velocity profile along the canal, an interface between the two layers is obtained for each drift. The depth of the interface along the length of the canal, determined by both methods, is shown in Figure 5 - 3 for Drifts A, B, C, and E and for Drift D in Appendix B. The interface may be additionally determined from the density profiles as described in Section 5.4.1.2. This study will assume that the zero velocity interface corresponds to the density interface. Note that if the flow were perfectly two-layered, as assumed in two-layer hydraulic theory, then $h_{1m.s.} = h_{1u=0}$.

If $a = 0$, (i.e. $u_1 = -u_2$), the point of maximum shear, $z = h_{1m.s.}$, equals the point where the velocity changes from positive-to-negative, $z = h_{1u=0}$. If $a \neq 0$, the point of zero velocity, $h_{1u=0}$, appears closer to the free surface if $a < 0$, (net flow to the harbour) and closer to the canal bottom if $a > 0$, (net flow to the lake). These results are summarized in Table 5 - 2.

Table 5 - 2 Interface location by the position of maximum shear and by the position of zero velocity.

Velocity offset	Interface	Appearance in canal	Velocity magnitude
$a = 0$	$ h_{1m.s.} = h_{1u=0} $	same	$ u_1 = u_2 $
$a > 0$	$ h_{1m.s.} < h_{1u=0} $	$h_{1u=0}$ closer to canal bottom	$ u_1 > u_2 $
$a < 0$	$ h_{1m.s.} > h_{1u=0} $	$h_{1u=0}$ closer to free surface	$ u_1 < u_2 $

In Figure 5 - 4, 3 sample velocity profiles are plotted with identical parameters except for the value of a . The effect of the velocity offset is examined by choosing $a = 5$ cm/s, $a = 0$ cm/s, and $a = -5$ cm/s. Drift C has a large velocity offset ($a > 0$) at the start of the drift (see Figure 5-2), so that $h_{1u=0}$ is much greater than $h_{1m.s.}$ (see Figure 5-3).

5.1.1.3 Thickness of Velocity Interface

The thickness of the velocity interface or shear thickness, δ , is the region where the velocity changes rapidly from the almost constant top layer velocity, u_1 , to the almost constant bottom layer velocity, u_2 . The shear thickness was determined from:

$$\delta = \frac{\Delta U}{\frac{du}{dz}_{max}} = 2d \quad (5.2)$$

where du/dz_{\max} is the maximum slope of the velocity profile occurring at the point of maximum shear. Shear thickness along the length of the canal for Drifts A, B, C, and E is presented in Figure 6 – 1. Drift D is presented in Appendix B.

Calculating the shear thickness from Equation (5.2) corresponds to solving for the depth from the 76% velocity of the top layer, $z_{76\%u1}$, to the 76% velocity of the bottom layer, $z_{76\%u2}$. The shear thickness, $\delta = z_{76\%u2} - z_{76\%u1} = 2 \cdot \text{atanh}(0.76) \cdot d = 2 \cdot d$.

The shear thickness may be predicted from Equation (3.11) as:

$$\delta = J_{\delta} F_{\Delta}^2 h \quad (5.3)$$

where the dimensionless bulk Richardson number from shear thickness, J_{δ} , is:

$$J_{\delta} = \frac{\delta}{F_{\Delta}^2 h} = \frac{\delta}{\Delta U^2 / g'} = \frac{dg'}{2b^2} 10^4 \quad (5.4)$$

and is presented in Figure 6-1.

5.1.1.4 Flow rates

The top layer, bottom layer, and net volumetric flow rates per unit width for the canal were obtained by integrating the velocity profiles with respect to depth. The width of the canal, W , was assumed to be constant along the length of the canal as was the velocity profile across the

width of the channel. Integrating from the free surface, $z = 0$, to the position of zero velocity, $z = h_{1u=0}$, yields the top layer flow rate,

$$q_1 = \int_{z=0}^{z=h_{1u=0}} u(z) dz = \frac{Q_1}{W} \quad (5.5)$$

where Q_1 is the volumetric flow rate for the top layer. Integrating from the position of zero velocity, $z = h_{1u=0}$, to the bottom of the canal, $z = h_b$ yields the bottom layer flow rate,

$$q_2 = \int_{z=h_{1u=0}}^{z=h_b} u(z) dz = \frac{Q_2}{W} \quad (5.6)$$

where Q_2 is the volumetric flow rate for the bottom layer. Integrating from the free surface, $z=0$, to the bottom of the canal, $z = h_b$, yields the total or net flow rate in the canal,

$$q = \int_{z=0}^{z=h_b} u(z) dz = \frac{Q}{W} = q_1 + q_2 \quad (5.7)$$

where Q is the net volumetric flow rate and should equal the sum of the layer flow rates.

The direction of positive flow is from Hamilton Harbour to Lake Ontario. In a pure exchange flow case, $q = 0$ and $q_1 = -q_2$ and the flow is steady, that is q_1 and q_2 remain constant over the drift. In Figure 5 - 5, the layer and net flow rates per unit width are displayed for Drifts A, B, C, and E. It is evident from the flow variation along the canal, that exchange flow is not

steady over the time to complete one drift as hoped. A measure of the strength of the exchange flow is the exchange flow strength parameter.

5.1.1.5 Exchange flow strength parameter

It is unlikely that either pure exchange flow or pure plug flow will occur for any substantial length of time in the Burlington Ship Canal. To classify the flows that do occur, it is useful to define an exchange flow strength parameter, R , given by:

$$R = \frac{|q_1 - q_2|}{|q_1 + q_2|} \quad (5.8)$$

and to describe flow according to the following classification scheme:

Table 5 - 3 Exchange flow strength classification.

Classification	Exchange flow strength parameter, R	Flow ratio
Pure exchange flow	$R = \infty$	$q_1 = -q_2$
Exchange flow	$R > 1$	$q_1/q_2 < 0$
Unidirectional flow	$R < 1$	$q_1/q_2 > 0$
Plug flow	$R = 0$	$q_1 = q_2$

For a steady flow, R is constant throughout the channel. Exchange flow is more prominent if $R > 1$ since q_1 and q_2 are of opposite sign. If $R < 1$, q_1 and q_2 are of the same sign and unidirectional flow is more prominent. At the extremes of the classification scheme, $R = \infty$ for pure exchange flow and $R = 0$ for plug flow. Exchange flow strength along the length of the

canal is presented for the drifts in Chapter 6, while the average values over the drift are given in Table 5 - 4.

5.1.2 Velocity variation along the canal

To visualize flow dynamics in the canal, velocity profiles for Drifts A, B, C, and E are plotted in Figure 5 - 6. See Appendix B for Drift D. Velocity is plotted as depth against distance along the canal. Considering this a snapshot in time assumes that the exchange is steady during the time of the drift. As seen from the flow variation, the flow in the canal is unsteady.

5.2 Equation of State

Density is calculated from temperature and salinity using an equation of state. The CTD probe measured *in situ* conductivity (conductivity at the field temperature). Salinity may be obtained after applying a series of equations to the *in situ* conductivity, C. First, the *in situ* conductivity, C, is converted to an uncalibrated conductivity at 25 °C, C'₂₅, by the following equation (P. Hamblin, personal communication, 1997):

$$C'_{25} = \frac{1827803 * C}{1 + 2.972 * 10^{-2} * T + 1.56 * 10^{-4} * T^2 - 7.89 * 10^{-7} * T^3} \quad (5.9)$$

where C is *in situ* conductivity in mS/cm and T is temperature in °C. The OS 200 CTD probe used in the field was calibrated against a Radiometer conductivity meter in the University of British Columbia Civil Engineering Environmental Lab using a 0.01 molar solution of potassium chloride (KCl) The calibration equation for the OS 200 is,

$$C_{25} = 11425 * C'_{25} - 0.1618 \quad (5.10)$$

where C_{25} is the calibrated conductivity at 25 °C in mS/cm. Finally, salinity, S , is obtained from the Practical Salinity scale (PSS-78) extended to low salinities as per *Standard Methods* (1995). A linear approximation to this equation over the temperature-conductivity range of interest is $S = 0.5 * C_{25}$ where salinity is measured in practical salinity units (psu) and C_{25} in mS/cm.

The equation of state provided by Chen & Millero (1986) for freshwater lakes is used to calculate density from temperature and salinity. Since the maximum depth in the canal is small (< 15m), pressure effects on density are negligible. Chen & Millero's equation for density at sea level is,

$$\begin{aligned} \rho = & 0.9998395 + 6.7914 * 10^{-5} * T - 9.0894 * 10^{-6} * T^2 + 1.0171 * 10^{-7} * T^3 \\ & - 1.2846 * 10^{-9} * T^4 + 1.1592 * 10^{-11} * T^5 - 5.0125 * 10^{-14} * T^6 \\ & + (8.221 * 10^{-4} - 3.87 * 10^{-6} * T + 4.99 * 10^{-8} * T^2) * S \end{aligned} \quad (5.11)$$

where ρ is density in g/cm^3 , T is temperature in °C, and S is salinity in psu. The equation is quoted as precise to $2 * 10^{-6} \text{ g/cm}^3$ for most freshwater lakes over a temperature range of 0-30 °C; a salinity range of 0-0.6 psu; and a pressure range of 0-180 bar. The harbour and lake temperatures, salinities and depths are within these limits ranging from 5 - 23 °C and 0.17 - 0.32 psu respectively, as depicted in Figure 5 - 7(a). Hamilton Harbour is warmer and slightly more saline, while Lake Ontario is cooler.

Density may be converted from g/cm^3 to kg/m^3 by:

$$\rho(\text{kg/m}^3) = 1000 * \rho(\text{g/cm}^3) \quad (5.12)$$

and to sigma-t units by:

$$\rho(\sigma\text{-t}) = \rho(\text{kg/m}^3) - 1000 \text{ kg/m}^3 \quad (5.13)$$

Sigma-t units are useful for representing small density changes. For example, in the canal, typically the upper layer is $0.998 \text{ g/cm}^3 = -2 \sigma_t$ and the lower layer is $1000.1 \text{ kg/m}^3 = 0.1 \sigma_t$.

Figures 5 - 8 (a)-(c) display the profiles for temperature, conductivity, and density as calculated by Chen & Millero's equation of state at one location in the canal. In general, density increases with conductivity and decreases with temperatures greater than $4 \text{ }^\circ\text{C}$. However, in the ship canal, temperature exerts a much greater influence on the density than conductivity. In fact, a typical temperature range of $7 \text{ }^\circ\text{C} - 22 \text{ }^\circ\text{C}$ (see Figure 5-8 (b)) results in a density difference of about $2.20 \sigma\text{-t}$ while a typical salinity range of $0.18 - 0.39 \text{ psu}$ corresponding to a conductivity range of $300 - 650 \text{ } \mu\text{S/cm}$ (see Figure 5-8 (a)) results in a density difference of only $0.09 \sigma\text{-t}$. Thus, although the salinity difference acts opposite to the temperature difference on density, temperature is much more significant and negates the salinity effect.

5.3 Temperature and Conductivity Data

Temperature and conductivity from the CTD are combined to obtain density. Temperature is plotted versus *in situ* conductivity in Figure 5 – 7(b) for all drifts. From this characteristic plot, the extreme values of the two water layers can be seen. The top layer (Hamilton Harbour) is 23° C and 680 μS/cm while the bottom layer (Lake Ontario) is 5 °C and 280 μS/cm. The points in between the two extremes values represent the mixed interfacial region.

5.3.1 Density Profiles

After calculating density using the equation of state, a hyperbolic tangent function was fitted to the density data in a manner similar to that described for the velocity data. The density of each layer, location of the interface and thickness of the density interface were determined from the fit parameters. Specifically, the density profiles were fitted to:

$$\rho(z) = A + B * \tanh\left[\frac{(z - C)}{D}\right] \quad (5.14)$$

where $\rho(z)$ is the density in the canal as a function of depth, z , and A , B , C , and D are fit parameters where:

- A = the horizontal density offset from the centre, $[\sigma_t]$
- B = the horizontal density scale, (described below) $[\sigma_t]$
- C = vertical distance to the interface from the free surface, and $[m]$
- D = vertical density scale (described below) $[m]$

Figure 5 – 1(b) shows a sample density profile, the fitted hyperbolic tangent density profile, and the associated squared error between the two. Note that the fit parameters for density are denoted by the uppercase letters: A, B, C, and D but the fit parameters for velocity are denoted by the lowercase letters: a, b, c, and d.

5.3.1.1 Density of each layer

The density of each layer is determined from the fitted hyperbolic tangent function. The density of the top layer, $\rho_1 = A - B$, and the density of the bottom layer, $\rho_2 = A + B$. Figure 5 - 9 shows the densities for each layer along the canal for Drifts A, B, C, and E. Results for Drift D are presented in Figure B-5. The density of each layer remains much more uniform over the drift in contrast to velocity.

5.3.1.2 Interface Position Along the Canal

The depth to the density interface, $h_{1\rho}$, is defined as the position where the density gradient, $|d\rho/dz|$, is a maximum. The position of the density interface below the surface is given by the hyperbolic tangent fit parameter C. Figure 5 - 10 shows the position of the density interface along the canal for Drifts A, B, C, and E. Drift D is presented in Figure B-6. Recall that data gaps result from time spent uploading the CTD instrument. Limited estimates of the interface from density are compared with complete records of the interface velocity in Chapter 6 when the linear theory is discussed.

5.3.1.3 Thickness of Density Interface

The thickness of the density interface, η , was calculated from:

$$\eta = \frac{\Delta\rho}{\frac{d\rho}{dz_{\max}}} = 2D \quad (5.15)$$

where $\Delta\rho = \rho_2 - \rho_1$ and $d\rho/dz_{\max}$ is the maximum gradient from the density profile. In Figure 6 – 2, the density thickness is plotted versus the length of the canal for Drifts A, B, C, and E. Drift D is plotted in Appendix B.

The thickness of the density interface corresponds to the distance from 76% of the upper layer density, $z_{76\%p1}$, to 76% of the lower layer density, $z_{76\%p2}$, from the hyperbolic tangent fit. In other words, $\eta = z_{76\%p2} - z_{76\%p1} = 2 \cdot \text{atanh}(0.76) \cdot D = 2 \cdot D$.

The thickness of the density interface may be predicted from:

$$\eta = J_{\eta} F_{\Delta}^2 h \quad (5.16)$$

where the dimensionless bulk Richardson number from density thickness, J_{η} , is

$$J_{\eta} = \frac{\eta}{F_{\Delta}^2 h} = \frac{\eta}{\Delta U^2 / g'} = \frac{Dg'}{2b^2} 10^4 \quad (5.17)$$

Note that the interfacial thickness, η , is estimated from the density profiles, while $\Delta U^2/g'$ is estimated from the velocity profiles. Interfacial mixing is determined and plotted for the field results in Chapter 6. The thickness of the density interface peaks along the canal at $x' = 0.2 - 0.3$ for all drifts. The bulk Richardson number associated with density is consistent for all drifts, except Drift D when additional mixing is caused by the passage of a ship.

5.3.2 Temperature Profiles

The distinct warm upper layer, cooler lower layer, and the rapidly changing interfacial layer can be seen in the temperature profiles. Temperature profiles are plotted along the length of the canal for Drifts A, B, C, and E in Figure 5 - 11. Drift D is displayed in Appendix B.

5.4 Parameter Summary

A summary of the characteristics for each of the five drifts is given in Table 5 - 4. For both layers, density, velocity, and flow rate per unit width, are averaged over the drift. Volumetric flow rate and the exchange flow strength parameter are calculated using average flows per unit width. The mean values (M) and the standard deviation from the mean (SD) are shown for all drifts.

Table 5 - 4 Density, velocity, and flow for each layer averaged over the drift.

	Units	M/SD	Drift A	Drift B	Drift C	Drift D	Drift E
¹ ρ ₁	[σ-t]	M	-1.932	-1.954	-1.978	-1.966	-2.076
		SD	0.041	0.042	0.028	0.097	0.039
¹ ρ ₂	[σ-t]	M	0.124	0.130	0.143	0.093	0.137
		SD	0.033	0.022	0.033	0.093	0.020
g'	[m/s ²]	M	0.0202	0.0204	0.0208	0.0202	0.0217
		SD	0.0006	0.0005	0.0005	0.0014	0.0002
¹ u ₁	[cm/s]	M	18.7	26.6	35.4	18.7	26.2
		SD	4.1	7.1	6.0	5.5	3.5
¹ u ₂	[cm/s]	M	-20.5	-15.2	-5.7	-19.7	-16.0
		SD	4.2	8.4	3.4	5.4	3.3
² q ₁	[m ² /s]	M	0.654	1.027	1.750	0.667	1.075
		SD	0.173	0.223	0.391	0.327	0.187
² q ₂	[m ² /s]	M	-1.171	-0.730	-0.272	-0.967	-0.812
		SD	0.257	0.303	0.212	0.333	0.142
² q	[m ² /s]	M	-0.517	0.297	1.485	-0.300	0.263
		SD	0.381	0.503	0.596	0.615	0.308
³ Q ₁	[m ³ /s]	M	58.2	91.4	155.7	59.4	95.6
³ Q ₂	[m ³ /s]	M	-104.2	-65.0	-24.2	-86.0	-72.3
³ Q	[m ³ /s]	M	-46.0	26.4	132.2	-26.7	23.4
⁴ R	[-]	M	3.5	5.9	1.4	5.5	7.2

Modified gravitational acceleration, calculated from the individual densities of each layer and gravitational acceleration, $g = 9.81 \text{ m/s}^2$, remains almost constant along the length of the canal; ranging from $g' = 0.020\text{-}0.022 \text{ m/s}^2$. Drift D has the greatest standard deviation due to the passage of the ship. Velocity, on the other hand, changes significantly from drift-to-drift as well as during each drift.

¹ These are the extreme values calculated from the hyperbolic tangent profiles at each location, then averaged over the length of the canal.

² Flow per unit width obtained by integrating the hyperbolic tangent velocity profiles with respect to depth.

³ Volumetric flow obtained assuming a constant channel width of 89 m.

⁴ Exchange flow strength parameter calculated assuming steady flow in the channel.

Using the classification scheme developed in Section 5.2, all drifts may be considered exchange flows ($R > 1$). However, Drift C has a large unidirectional flow component (net flow towards lake). All flows have a time-dependency (i.e. they are unsteady). Comparing the drifts, the exchange flow during Drift C is closest to steady flow. (See Figure 6-9).

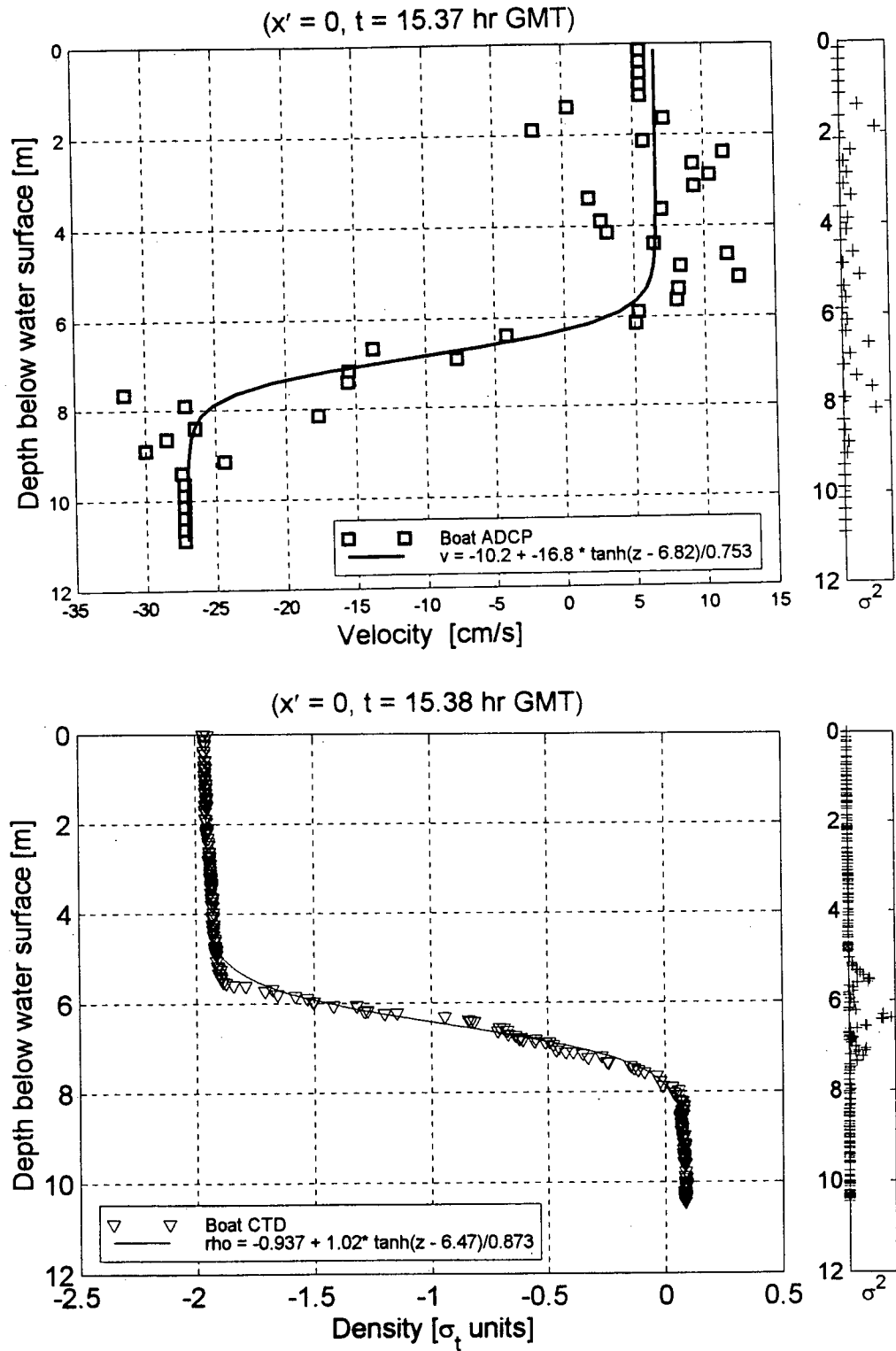


Figure 5 - 1 (a) Sample velocity and (b) density profiles with fitted hyperbolic tangent functions.

These profiles were taken near the Hamilton Harbour end of the canal on July 25, 1996. A hyperbolic tangent profile is fitted to the ADCP velocity profile and CTD density profile by minimizing the sum of the squared error, $\Sigma \sigma^2$, between the ADCP profile (\square) or CTD profile (∇) and the hyperbolic tangent fit (—). The largest individual squared error (+) $\sigma^2 = 75 \text{ cm}^2/\text{s}^2$ for velocity and $\sigma^2 = 0.041 \sigma_t^2$ for density.

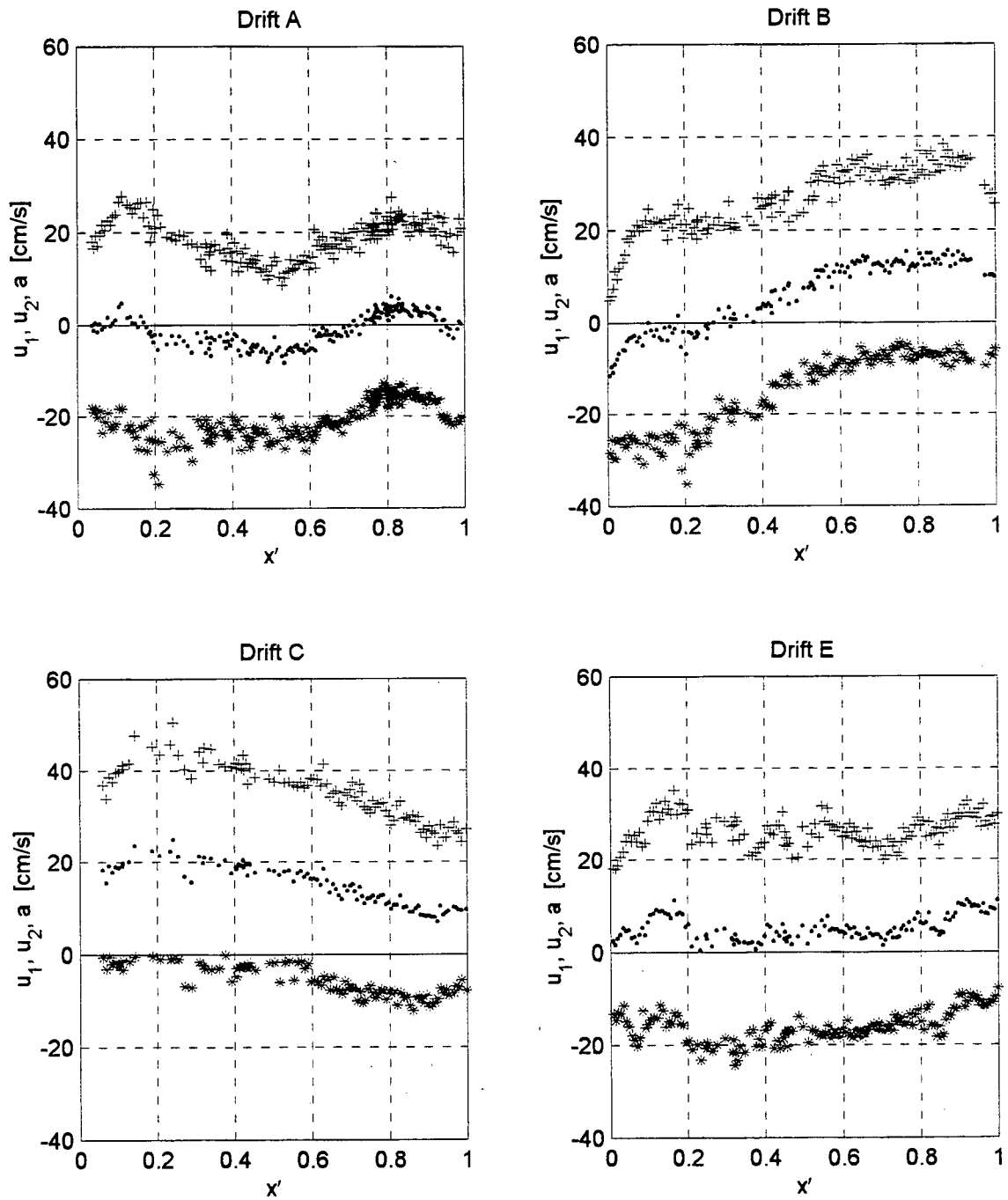


Figure 5 - 2 Layer velocities and barotropic component along the length of the canal for Drifts A, B, C, and E. The velocities of the top layer, u_1 (+), bottom layer, u_2 (*), and barotropic component, a (.), determined from the hyperbolic tangent fits to the velocity profiles vary along the length of the canal as shown. The plot for Drift D is presented in Appendix B, Figure B-1.

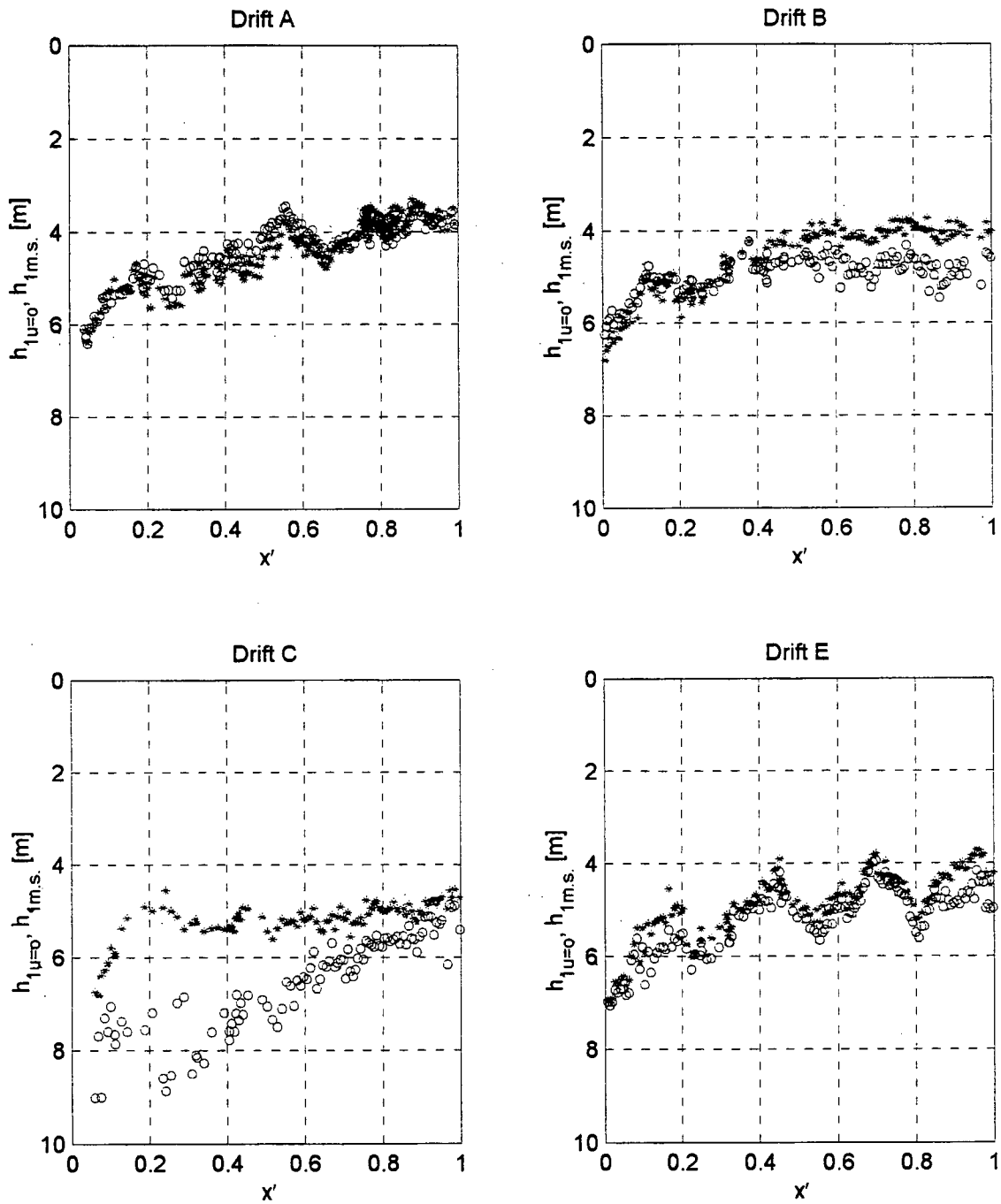


Figure 5 - 3 Interface height along the length of the canal from velocity for Drifts A, B, C, and E. Note the depth scale is positive downwards. The interface from the point of zero velocity, $h_{1u=0}$ (o), or the point of maximum shear, $h_{1m.s.}$ (+) determined from the fitted hyperbolic tangent velocity profiles. The plot for Drift D is presented in Appendix B, Figure B-2.

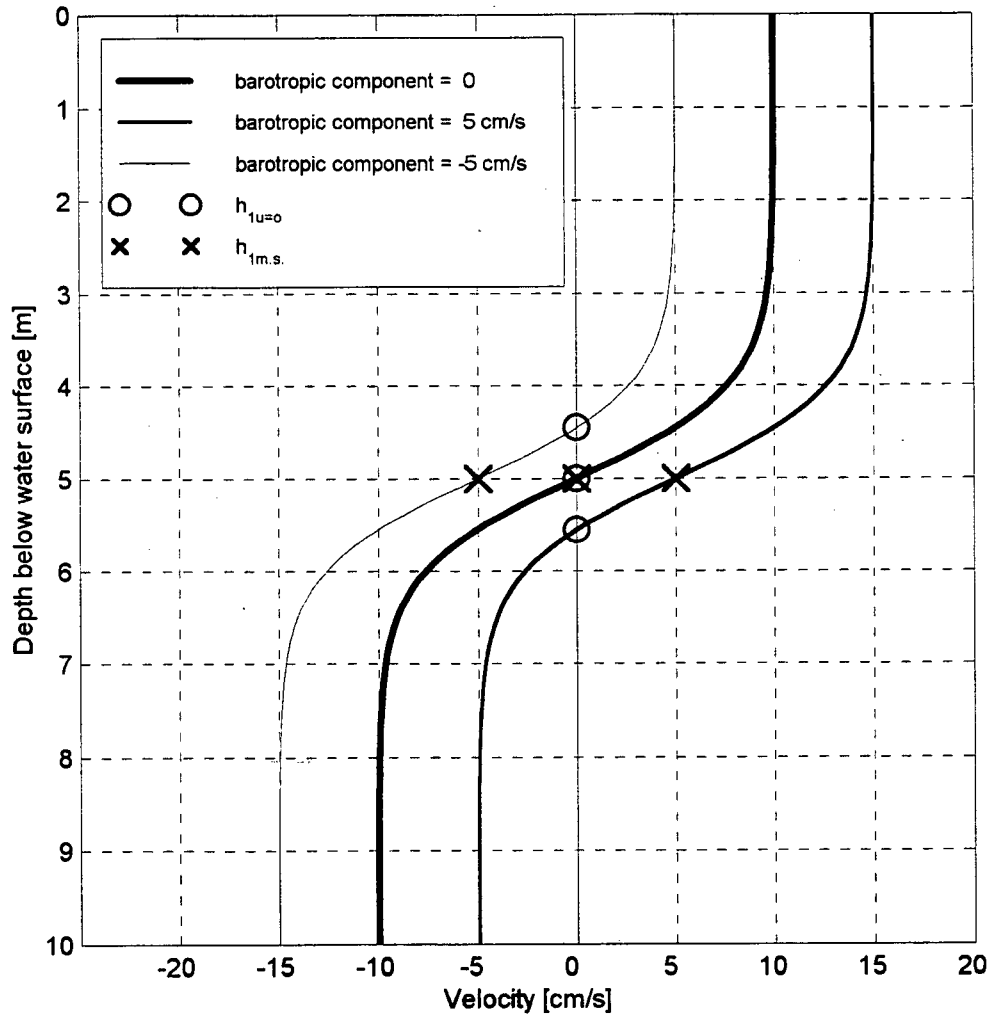


Figure 5 - 4 The difference in using the position of maximum shear, $h_{1m.s.}$, and position of zero velocity, $h_{1u=0}$, to locate the interface.

Three sample profiles are shown: zero barotropic velocity and positive/negative barotropic velocity. The position of the zero velocity interface (o) is higher than the position of the maximum shear interface (x) for the profile with negative barotropic component.

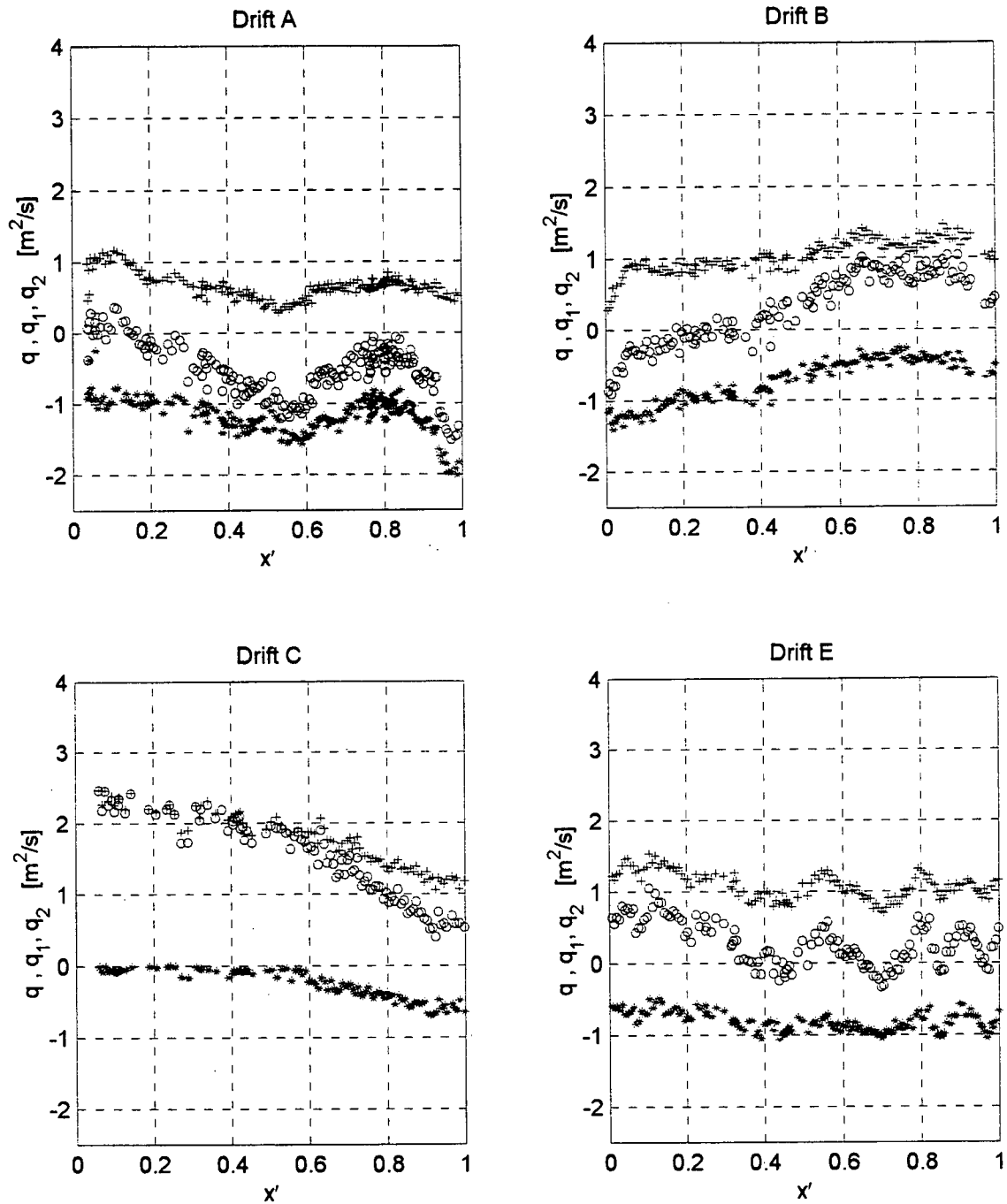


Figure 5 - 5 Layer and net flow rate per unit width along the length of the canal for Drifts A, B, C, and E. The flow rate per unit width for the top layer, q_1 (+), bottom layer, q_2 (*), and net, q (o), is determined by integrating the fitted velocity profiles. In a case of pure exchange flow, $q_1 = -q_2$ and $q = 0$. The plot for Drift D is presented in Appendix B, Figure B-3.

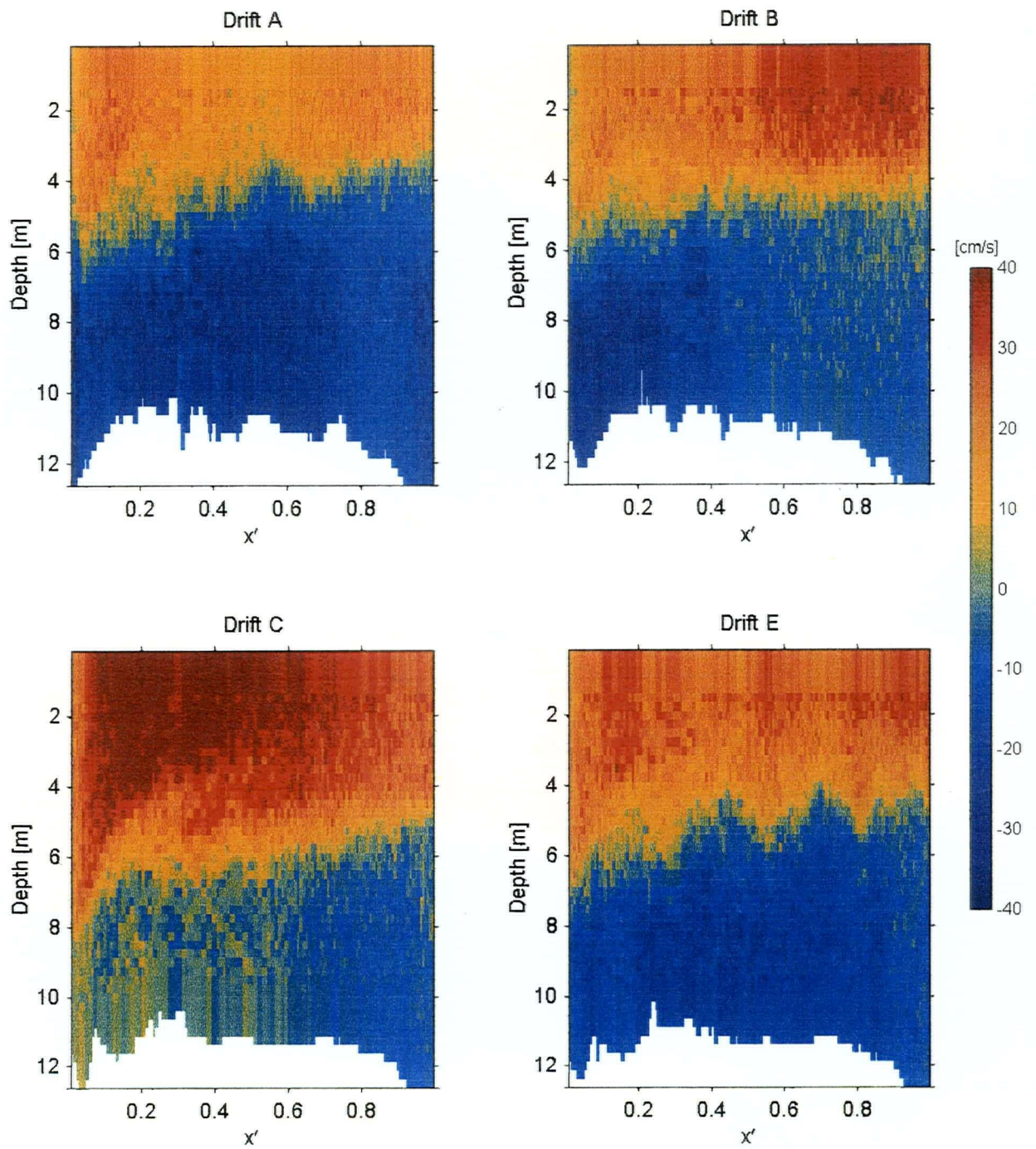


Figure 5 - 6 Velocity variation for Drifts A, B, C, and E.

Velocity (in cm/s) from the boat ADCP drifts in the Burlington Ship Canal are plotted on depth from water surface and position along the canal. Hot colours indicate a positive velocity (from Hamilton Harbour to Lake Ontario) while cool colors indicate a negative velocity (from Lake Ontario to Hamilton Harbour). The plot for Drift D is presented in Appendix B, Figures B-4.

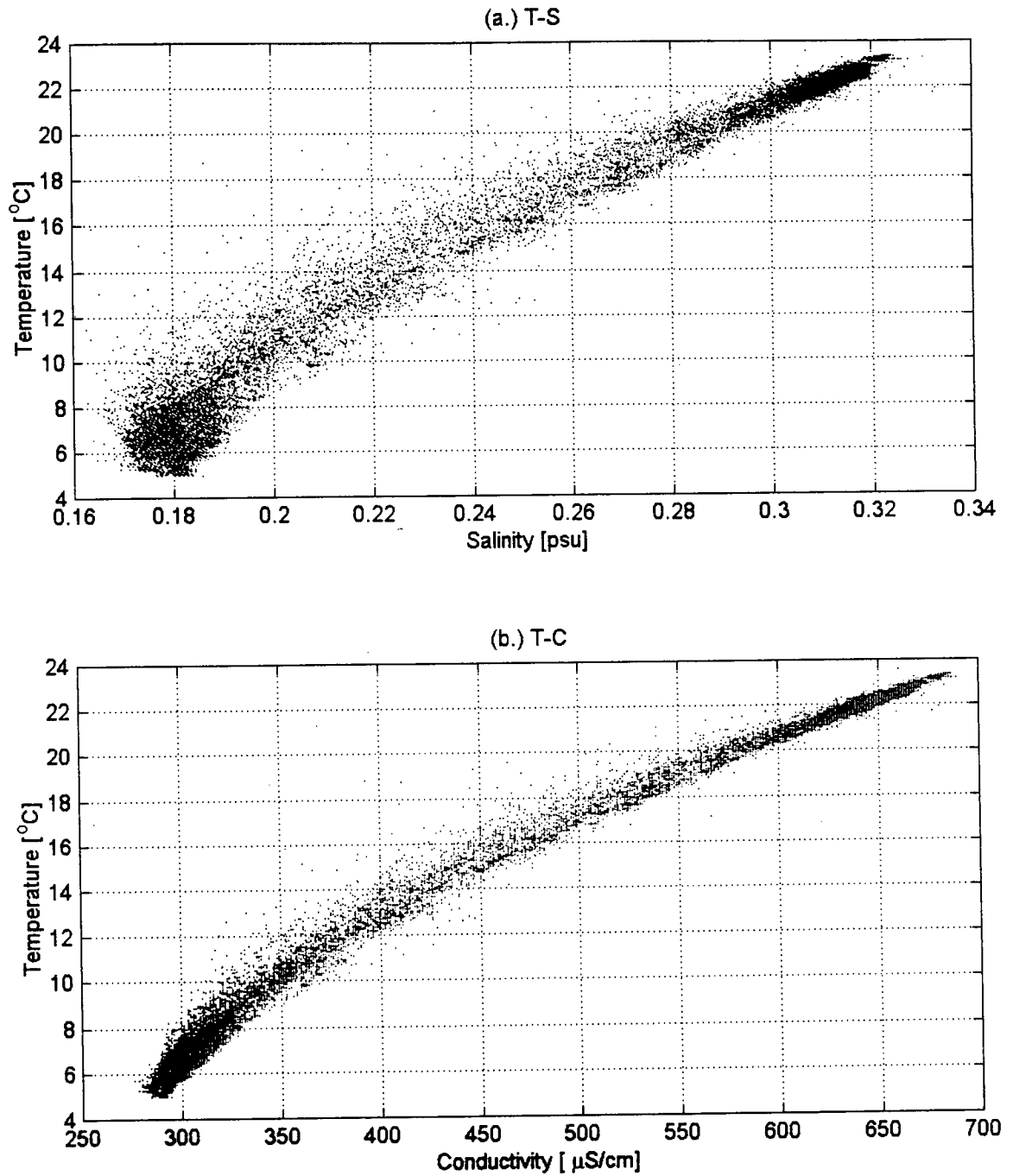


Figure 5 - 7 (a) Temperature-Salinity diagram and (b) Temperature-Conductivity plot for all Drifts.

Temperature, salinity, and *in situ* conductivity are plotted for all drifts on July 25, 1996. The cool, less saline cluster is water from Lake Ontario while the warm, slightly more saline cluster is water from Hamilton Harbour. Points in the middle represent the mixed interfacial region.

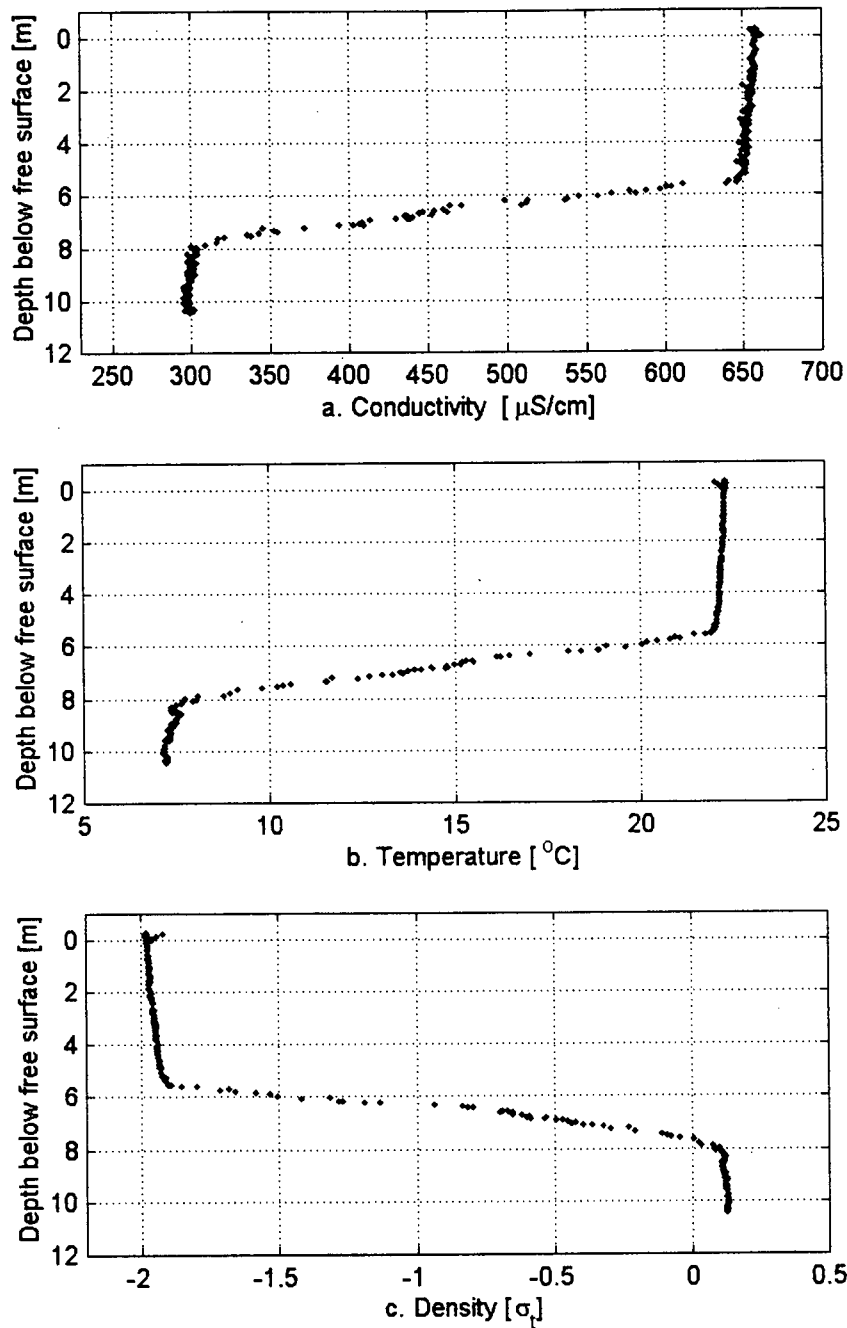


Figure 5 - 8 Sample (a) conductivity, (b) temperature, and (c) density profile. Temperature and in situ conductivity measured by the CTD are combined by the an equation of state to calculate density. The temperature difference has the greatest effect on the density. These profiles are taken from the Hamilton Harbour end of the Burlington Ship Canal ($x' = 0$) on July 25, 1996 at 15.38 hours (GMT).

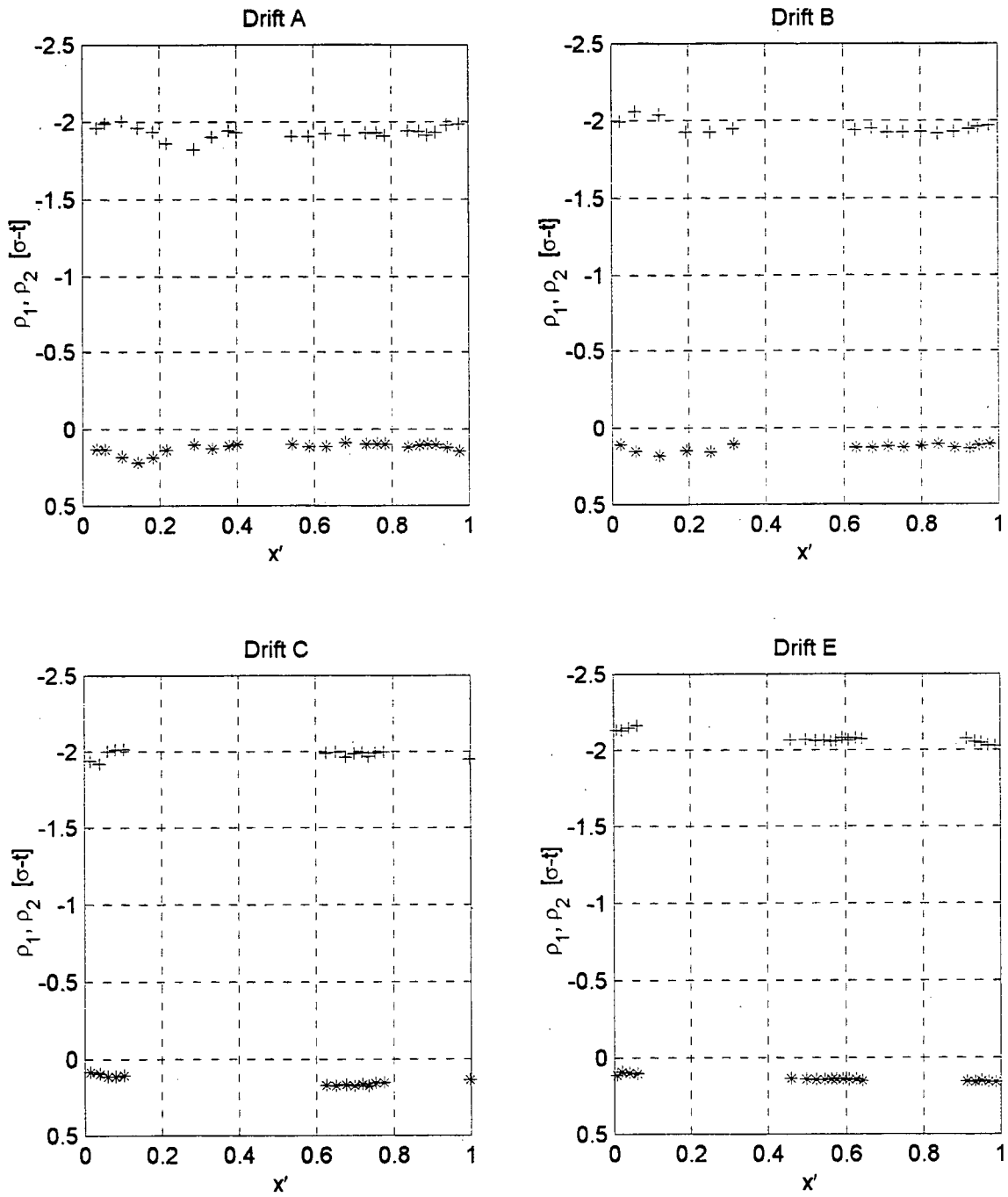


Figure 5 - 9 Density of top and bottom layers along the length of the canal for Drifts A, B, C, and E.

The density of the top layer, ρ_1 (+), and bottom layer, ρ_2 (*), determined from the hyperbolic tangent fits to the density profiles remains almost constant over the drift. The plot for Drift D is presented in Appendix B, Figure B-5. Recall that data gaps result from time spent uploading the CTD instrument.

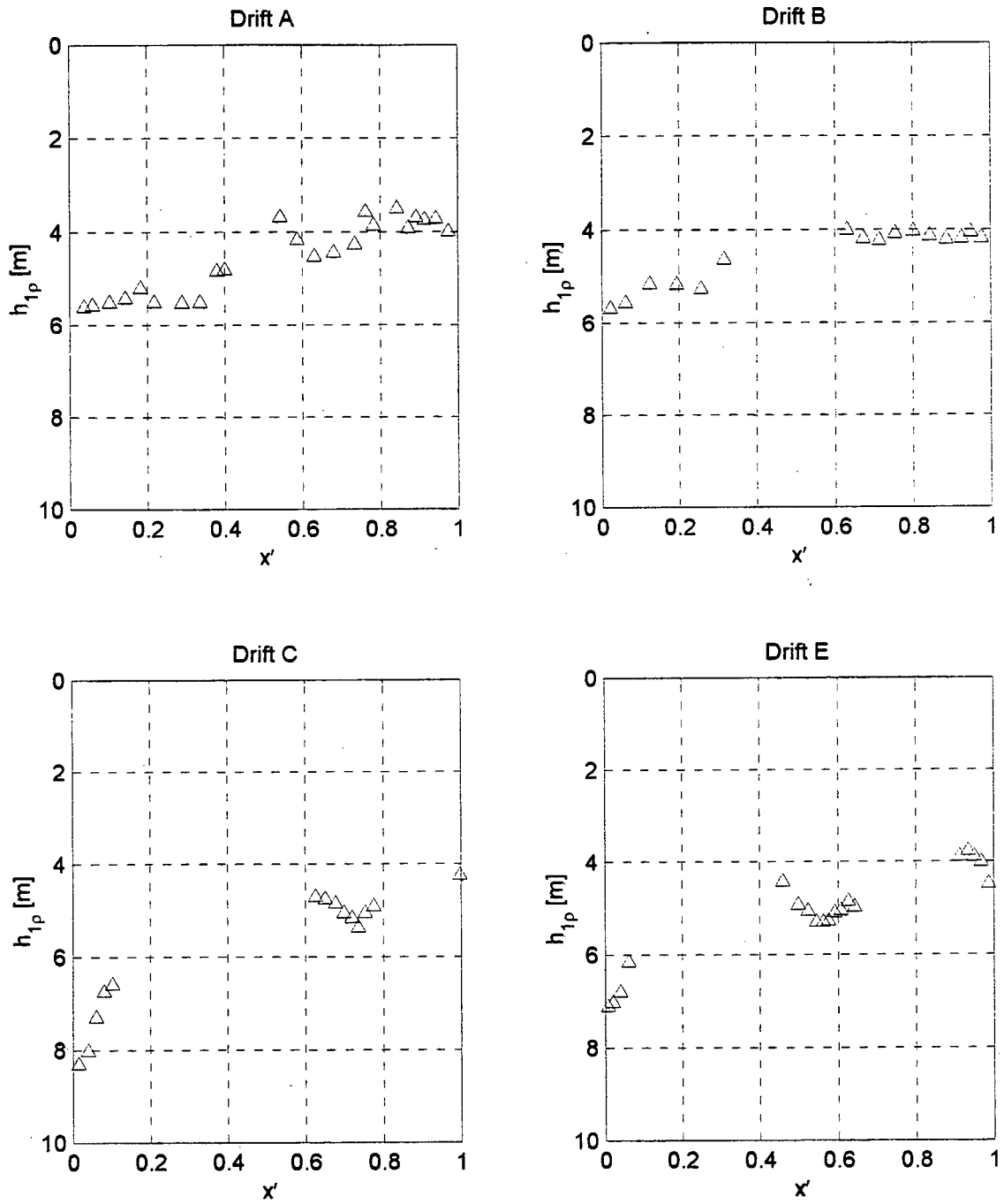


Figure 5 - 10 Interface height along the length of the canal from density for Drifts A, B, C, and E.

The depth of the interface, h_{1p} , is determined from the point of maximum density gradient from the hyperbolic tangent fits to the density profiles. The plot for Drift D is presented in Appendix B, Figure B-6.

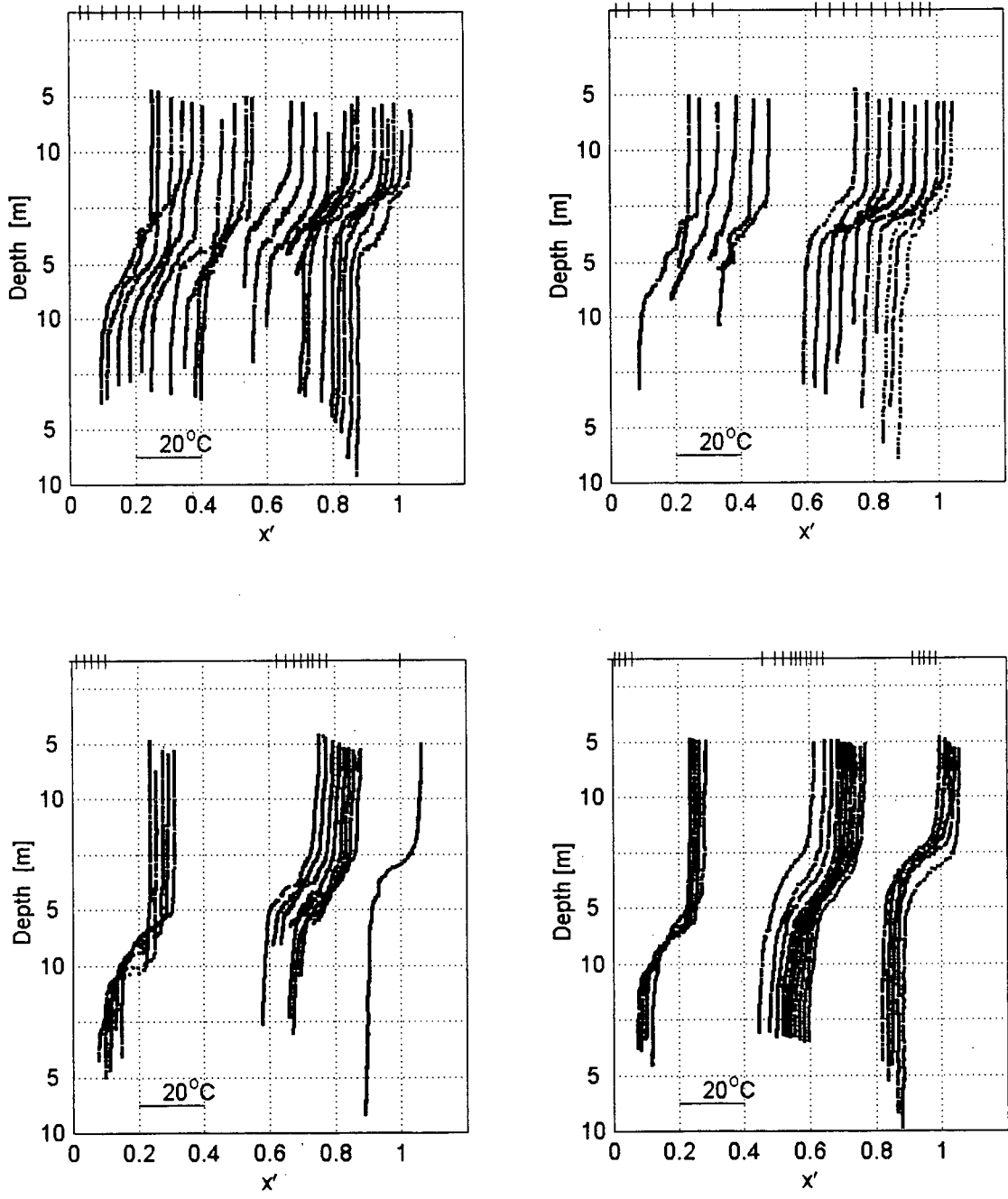


Figure 5 - 11 Temperature profiles from CTD along canal for Drifts A, B, C, and E. A distance of approximately $0.2x'$ corresponds to a temperature difference of about 20°C . Note that the horizontal offset of the temperature profiles is not to scale. Drift D is presented in Figure B-7.

6 DISCUSSION

This chapter discusses the most important results arising from analysis of the July 25, 1996 field data. The thickness of the interfacial layer and bulk Richardson numbers associated with mixing at the interface are examined in Section 6.1. Section 3.6 described an approximation to the solution of the two-layer hydraulic equations, which was called, for convenience, "linear theory". In Section 6.2, the results of linear theory will be compared to the field data and discussed.

6.1 Interfacial Mixing

An important feature of exchange flows is the mixing that can occur due to shear instabilities at the interface between the two layers. This mixing is important since it results in some "short-circuiting". For instance, some Hamilton Harbour water may be entrained from the upper layer into the lower layer and ultimately returned to Hamilton Harbour rather than being advected into Lake Ontario with the remainder of the upper layer. Therefore, it is important to be able to predict the amount of interfacial mixing since it affects the net exchange. In addition, the level of turbulence and mixing at the interface determines the magnitude of the interfacial shear stress, which also reduces the magnitude of the exchange.

Both the thickness of the velocity interface, δ , and the mixing length scale, $\Delta U^2/g'$, are relatively constant throughout Drifts A, B, C, and E¹ except when $0.1 < x' < 0.3$ where both have higher values; see Figure 6-1. This feature may be due to the change in bottom depth in this region; see Figure 4-9. The similar pattern in the behaviour of δ and $\Delta U^2/g'$ yields the very encouraging result that the bulk Richardson number, $J_\delta = g'\delta/\Delta U^2$, is quite uniform along the length of the channel. Although we have fewer density profiles, it appears that the density interfacial thickness, η , exhibits the same behaviour; see Figure 6-2.

The variation of δ and η are plotted against $\Delta U^2/g'$ in Figure 6-3 and 6-4, respectively. The average value for $J_\delta = 0.30$ for Drifts A, B, C, and E. The average for Drift D is $J_\delta = 0.48$, reflecting the disturbance caused by the ship. The average for all drifts except D ranges from $J_\delta = 0.28-0.31$, as shown in Table 6-1. Recall from Section 3.3.3 that previous theoretical, numerical and laboratory studies have yielded values of J_δ between 0.25 and 0.32. For Drifts A, B, C, and E, $J_\eta = g'\eta/\Delta U^2$ varies between 0.21 and 0.30 with an average value of 0.25. This result is slightly less than for the case of velocity and indicates that the density interface is slightly sharper than the velocity interface. However, insufficient data is available to make a definitive conclusion as the difference between the two is approximately the same size as the standard deviation for all drifts in Table 6-1.

The above results are potentially very useful, however we need to be able to predict ΔU before we can predict the interface thickness. This would be a relatively simple task if steady

¹ Drift D is not included because it varies significantly from the other drifts due to mixing caused by a ship passing through the canal. For Drift D results, see Appendix B.

internal hydraulic theory were applicable. However, the following section shows that the degree of unsteadiness in all of the drifts limits the applicability of steady internal hydraulic theory.

Table 6 - 1 Richardson Numbers.

Drift	J_δ		J_η	
	Mean	Standard Deviation	Mean	Standard Deviation
A	0.30	0.06	0.26	0.02
B	0.28	0.06	0.21	0.06
C	0.30	0.07	0.30	0.02
D	0.48	0.18	0.42	0.14
E	0.31	0.06	0.24	0.04
Average of A, B, C, E	0.30	0.06	0.25	0.05

6.2 Applicability of Two-Layer Hydraulics

The theoretical linear interface, described in Section 3.6, was determined by solving Equation (3.29). The equation is solved for h_1 using averaged values for q_1 , q_2 , and g' from the five drifts presented in Table 5 - 4. The average height of the canal is assumed to be, $h = 10$ m. For each drift, there are two real, positive solutions to Equation (3.29). The first solution, h_{1o} , corresponds to a thin lower layer which occurs at the Hamilton Harbour end ($x' = 0$). The second solution, h_{1f} , corresponds to a thin upper layer which occurs at the Lake Ontario end ($x' = 1$). Table 6 - 2 gives the values of h_{1o} and h_{1f} .

Table 6 - 2 Linear theory solutions for each of the five drifts.

DRIFT		A	B	C	D	E
h_{1o}	[m]	5.75	6.86	8.33	6.30	6.67
h_{1f}	[m]	2.98	3.88	5.35	2.94	3.95

A linear interface connecting h_{1o} to h_{1f} is assumed. This assumption circumvents the need to calculate frictional forces as described in Chapter 3. The interface location determined from the fitted profiles, along with the theoretical linear interface are shown in Figure 6 - 5 for Drifts A, B, C, and E and for Drift D in Figure B-12.

The linear interface provides an approximation to the actual data but there are some significant discrepancies. There are several possible sources for these discrepancies. One is the assumption that the channel is of constant depth, and another is the assumption of a linear variation between controls located at either end of the channel. However, even if these assumptions were relaxed, there would still be discrepancies. For instance, the interface elevation would still be predicted to increase monotonically as x' increases; whereas, Figure 6-5 shows that on a number of occasions, the interface elevation decreases.

A likely source of error, which unfortunately is beyond the scope of the present study to incorporate, is unsteadiness in the flow. Note that particular definition of internal energy (see Equations 3.16 and 3.27) and the adopted sign convention cause the internal energy to always increase monotonically in steady exchange flows when frictional effects are considered. However, the plots of internal energy for the drifts do not increase monotonically; see Figure 6-6. The internal energy decreases whenever the net flow rate, q , increases; for example,

between $x'=0.5-0.8$ in Drift A, for most of Drift B, for the start of Drift C, and for several short segments in Drift E. This result indicates that unsteady inertial effects are much greater than frictional effects during each of the drifts.

Helfrich, 1995, has shown that steady hydraulic theory is not appropriate when the parameter γ is of order 1 where:

$$\gamma = \frac{\sqrt{g' h T}}{L} \quad (6.1)$$

This non-dimensional parameter is a measure of the ratio of convective acceleration to inertial acceleration. For the Burlington Ship Canal, $g' = 0.02 \text{ m/s}^2$; $h \approx 10 \text{ m}$; $L = 836 \text{ m}$; and T , the characteristic period over which the velocity varies, is of order 30 minutes. These values yield $\gamma \approx 1$ indicating that time dependence should be considered.

The value of G^2 is often at or near 1 in each of the drifts, but no distinct points of control can be identified, either at the ends of the channel or elsewhere within the channel; see Figure 6-7. This result is consistent with Helfrich's (1995) finding that the usual concept of hydraulic control does not apply for flows where γ is of order 1.

Another potential difficulty in applying internal hydraulic theory to the flows results from the fact that there are instances when the stability Froude number exceeds one in all drifts. As displayed in Figure 6-8, this occurs where the shear between the layers is greatest ($x' = 0.1-$

0.3). This violates Long's stability criterion for long internal waves and internal hydraulic analysis may not be appropriate.

An indication of the degree of unsteadiness in each of the drifts is the variation in the exchange flow strength parameter, R . For steady flow, R remains constant along the length of the channel. In Figure 6-9, the exchange flow strength parameter varies substantially in all drifts. Although in Drift C, R is quite constant for $x' < 0.5$ indicating that on occasion, steady flow may persist for relatively long periods.

Recall that $R > 1$ for flows with a larger exchange component and $R < 1$ for flows with a larger unidirectional component. All flows can be classified as exchange flows since $R > 1$. Weak exchange flows occur when R is close to 1 during portions of Drift D (see Figure B-16) and for a significant portion of Drift C ($0 < x' < 0.6$).

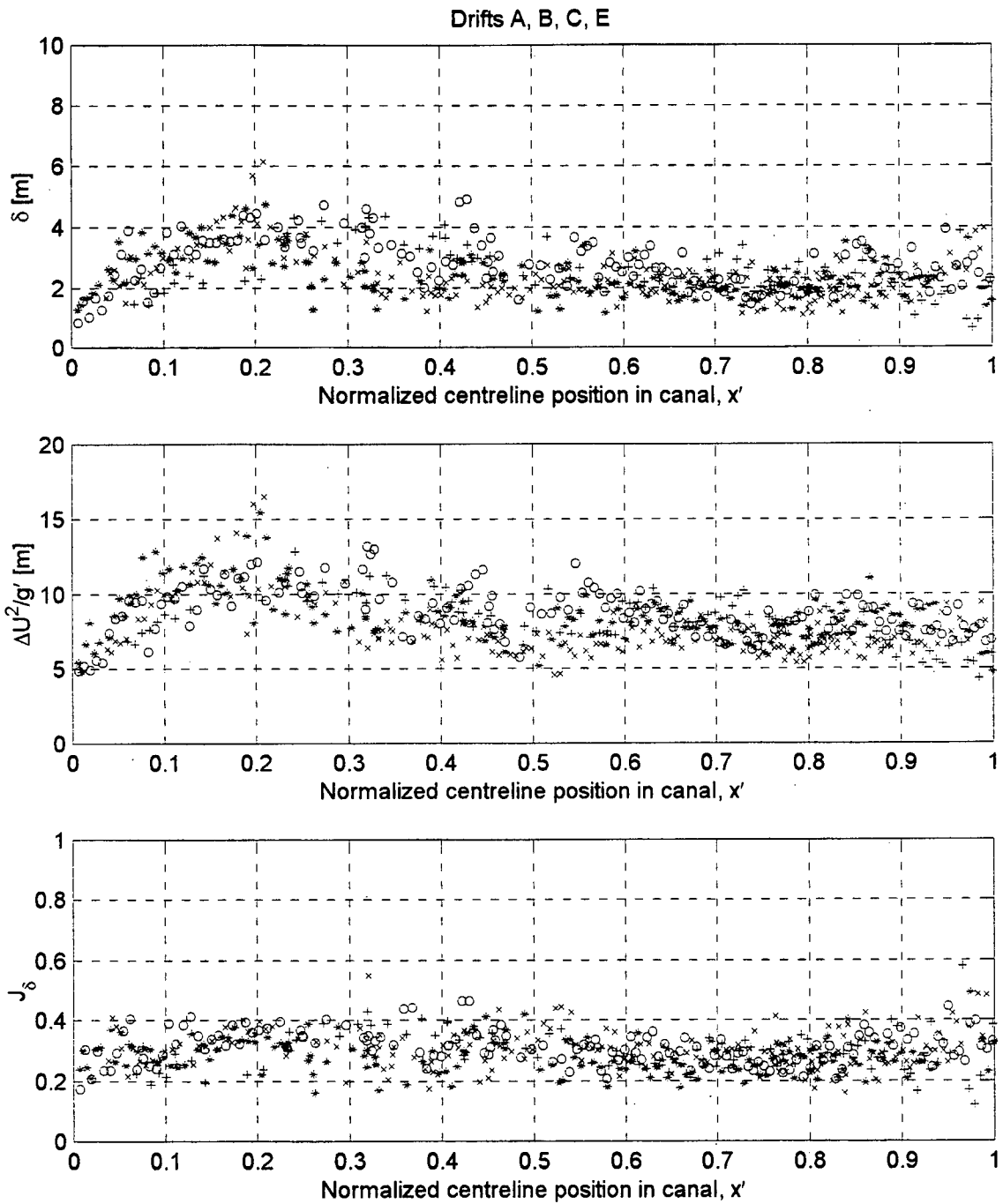


Figure 6 - 1 Thickness of the velocity interface, δ , mixing length scale, $\Delta U^2/g'$, and bulk Richardson number from velocity profiles, J_δ , for Drifts A, B, C, and E. For Drifts A (x); B (*); C (+); and E (o): δ , $\Delta U^2/g'$ and $J_\delta = \delta/(\Delta U^2/g')$ are calculated from the fitted hyperbolic tangent velocity profiles in the top, middle, and bottom plots, respectively. Drift D is presented in Appendix B, Figure B-8.

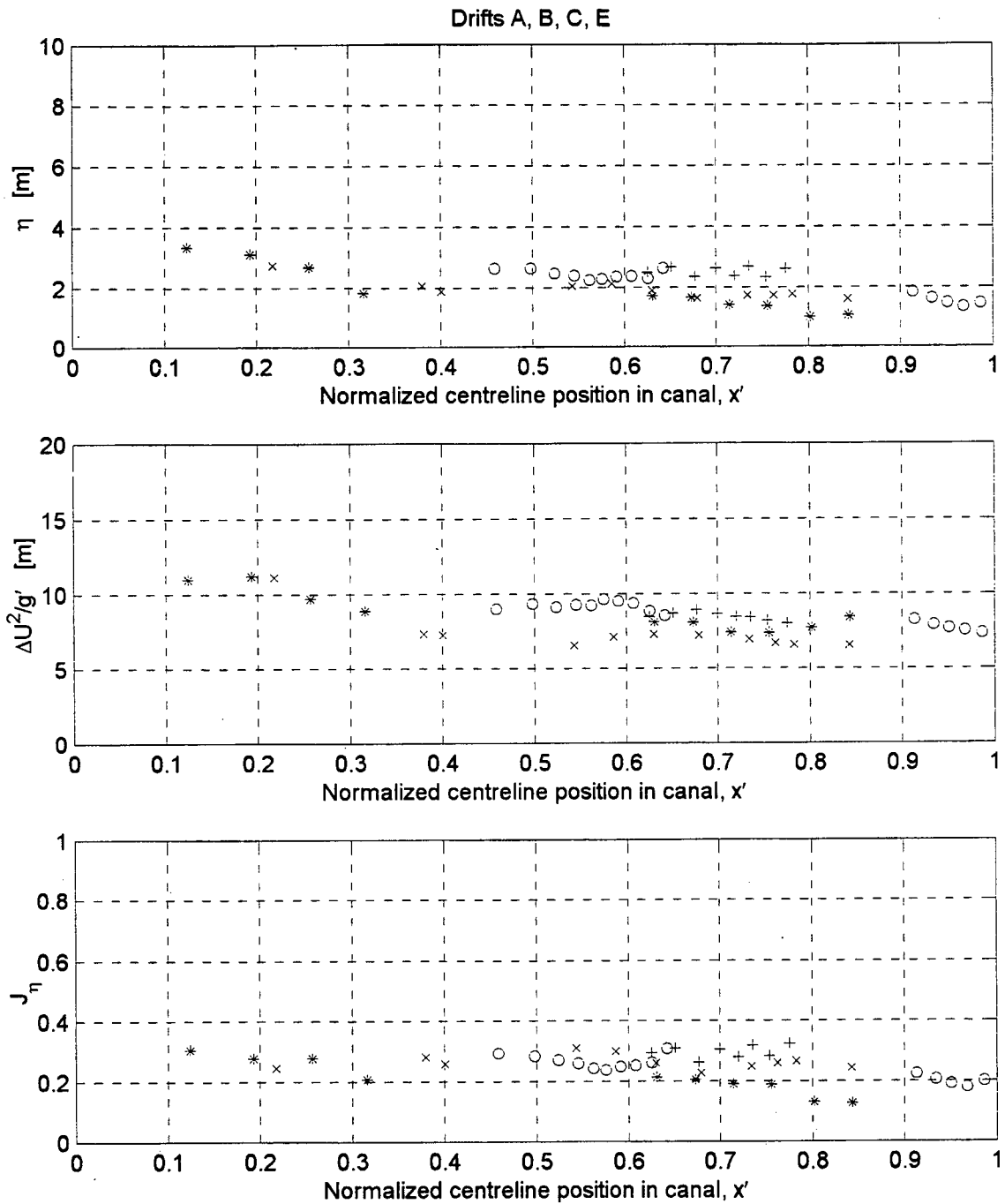


Figure 6 - 2 Thickness of the density interface, η , mixing length scale, $\Delta U^2/g'$, and bulk Richardson number from density profiles, J_η , for Drifts A, B, C, and E. For Drifts A (x); B (*); C (+); and E (o): η , $\Delta U^2/g'$ and $J_\eta = \eta/(\Delta U^2/g')$ are calculated from the fitted hyperbolic tangent density profiles in the top, middle, and bottom plots, respectively. Drift D is presented in Appendix B, Figure B-9.

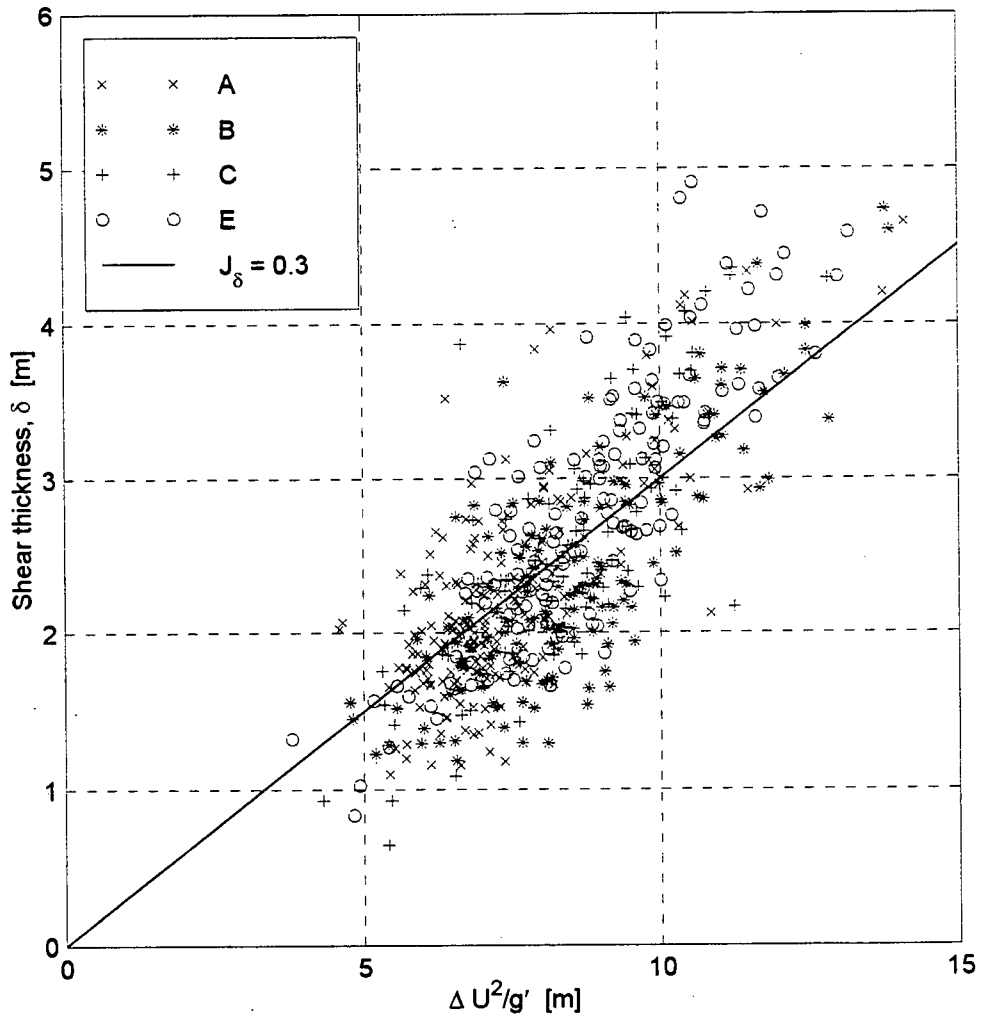


Figure 6 - 3 Bulk Richardson number from velocity for Drifts A, B, C, and E. The line $J_\delta = 0.3$ is the average for Drifts A (x); B (*); C (+); and E (o). Drift D is shown in Figure B-10.

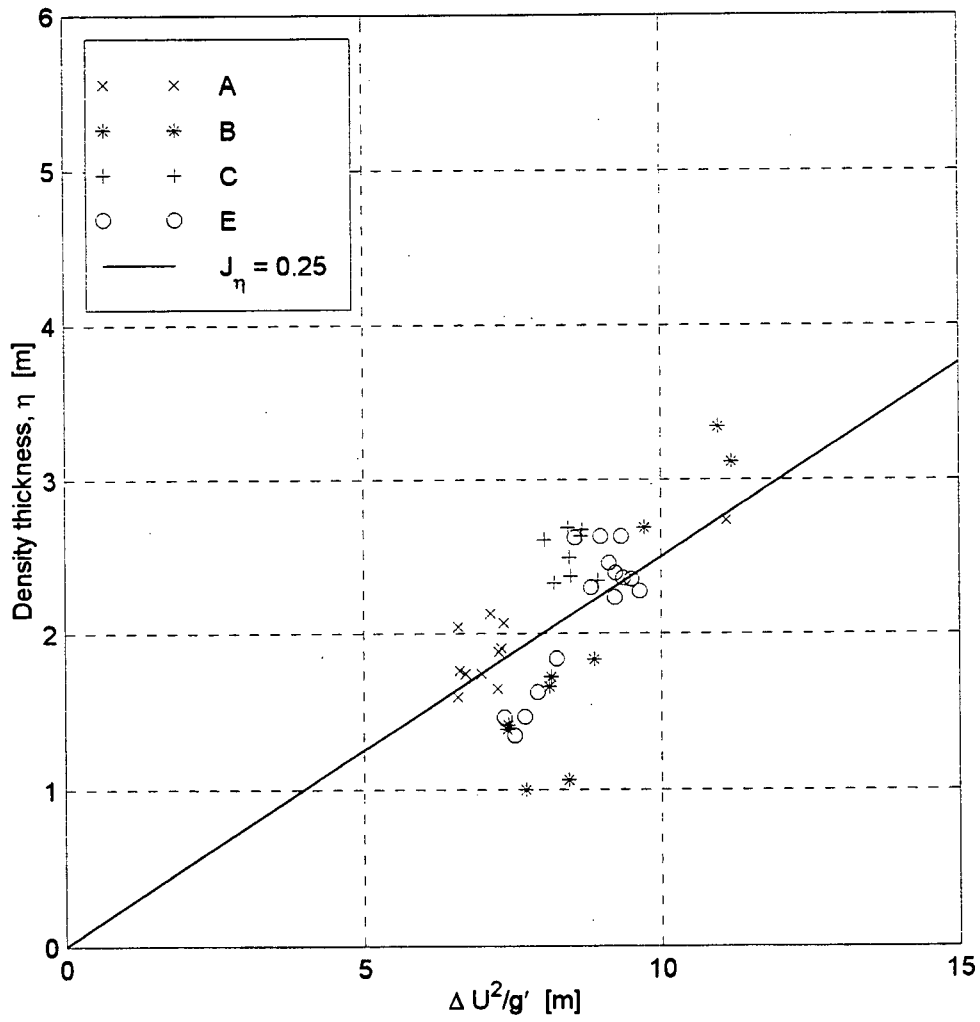


Figure 6 - 4 Richardson number from density for Drifts A, B, C, and E. The line $J_\eta = 0.25$ is the average for Drifts A (x); B (*); C (+); and E (o). The average for Drift D is higher (see Figure B-11) because of mixing that took place due to the passage of a large ship through the canal just before the drift.

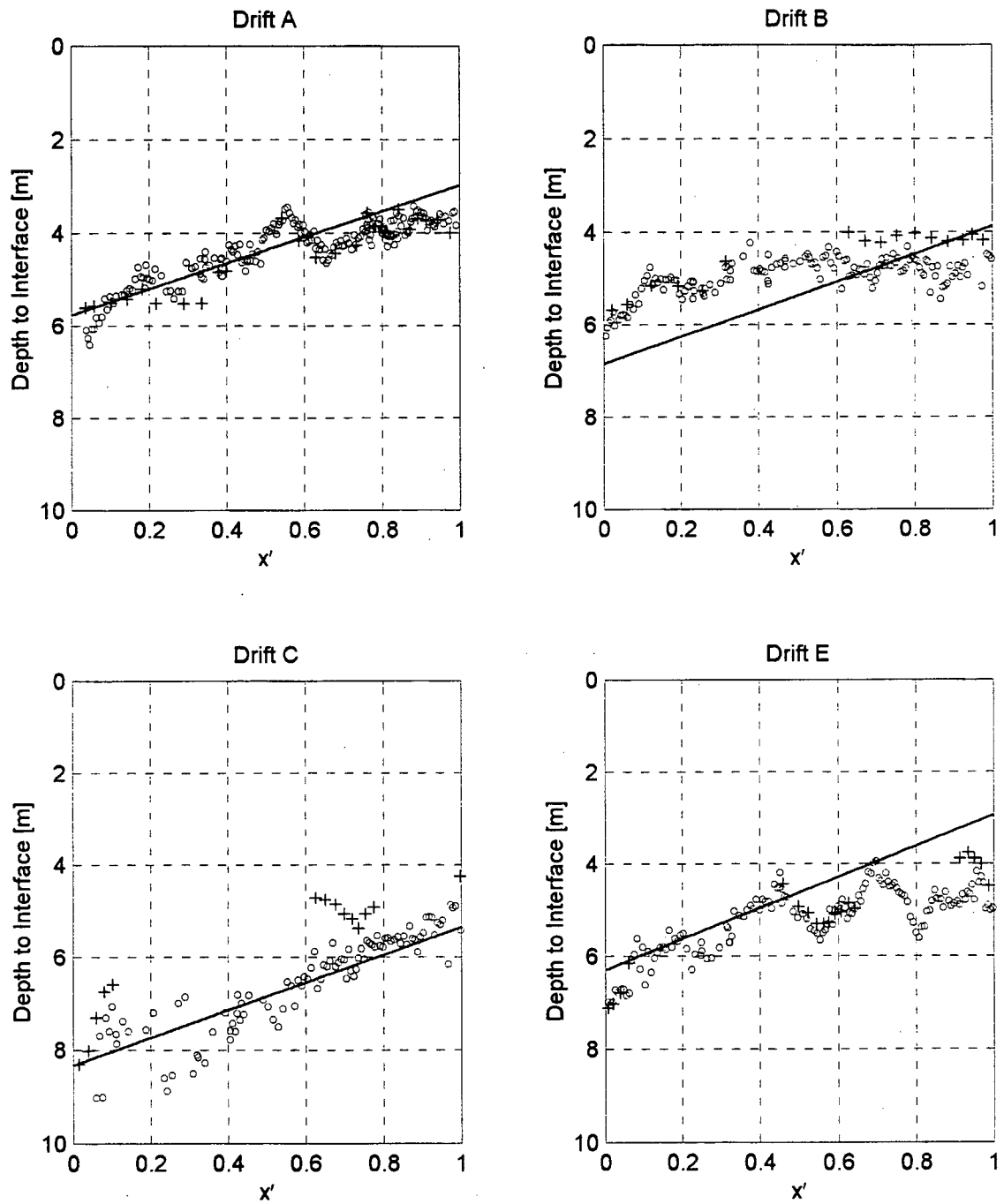


Figure 6 - 5 Interface from density and velocity profiles compared to linear interface for Drifts A, B, C, and E.

The points represent the interface determined from the hyperbolic tangent function fits to the velocity, $h_{1u=0}$ (o) and density profiles, $h_{1\rho}$ (+). The line represents the interface determined from solving $G^2 = 1$ at the ends of the ship canal with the layer depths at ends shown in Table 6 - 2. Drift D is plotted in Figure B-12.

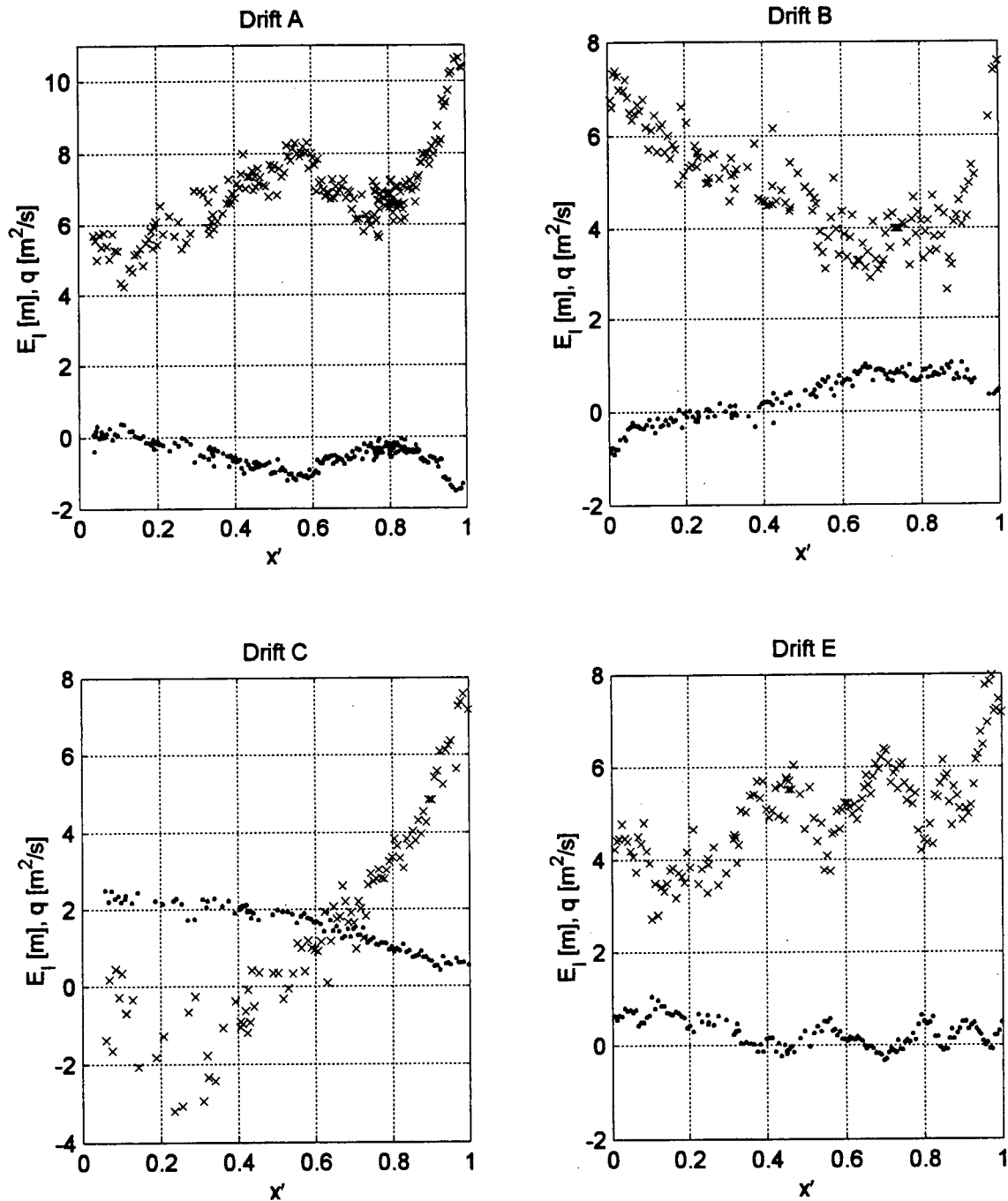


Figure 6 - 6 Variation of internal energy head, E_1 , and net flow, q , along the length of the canal for Drifts A, B, C, and E.

Note that periods when the energy slope $E_1(x)$ is negative correspond to periods of unsteady flow when $q(\cdot)$ is increasing. Drift D is presented in Figure B-13.

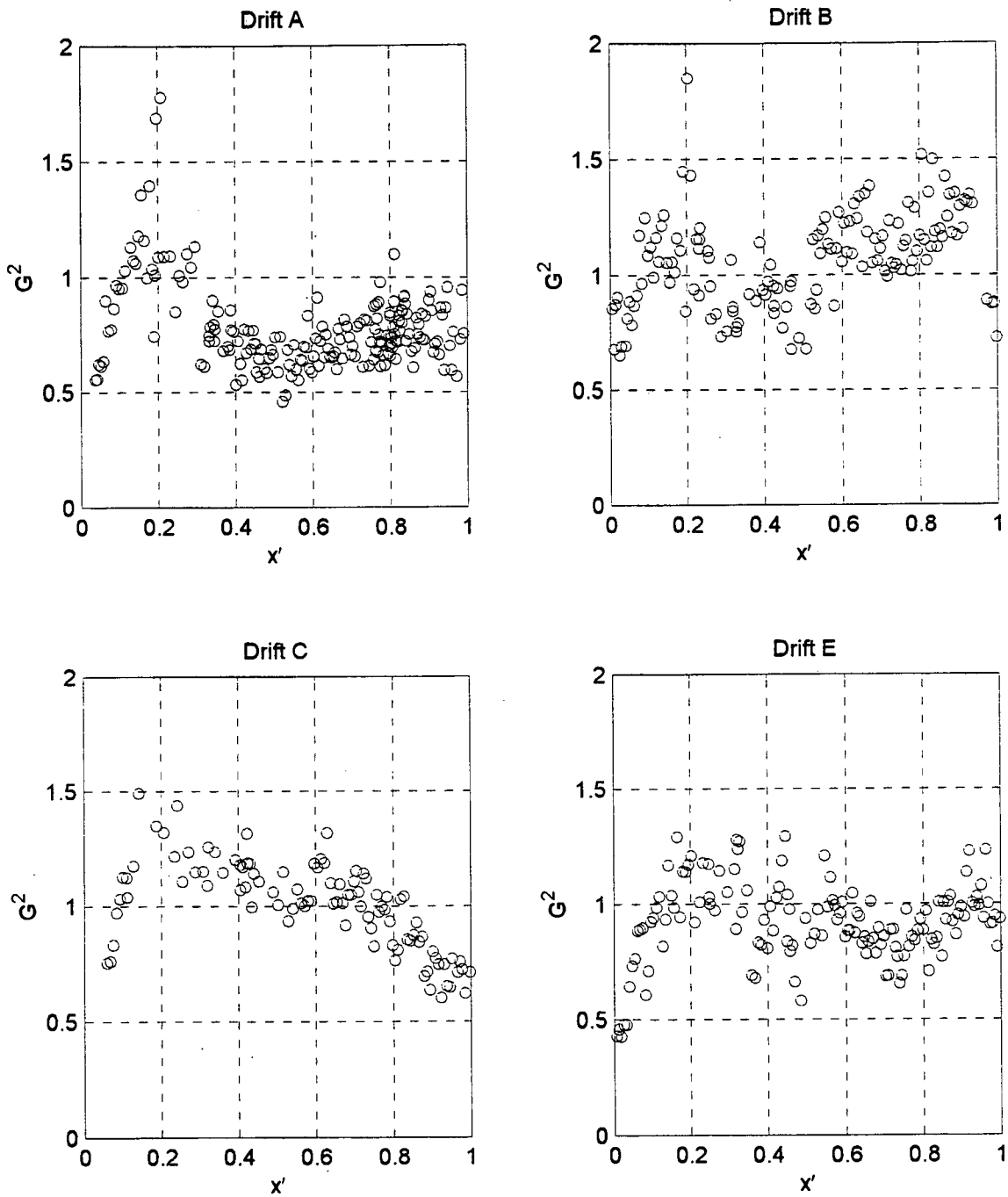


Figure 6 - 7 Variation of composite Froude number along the length of the canal for Drifts A, B, C, and E.

Markers indicate the composite Froude number, G^2 (o). The value of G^2 is often at or near 1 in each of the drifts, but no distinct points of control can be identified, either at the ends of the channel or elsewhere within the channel. See Figure B-14 for the Drift D plot.

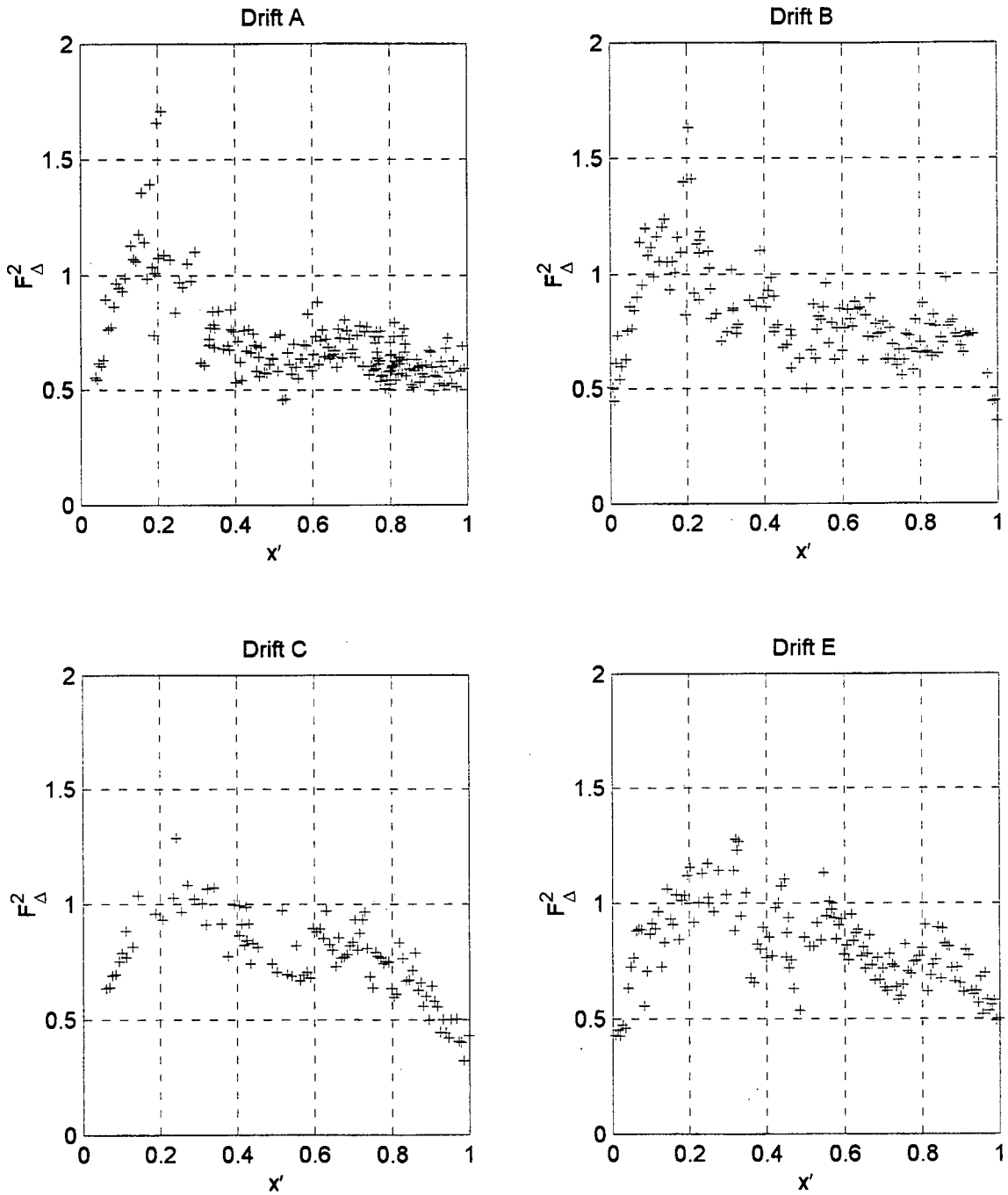


Figure 6 - 8 Variation of stability Froude number along the length of the canal for Drifts A, B, C, and E.

Markers indicate the stability Froude number, F_{Δ}^2 (+). Note that F_{Δ}^2 exceeds 1 inside the canal. This indicates that internal hydraulic theory may not apply. Drift D is presented in Figure B-15.

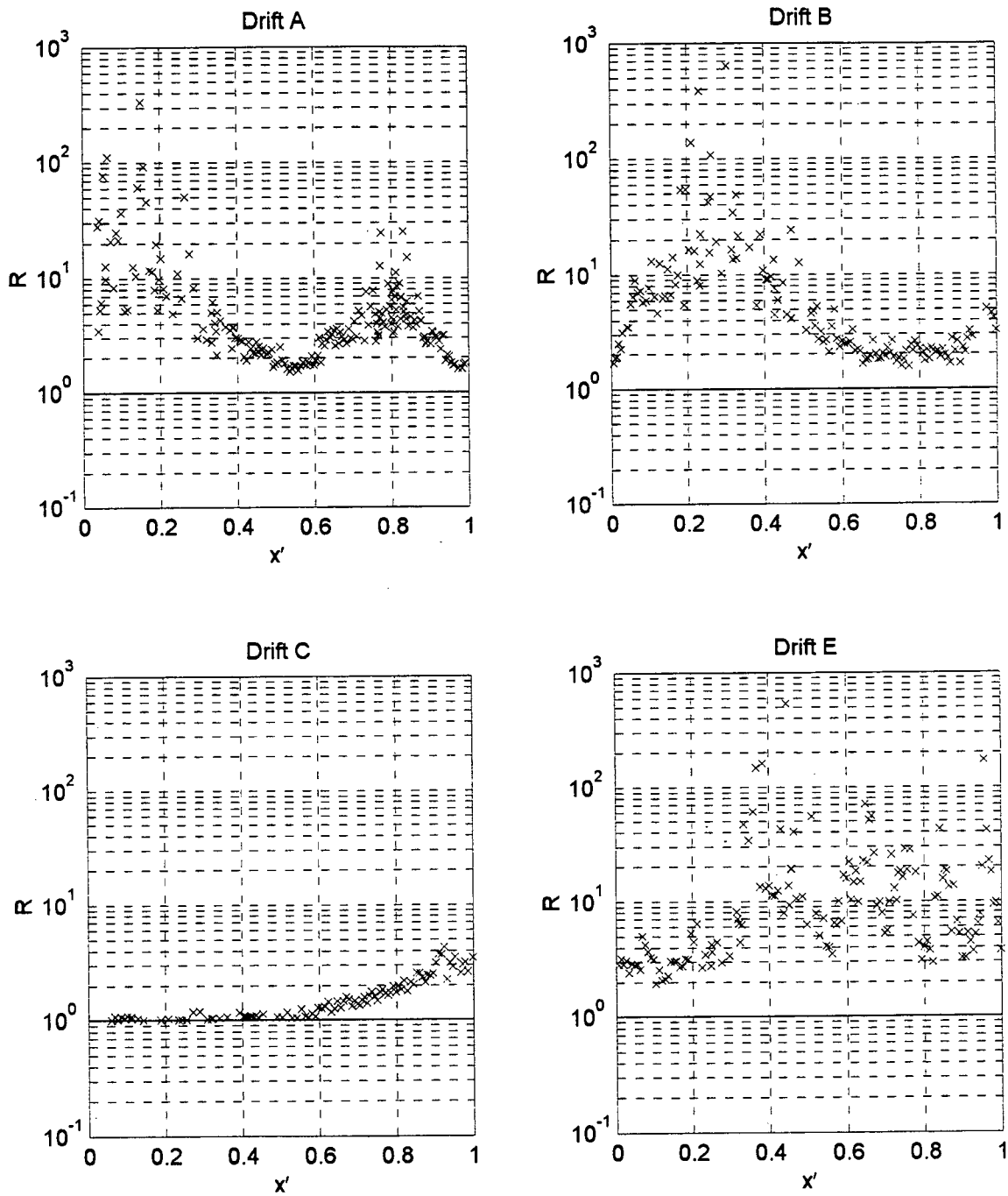


Figure 6 - 9 Exchange flow strength parameter for Drifts A, B, C, and E. All flows are classified as exchange flows ($R > 1$). Note the period of steady flow in Drift C (constant R) and periods of unsteady flow in all drifts. Drift D is presented in Figure B-16.

7 CONCLUSIONS AND RECOMMENDATIONS

A two-month sampling program in the Burlington Ship Canal from July 4 to August 15, 1996 collected data from summertime two-layer exchange flow between Hamilton Harbour and Lake Ontario. The focus of this work was analyzing velocity and density data collected from a boat traversing the length of the canal on July 25, 1996 in order to improve understanding of exchange flow dynamics, determine the applicability of two-layer hydraulic theory, and estimate the interfacial mixing that occurs between the layers in the canal.

A linear interface between the two layers was calculated by assuming that controls occurred at the ends of the ship canal (i.e. $G^2 = 1$ at the ends $x' = 0$ and $x' = 1$) and using the averaged, steady flow rate for each layer (from Table 5 - 2). The linear fit for the interface provides a reasonable initial fit to the data profiles. However the assumptions made to obtain the fit are both violated. Locations where $G^2 = 1$ are plentiful, but in general $G^2 \neq 1$ at the ends of the channel. Unsteadiness in the flow results in substantial variations in the internal energy and the exchange flow strength during each drift. This is consistent with the results of Helfrich (1995) who shows that steady hydraulic analysis is unsuitable when the non-dimensional parameter, γ is of order 1. Long's stability criterion for long internal waves is also violated.

One of the drifts, Drift D behaved erratically compared to the other drifts due to the passage of an ore laker through the canal just prior to the drift that caused significant vertical mixing and internal wave activity in the canal. This drift is excluded from the mixing analysis. Mixing between the layers was very consistent for all Drifts except for Drift D. The bulk Richardson number for velocity was determined to be, $J_s = 0.30 \pm 0.06$ and for density, $J_n = 0.25 \pm 0.05$. The interfacial thickness determined by the density and velocity profiles was greatest near the Hamilton Harbour end of the canal at $x' = 0.2 - 0.3$. The bathymetry of the canal likely influences the location of the peak. It is interesting that even though the flow is unsteady and the interface cannot be predicted with certainty, the mixing in the canal due to interfacial instabilities is predictable. The two-layer flow appears to have a sharper density profile than velocity profile ($J_n < J_s$) although the difference is small in relation to the scatter in the data.

It is evident that the assumption of steady exchange flow is violated for all drifts. Flow rates and the exchange flow strength parameter varied in the time it took to complete one drift. In the future, incorporating unsteady effects into the analysis of flow in the Burlington Ship canal should be considered.

7.1 Suggestions for further research

Future studies should attempt to:

- extend the analysis to incorporate unsteady flow effects following the approach of Helfrich (1995),
- include frictional forces and barotropic effects in the hydraulic analysis, and
- incorporate entire channel geometry (mainly bottom topography).

BIBLIOGRAPHY

American Public Health Association, Washington. 1995 *Standard Methods for the Examination of Water and Wastewater, 19th Edition*. Section 252B, 2-47.

Armi, L. 1986 The hydraulics of two flowing layers of different densities. *J. Fluid Mech.* 163: 27-58.

Armi, L. & Farmer, D.M. 1986 "Maximal two-layer exchange flow through a contraction with barotropic net flow". *J. Fluid Mech.* 164:27-51.

Barica, J., Poulton, D.J., Kohli, B., & Charlton, M.N. 1988 "Water exchange between Lake Ontario and Hamilton Harbour: Water Quality Implications". *Water Pollution Research J. Canada*, 23(2):213-236.

Chen & Millero. 1977 "The use and misuse of pure water PVT properties for lake waters". *Nature*, 266:707-708.

Cheung, E.A. 1990 *Two-layer exchange flow through a contraction with frictional effects*. M.A.Sc. Thesis, University of British Columbia, Vancouver.

Corcos, G.M. & Sherman, F.S. 1976 Vorticity concentration and the dynamics of unstable free shear layers. *J. Fluid Mech.* 73:241.

Dick, T.M., & Marsalek, J. 1973 "Exchange flow between Lake Ontario and Hamilton Harbour". *Environment Canada Inland Waters Directorate, Scientific Series No. 36*.

Farmer, D.M. & Armi, L. 1986 "Maximal two-layer exchange over a sill and through the combination of a sill and contraction with barotropic flow". *J. Fluid Mech.* 164:53-76.

Greco, S.L. 1998 "Exchange flow in the Burlington Ship Canal". *Proceedings of the CWRA 51st Annual National Conference*, Victoria, British Columbia, June 10-12th, '98, pp. 147-151.

Hamblin, P.F. 1989 *Notes on the Hydraulics of Hamilton harbour* Environ. Canada. NWRI Contribution No. 89-36.

Hamblin, P.F. 1995 "Exchange flows in lakes". *Proceedings of the IUTAM Symposium on Physical Limnology*, Broome, Australia, September '95, pp. 163-170.

- Hamblin, P.F., & Lawrence, G.A. 1990 "Exchange flows between Hamilton Harbour and Lake Ontario". *Proceedings of the 1st Biennial Environmental Specialty Conference, CSCE*, 1:140-148.
- Hazel, P. 1972 "Numerical Studies of the stability of inviscid stratified shear flows". *J. Fluid Mech.* 51:39.
- Helfrich, K.R. 1995 "Time-Dependent Two-Layer Hydraulic Exchange Flows". *Journal of Physical Oceanography*. 25:359-373.
- Henderson, F.M. 1966 *Open Channel Flow*. MacMillan, 522 pp.
- Howard, L.N. 1961 Note on a paper of John W. Miles. *J. Fluid Mech.* 10:509.
- Kinder, T.H., & Bryden, H.L. 1987 "The 1985-86 Gibraltar experiment: data collection and preliminary results." *EOS*. 68(40): 746.
- Klapwijk, A., & Snodgrass, W.J. 1985 "Model for Lake-Bay Exchange Flow". *J. Great Lakes Res.* 11(1):43-52.
- Kohli, B. 1979 "Mass Exchange between Hamilton Harbour and Lake Ontario". *J. Great Lakes Research*, 5(1):36-44.
- Koop, C.G. & Browand, F.K. 1979 "Instability and turbulence in a stratified fluid with shear". *J. Fluid Mech.* 93:135.
- Lawrence, G.A. 1985 *Mixing in steady two-layer flow over topography*. Ph.D. Thesis, University of California, Berkeley.
- Lawrence, G.A. 1990a "On the hydraulics of Boussinesq and non-Boussinesq two-layer flows". *J. of Fluid Mechanics* 215:457-480.
- Lawrence, G.A. 1990b "Can Mixing in Exchange Flows be Predicted Using Internal Hydraulics?" *The Physical Oceanography of Sea Straits*, (Ed. Pratt, L.J.) Kluwer Academic Publishers, p. 519-536.
- Lawrence, G.A., Browand, F.K. & Redekopp, L.G. 1991 "The stability of a sheared density interface". *Physics of Fluids A3*(10), 2360-2370.
- Ling, H., Diamond, M., & MacKay, D. 1993 "Application of the QWASI Fugacity/Aquivalence Model to Assessing Sources and Fate of Contaminants in Hamilton Harbour". *J. Great Lakes Research*, 19(3):582-602.

- M.O.E. (Ontario Ministry of the Environment) 1986 *Impact of Hamilton Harbour on Western Lake Ontario*. Water Resources Branch, Toronto, Ontario, 126 p.
- M.O.E. (Ontario Ministry of the Environment). 1989 "Stage 1 Report: Environmental conditions and problem definitions." *Remedial Action Plan for Hamilton Harbour*.
- M.O.E. (Ontario Ministry of the Environment). 1992 "Stage 2A Report: Goals, options and recommendations." *Remedial Action Plan for Hamilton Harbour*.
- Miles, J.W. 1961 "On the stability of heterogeneous shear flows". *J. Fluid Mech.* 10:496.
- Palmer, M.D., & Poulton, D.J. 1976 "Hamilton Harbour: Periodicities of the physiochemical process" *Limnol. Oceanog.* 21:118-127.
- Patnaik, P.C., Sherman, F.S., and Corcos, G.M. 1976 "A numerical simulation of Kelvin-Helmholtz waves of finite amplitude" *J. Fluid Mech.* 73:215-240.
- Pratt L.J. 1990 *The Physical Oceanography of Sea Straits*, Kluwer Academic Publishers, NATO/ASI Series C *Proceeding of the NATO Advanced Research Workshop on the Physical Oceanography of Sea Straits*, Les Arcs, France, July 5-9, 1989.
- RD Instruments Corporate Office 1998 9855 Businesspark Avenue, San Diego, California (<http://www.rdinstruments.com>).
- Spiegel, R.H. 1989 *Some aspects on the physical limnology of Hamilton Harbour*. Environ. Can. NWRI Contribution No. 89-08.
- Stirrup, M. 1996 "Implementation of Hamilton-Wentworth Region's Pollution Control Plan". *Water Quality Research J. of Canada*, 31(3):453-472.
- Thorpe, S. A. 1973 "Turbulence in stably stratified fluids: a review of laboratory experiments. *Boundary Layer Meteorol.* 5, 95.
- Zhu, Zhiwei. 1996 *Exchange flow through a channel with an underwater sill*. Ph.D. Thesis, University of British Columbia, Vancouver.

APPENDIX A – LIST OF COMPUTER PROGRAMS FOR DATA ANALYSIS

PROGRAM NAME	DESCRIPTION
adcp_position.m	Calculates position in Burlington Ship Canal & 'bsc' vector that is 1 for inside & NaN for outside canal
addtop.m	Adds evenly spaced points to fill boat ADCP velocity to 0 m mark (1 of 5 programs to read-in ADCP data)
bot_depth_adcp.m	ADCP estimate of the bottom depth in the Burlington Ship Canal
box.m	Uses a running average (boxcar averaging) for a specified number of points to average data
colfiltt.m	ADCP filtering program (1 of 5 programs to read-in ADCP data)
cutlobe.m	Cuts NaN's at bottom and 15% of depth due to sidelobe contamination (1 of 5 programs to read-in ADCP data)
density.m	Returns density to OS 200 data after input of C,T,D using Chen & Millero's equation of state for freshwater lakes. Applies C25 and OS 200 conductivity calibration equations.
drift_linear.mat	Stores h_{10} and h_{1f} for $G^2=1$ at ends
drift_param.txt	Summary information for all 5 drifts
fiterror.m	Function that minimizes the sum of the squared error for fitting hyperbolic tangent function to density and velocity profiles.
fittanh.m	Program to fit a hyperbolic tangent function to ADCP data
fittanhos.m	Program to fit a hyperbolic tangent function to CTD data fits.
find_J	Calculates stability, composite, internal Froude numbers for linear theory and boat data.
gps_cart_os200.m	
gps_cart_all.m	Reads in GPS data and converts it to Cartesian co-ordinates in the Burlington Ship Canal. It makes a linear fit through stations 901, 924, 925 and takes out data NOT in Burlington Ship Canal then calls norm_bsc1022 to normalize centreline length.

PROGRAM NAME	DESCRIPTION
july25.m	Plots moored ADCP July 25, 1996 data july25.mat holds dept, velocity, time for moored instrumentation
july25_3reg.m	Plots 3 regimes of flow: -exchange flow; unidirectional flow; and mixed flow
meanu.m	Calculates and stores mean velocity.
norm_bsc.m	Normalizes the length of the canal so that Hamilton Harbour end = 0 and Lake Ontario end = 1. To be used with gps_cart.m
os200.mat	Stores CTD data (conductivity, temperature, depth, and time).
os200_position.m	Determines CTD position in Burlington Ship Canal.
q_new.m	Integrates the hyperbolic tangent velocity fit to the ADCP data with respect to depth to obtain top-layer flow, bottom-layer flow, and net flow.
rcast.m	Cuts upcasts of os200 data
rhoi.m	Calculates density of top and bottom layer from hyperbolic tangent fit to OS 200 density profiles
split_drift.m	Splits ADCP drifts up into A, B, C, D, E
split_os200_2.m	Splits CTD drifts up into A, B, C, D, E
time_os200.m	Interpolates OS 200 position in Burlington Ship Canal based on time interpolation of GPS data
time16.m-time36.m	Files that read in OS 200 data, assign a time to each data reading, and return the midpoint of the downcasts (Casts33 is empty).
ui1022.m	Calculates top and bottom layer densities based on hyperbolic tangent fit to ADCP velocity profiles
vproject.m	Projects velocity to 55°N (1 of 5 programs to read-in ADCP data)

APPENDIX B – DRIFT D RESULTS

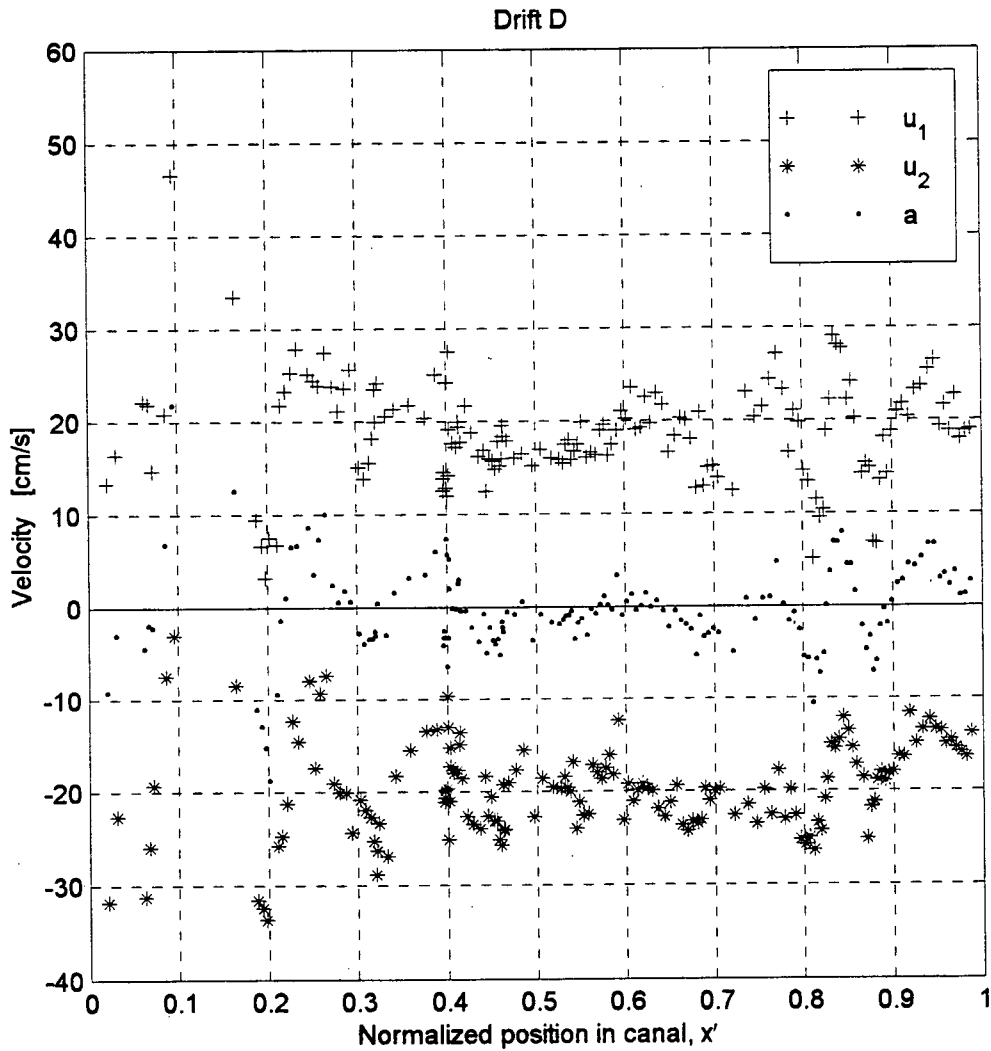


Figure B - 1 Layer velocities and barotropic component along the length of the canal for Drift D.

The velocities of the top layer, u_1 (+); bottom layer, u_2 (*); and barotropic component, a (.); determined from the hyperbolic tangent fits to the velocity profiles vary along the length of the canal as shown.

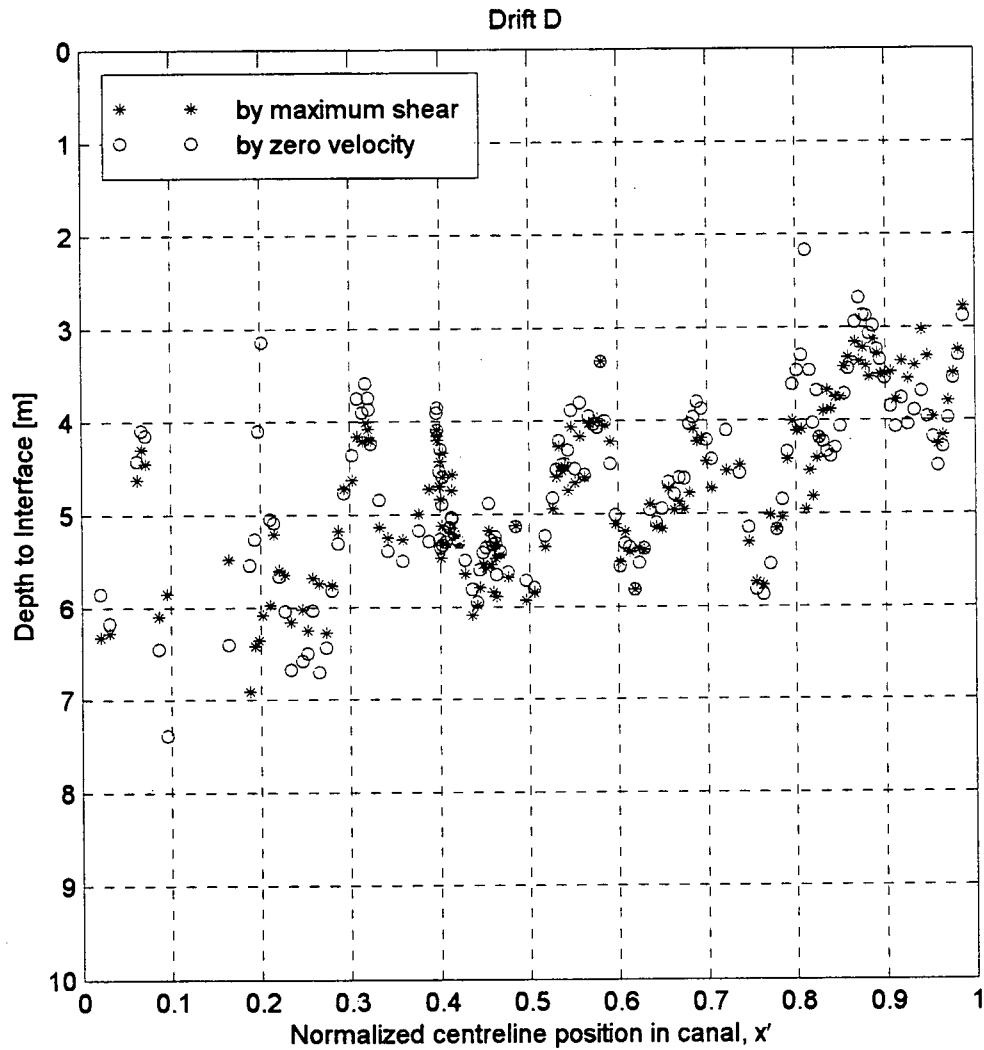


Figure B - 2 Interface height along the length of the canal for Drift D. The interface along the canal is the point of zero velocity (o) or the point of maximum shear (*) determined from the fitted hyperbolic tangent velocity profiles.

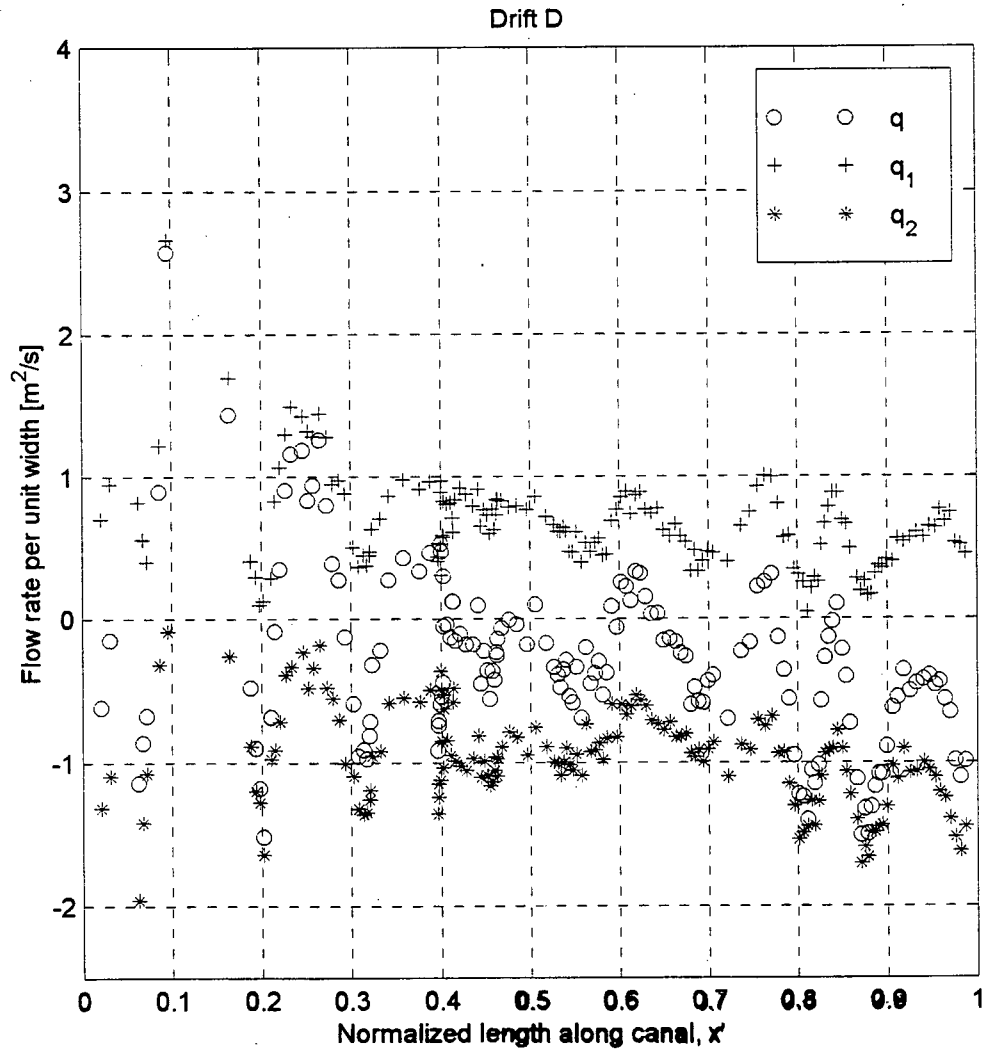


Figure B - 3 Flow rate per unit width in top and bottom layers along the length of the canal determined from velocity profiles for Drift D. Flow rate per unit width for the top layer, q_1 (+); bottom layer, q_2 (*), and net flow rate, q (o) are determined from integrating the fitted hyperbolic tangent velocity profiles with respect to depth.

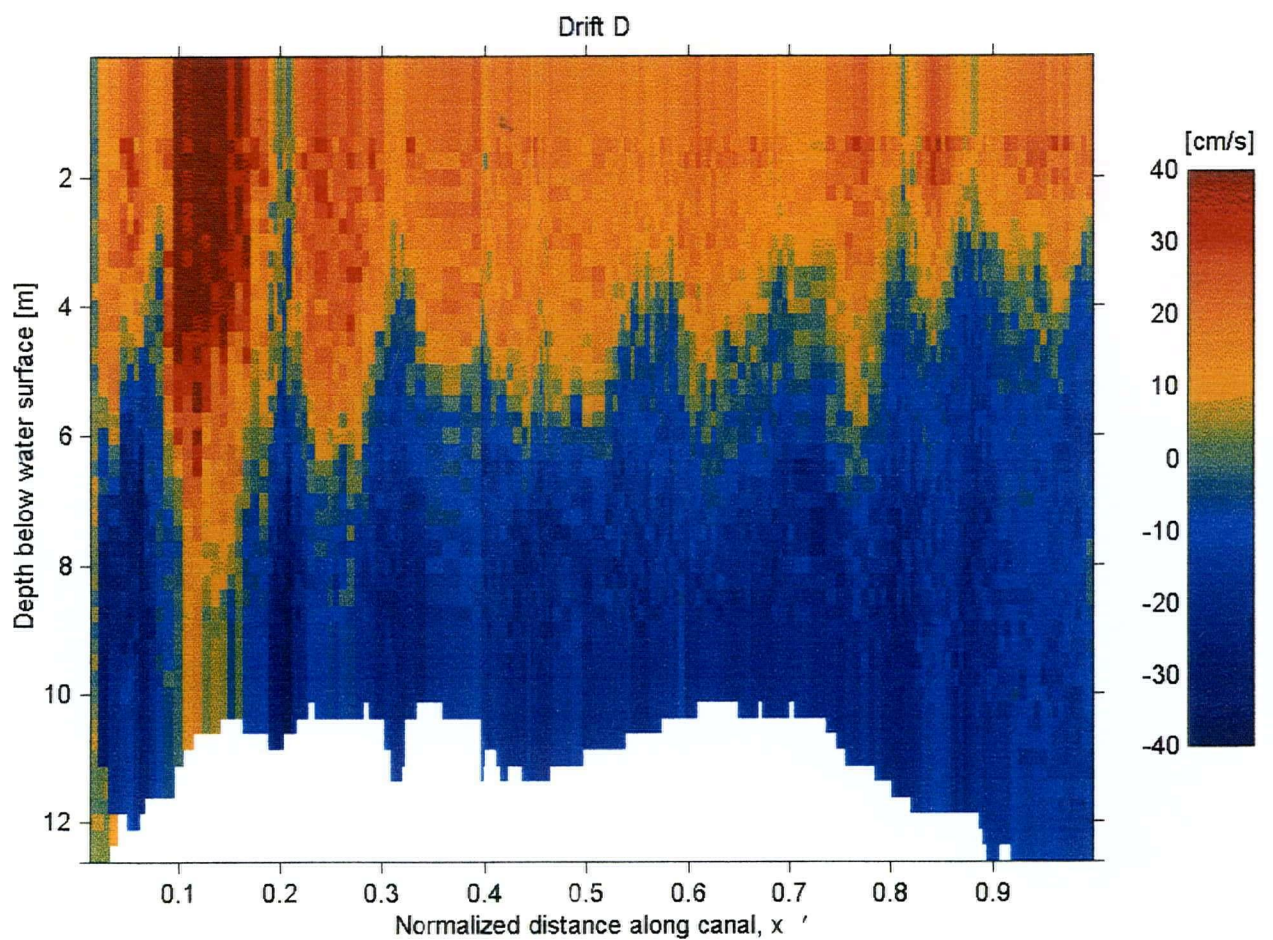


Figure B - 4 Velocities plotted depth against distance for Drift D. Velocities (in cm/s) from the boat ADCP drifts in the Burlington Ship Canal are plotted on depth from water surface and position along the canal. Hot colours indicate a positive velocity (from Hamilton Harbour to Lake Ontario) while cool colors indicate a negative velocity (from Lake Ontario to Hamilton Harbour).

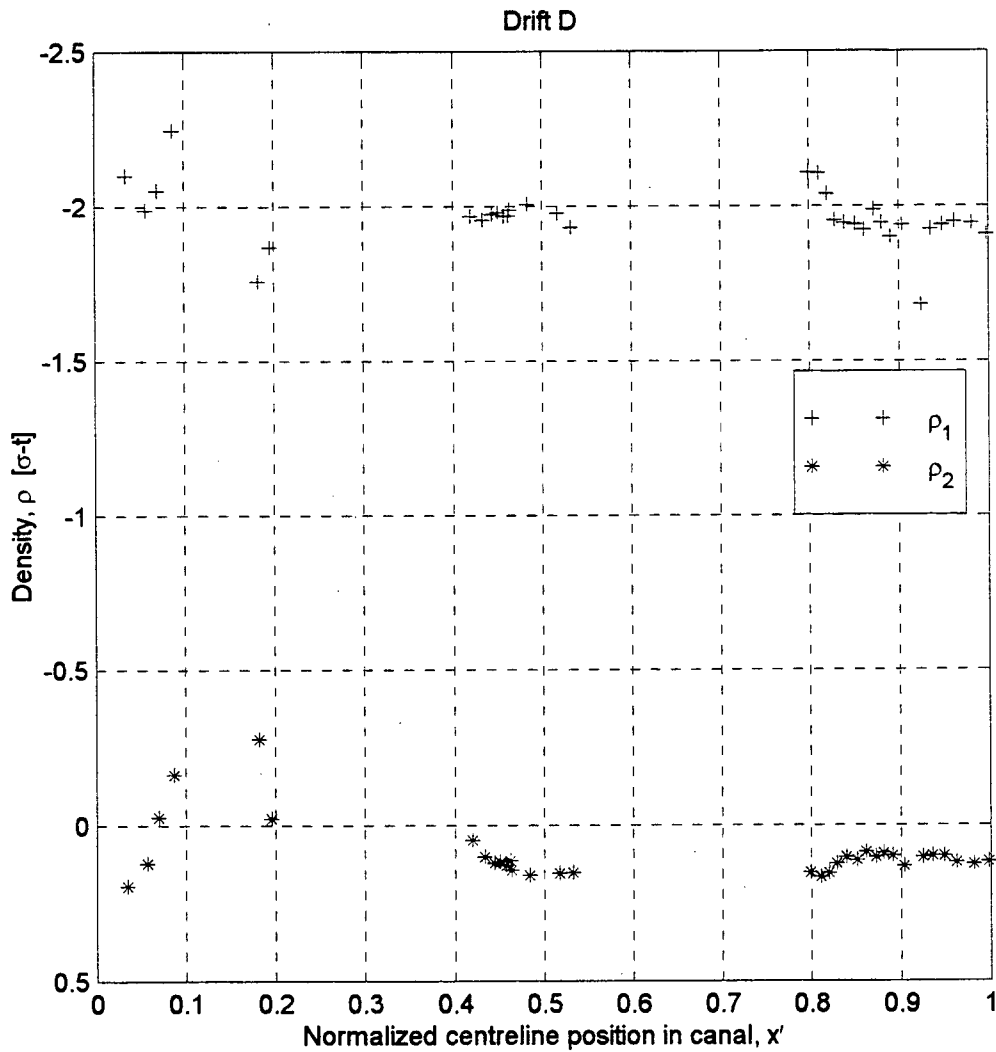


Figure B - 5 Density of top and bottom layers along the length of the canal for Drift D. Density for the top layer, ρ_1 (+), and bottom layer, ρ_2 (*), are determined from the fitted hyperbolic tangent density profiles.

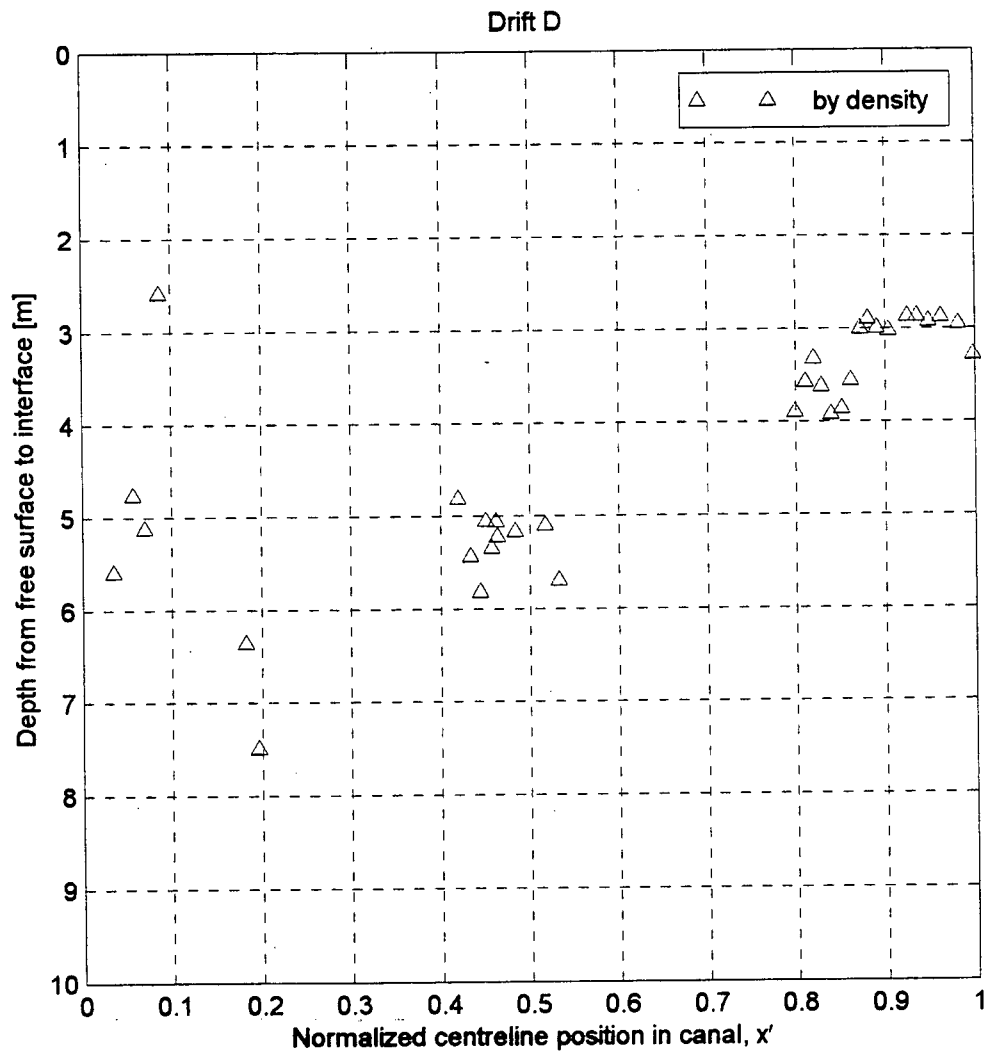


Figure B - 6 Interface height along the length of the canal from density profiles for Drift D. The depth of the interface is determined using the hyperbolic tangent fits of the density profiles.

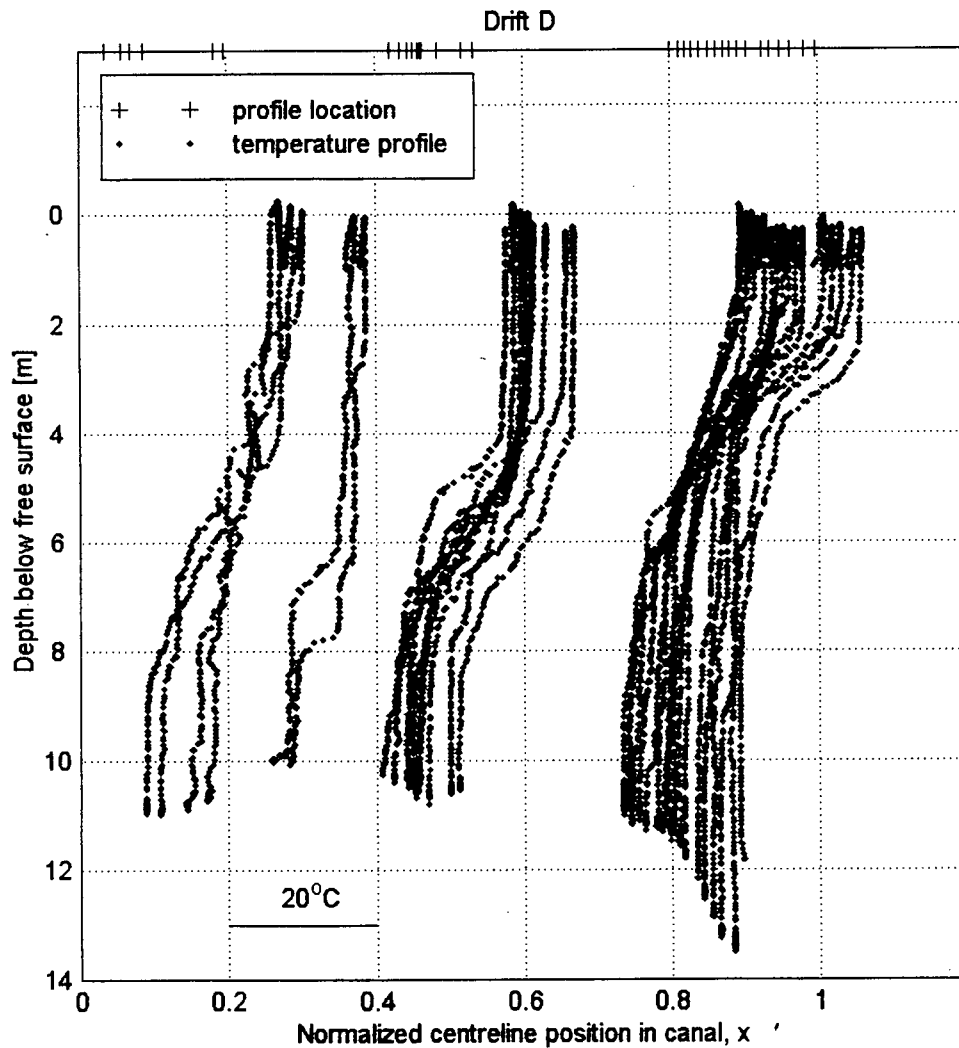


Figure B - 7 Temperature profiles along the length of the canal for Drift D. Temperature profiles from CTD casts along the canal are. A distance of approximately $0.2x'$ corresponds to a temperature difference of about 20°C . Note that the horizontal offset of the temperature profiles is not to scale.

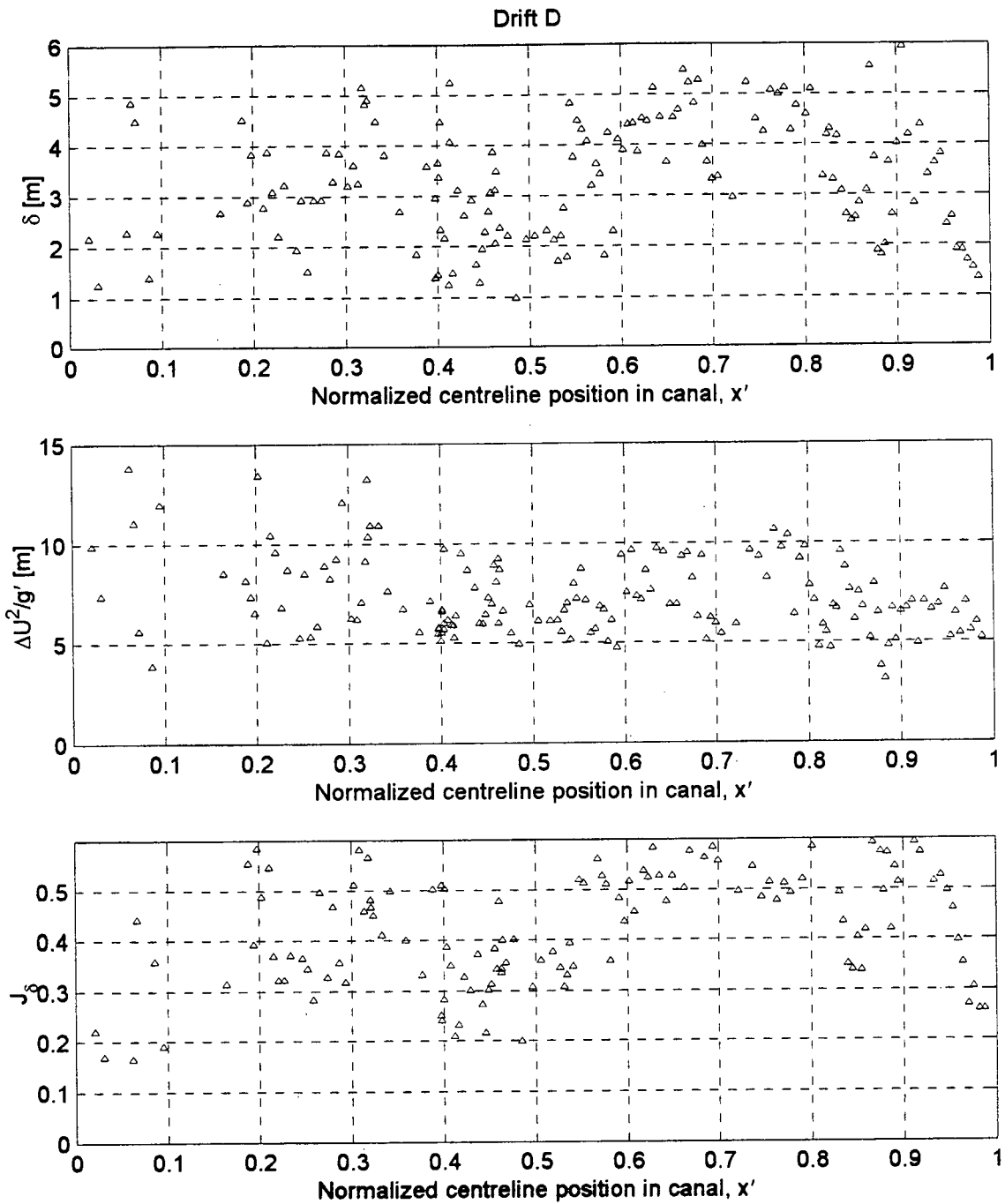


Figure B - 8 Thickness of the velocity interface, δ , mixing length scale, $\Delta U^2/g'$, and bulk Richardson number from velocity profiles, J_s , for Drift D.
 For Drift D: δ , $\Delta U^2/g'$ and $J_s = \delta/(\Delta U^2/g')$ are calculated from the fitted hyperbolic tangent velocity profiles in the top, middle, and bottom plots, respectively.

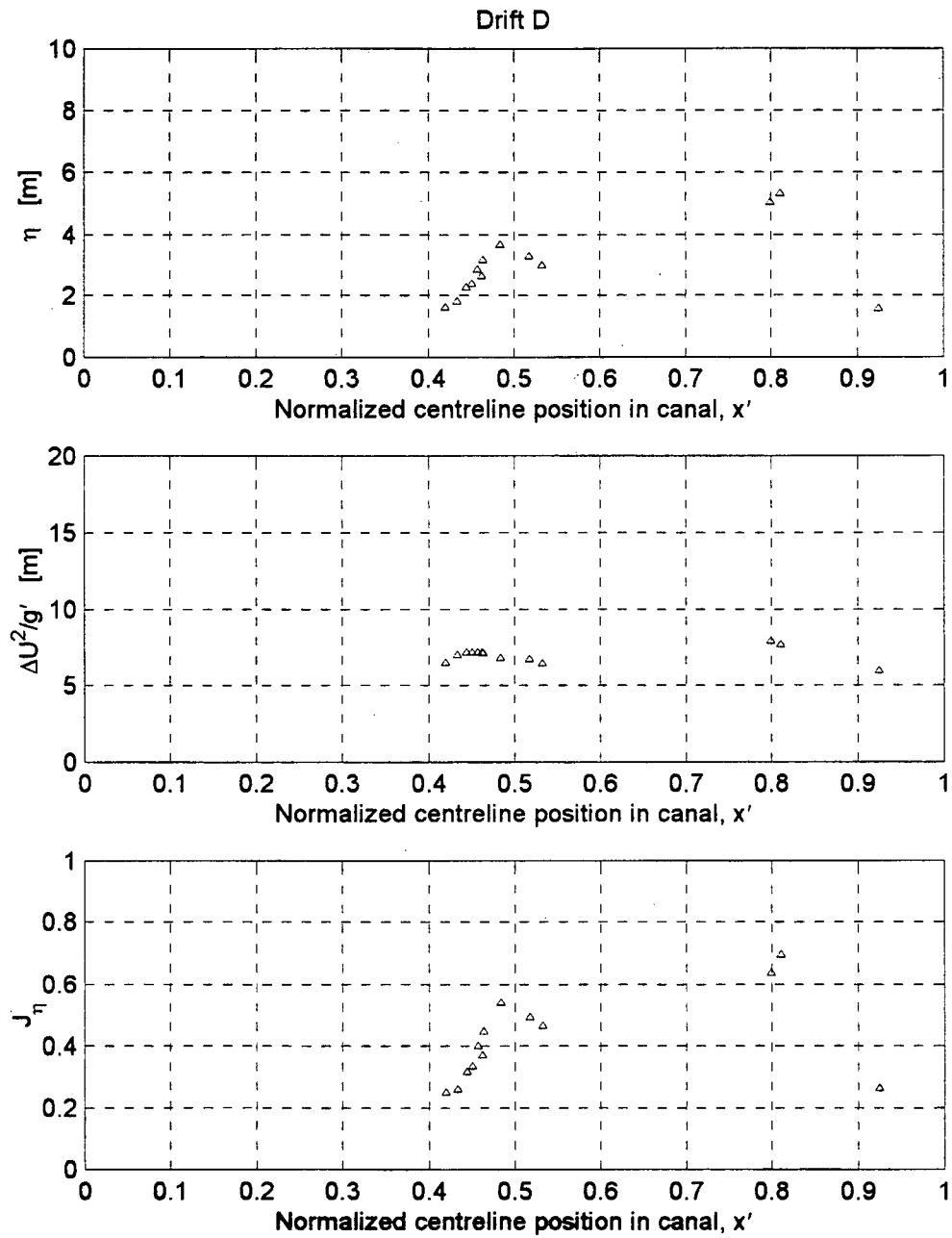


Figure B - 9 Thickness of the density interface, η , mixing length scale, $\Delta U^2/g'$, and bulk Richardson number from density profiles, J_η , for Drifts A, B, C, and E. For Drift D: η , $\Delta U^2/g'$ and $J_\eta = \eta/(\Delta U^2/g')$ are calculated from the fitted hyperbolic tangent density profiles in the top, middle, and bottom plots, respectively.

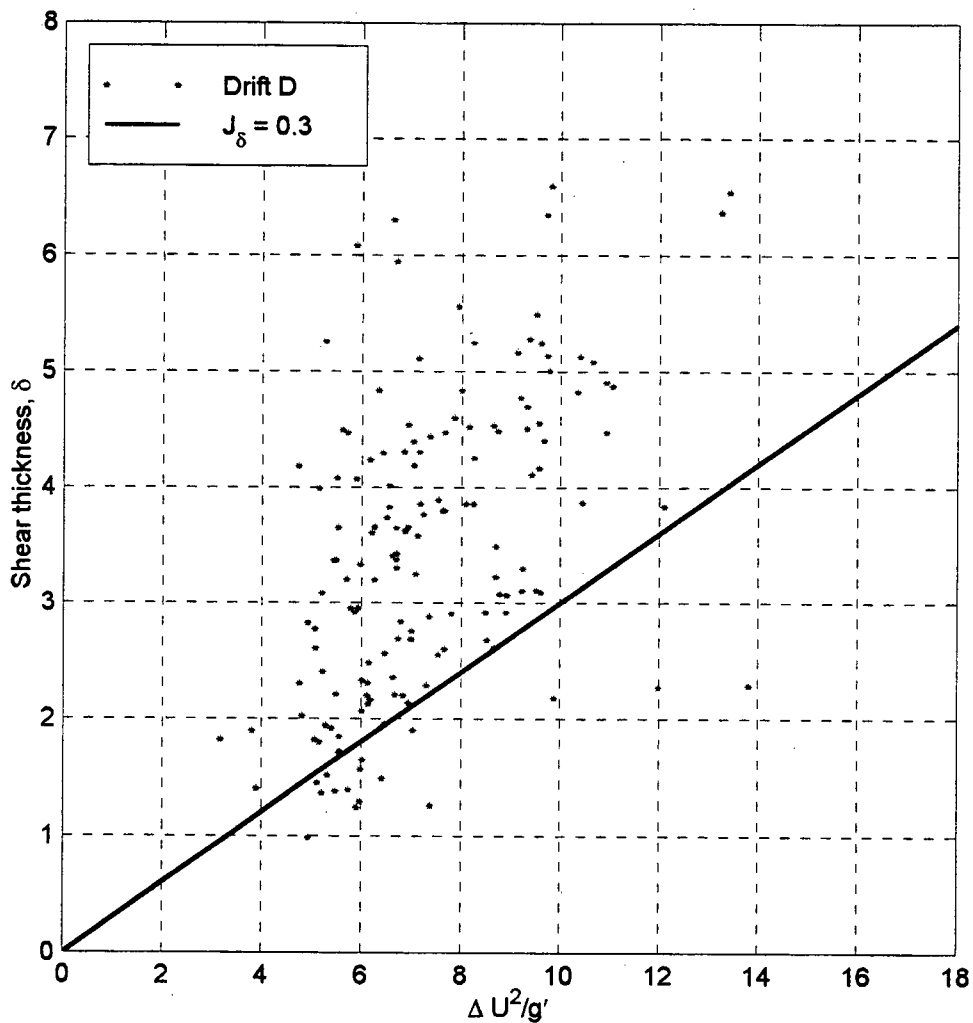


Figure B - 10 Bulk Richardson number plot for velocity for Drift D. The line of $J_\delta = 0.3$ is the average for Drifts A, B, C, and E. The average for Drift D is higher (see Table 6-1) because of mixing that took place due to the passage of a large ship through the canal just before the drift.

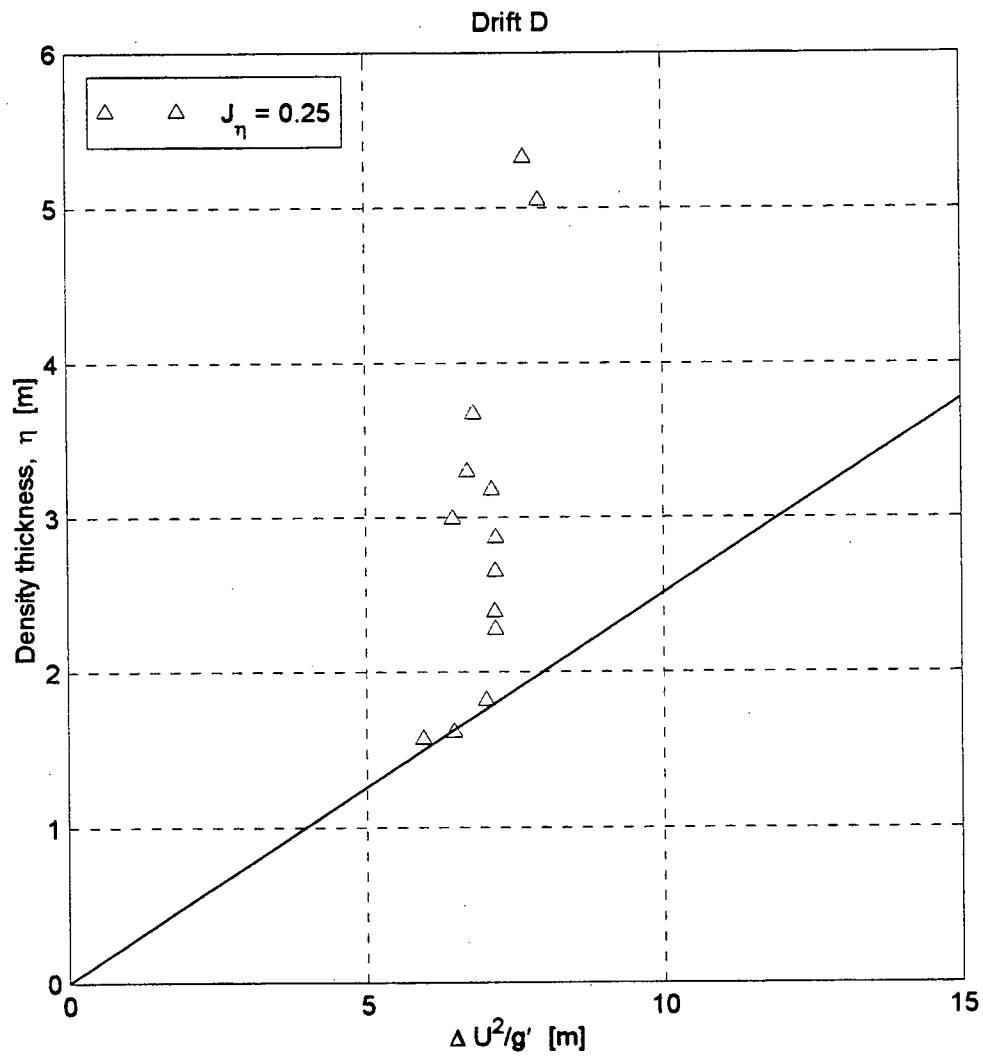


Figure B - 11 Bulk Richardson number plot for density for Drift D. The line of $J_{\eta} = 0.25$ is the average for Drifts A, B, C, and E. The average for Drift D is higher (see Table 6-1) because of mixing that took place due to the passage of a large ship through the canal just before the drift.

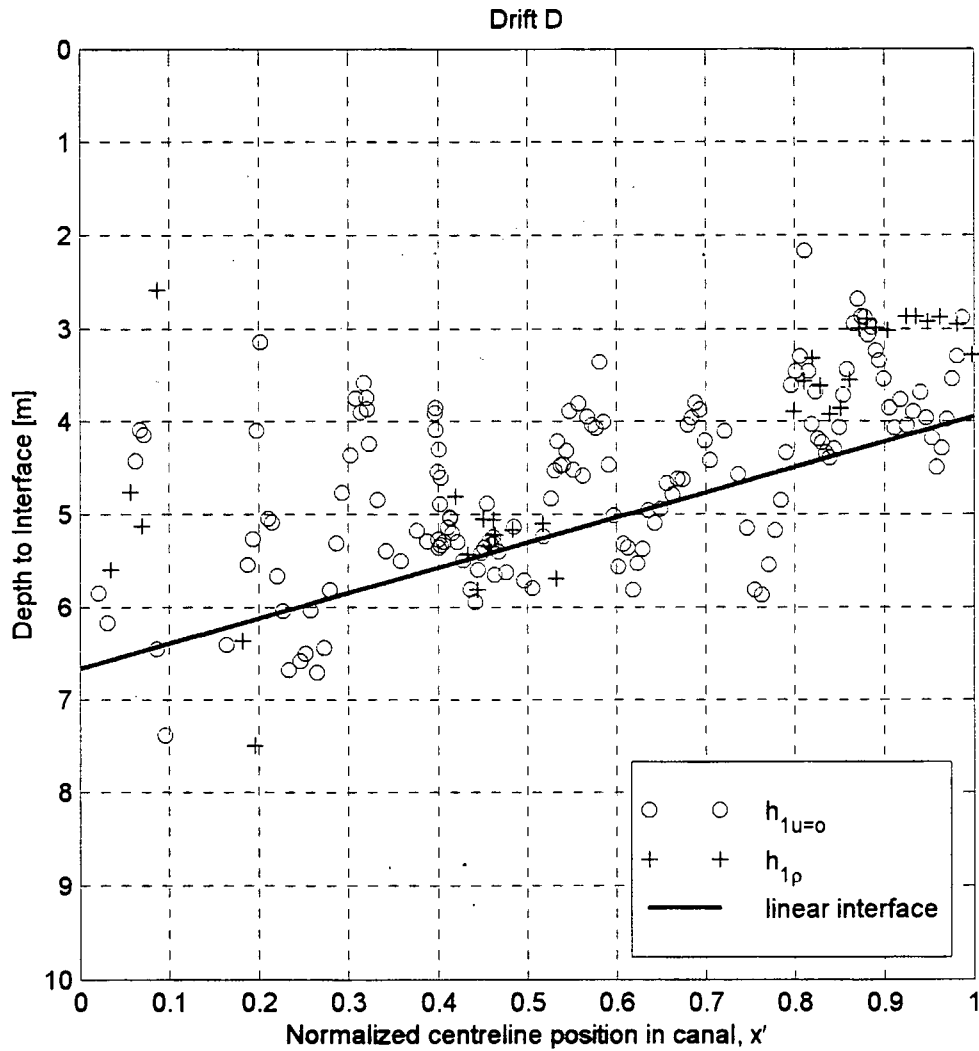


Figure B - 12 Comparison of interface location with linear interface for Drift D.

The points represent the interface determined from the hyperbolic tangent fits to the actual velocity/density profiles from the height of maximum shear, $h_{1m.s.}$ (*); the height of zero velocity, $h_{1u=0}$ (o); and centre of the centre of the density profile, h_{1p} (+). The line represents the linear interface determined from solving $G^2 = 1$ at the ends of the ship canal as described in Section 6.1.1. Endpoints are shown in Table 6 - 1.

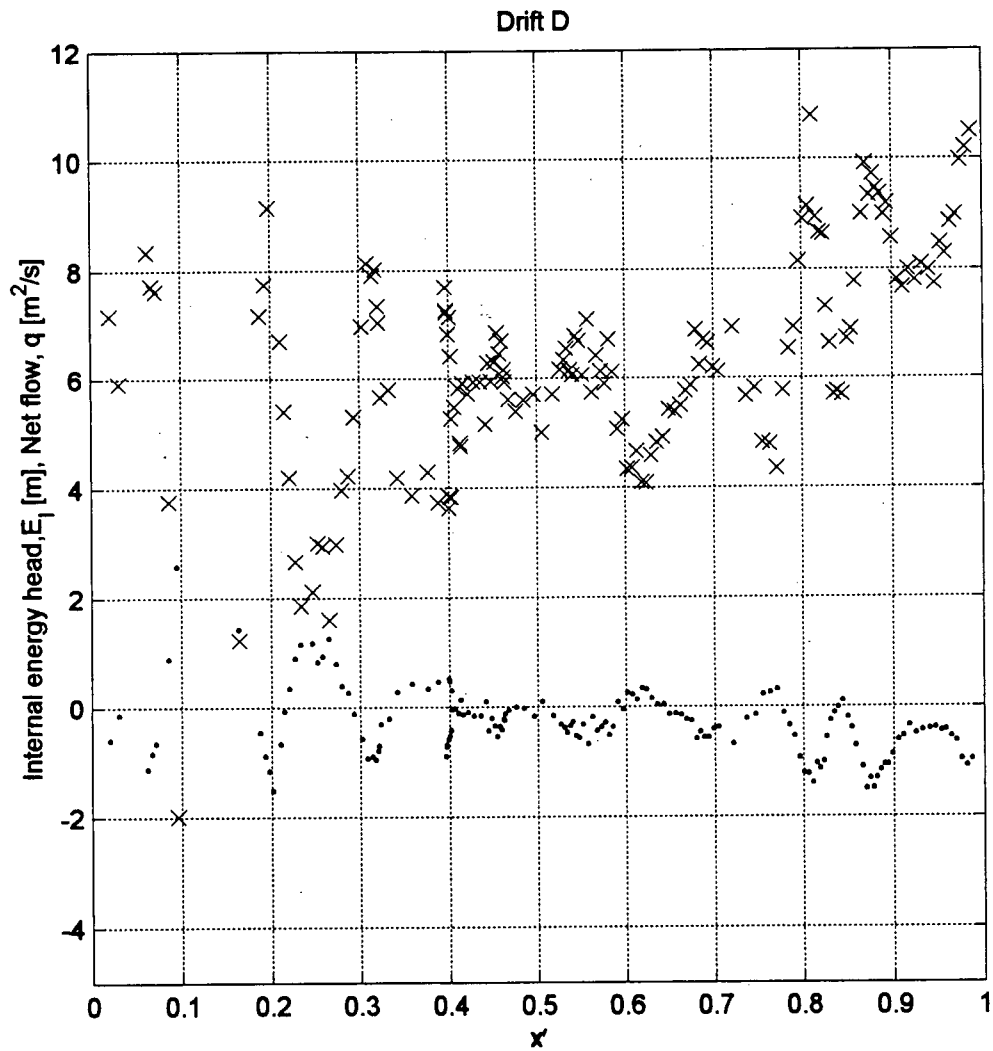


Figure B - 13 Variation of internal energy head, E_I , and net flow, q , along the length of the canal for Drift D.

Note that periods when the energy slope $E_I(x)$ is negative correspond to periods of unsteady flow when $q(\cdot)$ is increasing.

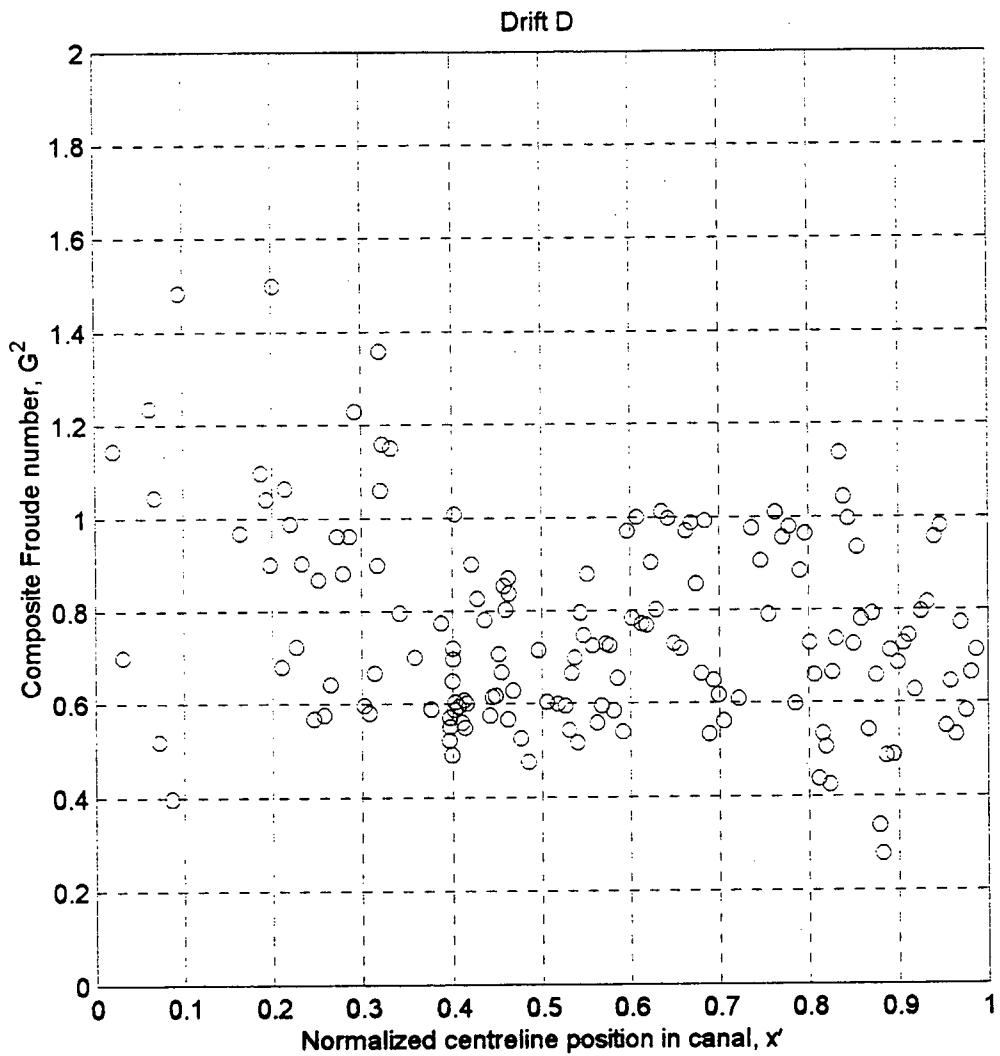


Figure B - 14 Variation of composite Froude number along the length of the canal for Drift D.

Markers indicate the composite Froude number, G^2 (o). The value of G^2 is often at or near 1 in each of the drifts, but no distinct points of control can be identified, either at the ends of the channel or elsewhere within the channel.

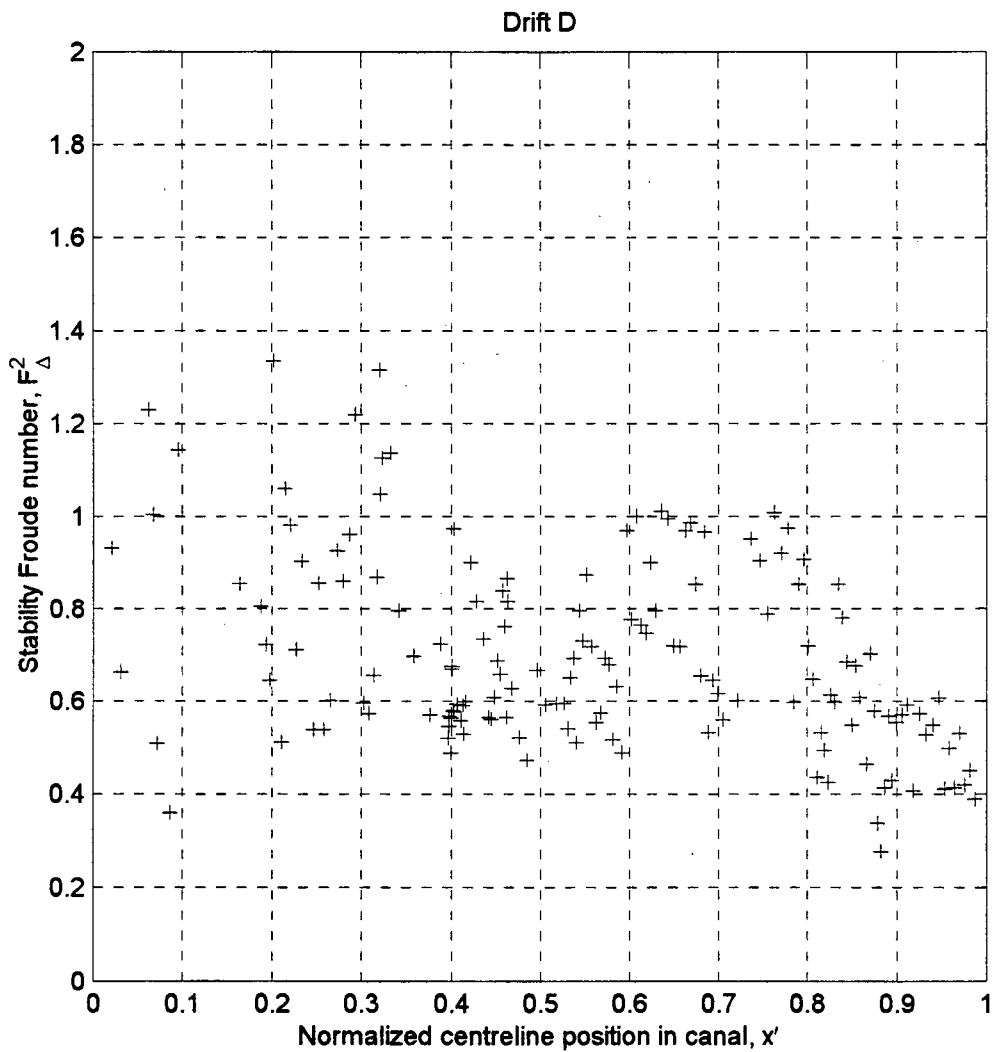


Figure B - 15 Variation of stability Froude number along the length of the canal for Drift D. Markers indicate the stability Froude number, F_{Δ}^2 (+). Note that, F_{Δ}^2 exceeds 1 inside the canal.

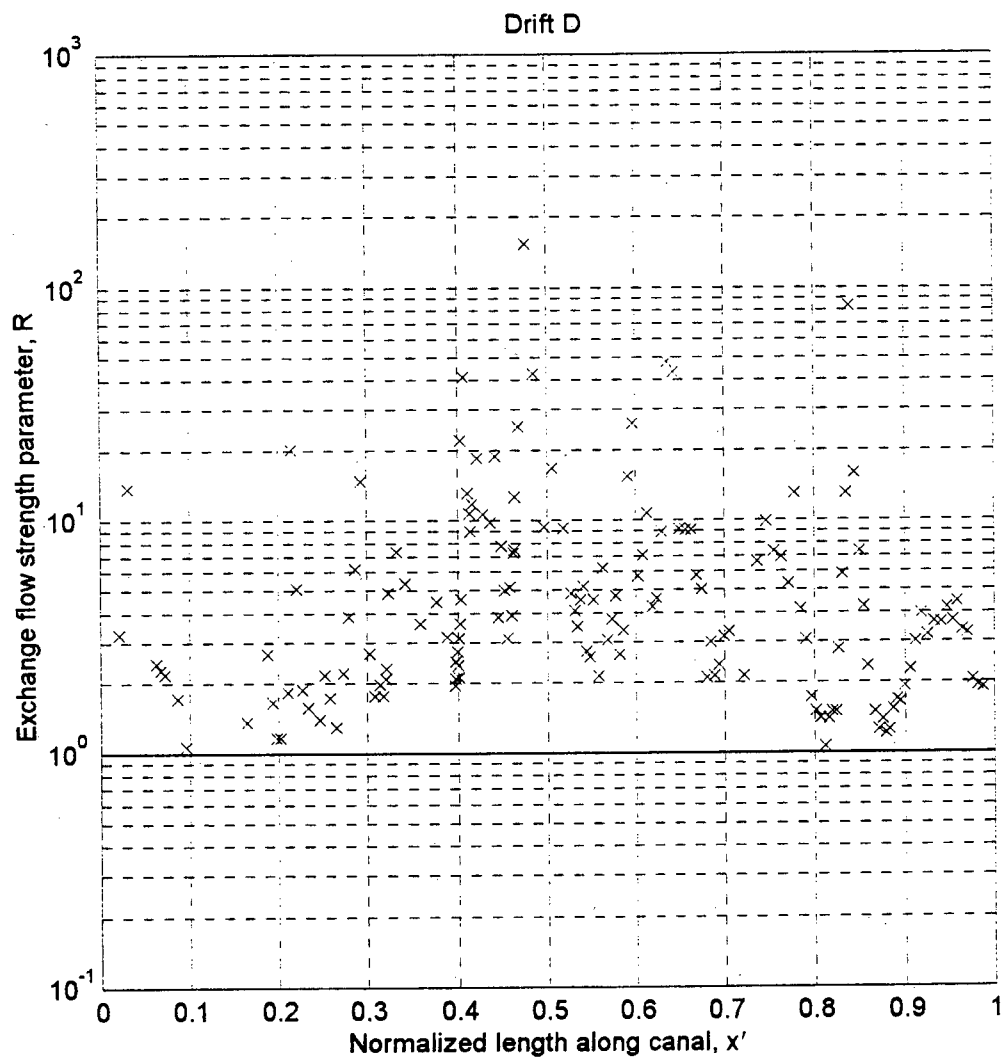


Figure B - 16 Exchange flow strength parameter for Drift D.
 When $R > 1$, the flow has a stronger exchange component while when $R < 1$, the flow has a stronger plug component.